UNIVERSITY OF ÇUKUROVA
INSTITUTE OF NATURAL AND
APPLIED SCIENCES

MSc THESIS

Ömer Evren İNAN

INVESTIGATION OF STOP AND PASS BANDS IN THE SPECTRUM OF A PERIODICALLY CORRUGATED WAVEGUIDE

DEPARTMENT OF ELECTRICAL AND
ELECTRONICS ENGINEERING

ADANA, 2005

ÇUKUROVA ÜNİVERSİTESİ

FEN BİLİMLERİ ENSTİTÜSÜ

INVESTIGATION OF STOP AND PASS BANDS IN THE SPECTRUM OF A PERIODICALLY CORRUGATED WAVEGUIDE

Ömer Evren İNAN

YÜKSEK LİSANS TEZİ

ELEKTRİK-ELEKTRONİK ANABİLİM DALI

Bu tez 21.09.2005 Tarihinde Aşağıdaki Jüri Üyeleri Tarafından Oybirliği/~~Oyçokluğu~~ İle Kabul Edilmiştir.

İmza............................	İmza............................	İmza............................
Prof. Dr. Victor POGREBNYAK	Prof. Dr. Süleyman GÜNGÖR	Doç. Dr. Turgut İKİZ
DANIŞMAN	ÜYE	ÜYE

Bu tez Enstitümüz Elektrik-Elektronik Anabilim Dalında hazırlanmıştır.

Kod No

Prof Dr. Aziz ERTUNÇ
Enstitü Müdürü

ABSTRACT

MSc. THESIS

INVESTIGATION OF STOP AND PASS BANDS IN THE SPECTRUM OF A PERIODICALLY CORRUGATED WAVEGUIDE

Ömer Evren İNAN

DEPARTMENT OF ELECTRICAL AND ELECTRONICS ENGINEERING
INSTITUTE OF NATURAL AND APPLIED SCIENCES
UNIVERSITY OF ÇUKUROVA

Supervisor: Prof. Dr. Victor POGREBNYAK
Year: 2005, Page: 142
Jury: Prof Dr. Victor POGREBNYAK
Prof. Dr. Süleyman GÜNGÖR
Ass. Prof. Dr. Turgut İKİZ

Bragg reflection phenomenon that is revealed by electromagnetic waves traveling in periodic structures is used in many microwave devices and antennas. Bragg reflection occurs because of the constructive interference of the longitudinal modes of the electromagnetic wave propagating in the waveguide. The Bragg reflection gives rise to band gap (stop band) in the frequency spectrum of the periodically corrugated waveguide. Bragg reflection phenomena have described well theoretically by the coupled-waves equation method and studied experimentally. Wave phenomenon arising in the frequency range located far from the Bragg reflections, non-Bragg phenomena, have studied theoretically in a planar periodically corrugated waveguide. Non-Bragg reflections occur because of the interaction between transverse modes of the different space harmonics of the electromagnetic wave propagating in the waveguide.

In this thesis, stop and pass bands in the spectrum of a planar periodically corrugated waveguide are investigated in detailed theoretically and experimentally. Experimentally such wave phenomenons have been investigated respectively; observation of stop and pass bands and transmitted power on changing of phase shift between parallel plates, dependency of transmitted power and stop and pass band's width and location in the frequency spectrum on distance between antennas and average distance between parallel plates, distribution of scattered power along the corrugation. In addition of these, evolution of stop and pass band's width and location in the frequency spectrum and distribution of scattered power along the corrugation have been investigated upon gradual transformation from periodic waveguide to smooth waveguide.

Keywords: periodic waveguide, pass band, stop band, frequency spectrum

ÖZ

YÜKSEK LİSANS TEZİ

PERİYODİK OLARAK OLUKLU DALGA KILAVUZUNUN SPEKTRUMUNDA DURDURAN VE GEÇİRGEN BANTLARIN İNCELENMESİ

Ömer Evren İNAN

ELEKTRİK-ELEKTRONİK MÜHENDİSLİĞİ BÖLÜMÜ
FEN BİLİMLERİ ENSTİTÜSÜ
ÇUKUROVA ÜNİVERSİTESİ

Danışman: Prof. Dr. Victor POGREBNYAK
Yıl: 2005, Sayfa: 142
Jüri: Prof Dr. Victor POGREBNYAK
Prof. Dr. Süleyman GÜNGÖR
Doç. Dr. Turgut İKİZ

Periyodik yapılar içinde yayılan elektromanyetik dalgalarla açıklanan Bragg yansıma olgusu, çoğu mikrodalga cihazlarda ve antenlerde kullanılır. Bragg yansıması, dalga kılavuzu içinde yayılan elektromanyetik dalganın boyuna modlarının yapıcı girişimlerinden kaynaklanmaktadır. Bragg yansıması, periyodik olarak oluklu dalga kılavuzunun frekans spektrumunda bant aralığının (durdurma bantları) oluşmasına sebep olur. Bragg yansıma olgusu, teorik olarak çiftli-dalga denklemi metoduyla tanımlanmıştır. Ayrıca deneysel olarak da çalışılmıştır. Bunun yanında Bragg yansımasından uzak yerlerdeki frekans aralıklarında oluşan dalga olgusu, non-Bragg olgusu, da düzlemsel olarak oluklu dalga kılavuzunda teorik olarak çalışılmıştır. Non-Bragg yansıması, dalga kılavuzu içinde yayılan elektromanyetik dalganın değişik uzay harmoniklerinin dikine modları arasındaki etkileşimden kaynaklanır.

Bu tezde; düzlemsel, periyodik olarak oluklu dalga kılavuzunun spektrumunda durduran ve geçirgen bantlar teorik ve deneysel olarak detaylı bir şekilde incelenmiştir. Deneysel olarak şu dalga olguları sırasıyla incelenmiştir: durduran ve geçirgen bantların ve iletilen gücün paralel plakalar arasındaki faz farkının değişimine olan bağlılığı, iletilen gücün ve durduran ve geçirgen bantların frekans spektrumundaki yerlerinin ve genişliklerinin antenler arasındaki uzaklığa ve paralel plakalar arasındaki ortalama uzaklığa olan bağlılığı, oluklar boyunca saçılan gücün dağılımı. Bunlara ek olarak, durduran ve geçirgen bantların frekans spektrumundaki yerlerinin ve genişliklerinin ve oluklar boyunca saçılan gücün dağılımının, periyodik olarak oluklu dalga kılavuzundan düz dalga kılavuzuna doğru kademeli olarak geçişteki evrimi deneysel olarak incelendi.

Anahtar Kelimeler: periyodik dalga kılavuzu, geçirgen bant, durduran bant, frekans spektrumu

ACKNOWLEDGMENT

Science is an activity which interrogates our theories and expectations related to nature. And science history is a source of learnedness and humanism. It teaches us to interrogate our ideas continuously, to rescued arrogant, to don't carried away null hope and to go forward quietly with study through success. And human beings comes today's status thanks to scientist.

I would like to say my respectful and thankful feelings to my supervisor Prof. Dr. Victor Pogrebnyak. He has much contributes to my education and academic carrier in both theoretical and experimental knowledge. From Prof. Dr. Pogrebnyak, I learnt how a scientific working should do. And he always believes and supports me. Also I would like to thank to Prof. Dr. Hamit Serbest who always inspired me with his scientific portrait and academic success.

I would like to thank to my father Sıtkı İnan, my mother Nalan İnan, my brother Erkin İnan and my aunt Nazan Uysal very much. Always, especially in my hard times, they support me in every way. And my friends Güzide Pelin Ayhan, Uğur Cem Hasar and Neşet Küçükaltun for their intimate friendship. Experimental measurements were done with MSc. student Neşet Küçükaltun and PhD. student Uğur Cem Hasar.

To my father Sıtkı İNAN

CONTENTS **PAGE**

LIST OF FIGURES **PAGE**

1. INTRODUCTION PART

1.1. Introduction

Analysis of electromagnetic wave propagation in periodic structures is very interesting subject in all around the world especially in near time. And its importance is increasing in time because of its extensive use in many fields of modern optics such as integrated optics, optoelectronics, photonic crystals, fiber sensors as well for the close relation of the this problem to investigation of a two-dimensional electron gas and the electronic stripe phase in high temperature superconductors. The periodic structures have been extensively studied theoretically as well as experimentally in above mentioned specific fields from different points of view. An incomplete list of the branches implies a huge number of publications devoted to wave propagation in the periodic structures. Important advances have been done in this subject via the computational methods in near time. Numerical techniques that are based on the particular physical models enable detailed investigation into practical periodic structures.

Although the field is well developed, there are still some basic problems that should be investigated both theoretically and experimentally in detail. For example, resonance phenomenon between transverse modes (standing-waves) in a periodically corrugated waveguide and effect of the phase shift between two periodic boundaries on wave propagation. For our knowledge, these problems had not been studied sufficiently. These problems can be solved analytically by using the standard perturbation theory. As a result, in this thesis, according to our theoretical and experimental investigations, new fundamental properties are revealed in such a periodic structure.

Bragg reflection or Bragg resonance phenomena that is the principal physical phenomenon in periodic structures is occurred because of periodicity. Because of this phenomenon, forbidden gap (stop band) is opened in the electromagnetic spectrum of the periodic structure. The Bragg reflection occurs both in the case of unbounded periodic medium as well as in the case of bounded periodic structure like a periodic waveguide. Besides, in both cases the Bragg reflection occurs at Bragg's law. Bragg's law is the mathematical formulation of the constructive interference of the longitudinal modes. Bragg reflection is also named as longitudinal phase matching in integrated optics.

In this thesis, it is shown that non-Bragg reflection is occurred by the resonance interaction between transverse modes. And again it is shown that interference of the transverse modes (standing-waves) essentially affects the wave propagation in the periodically corrugated waveguide or electronic states in the periodic quantum well.

The analysis shows dependency of the location and width of the forbidden gap (stop band) in the spectrum of a periodically corrugated waveguide on the phase shift between the periodic profiles of two boundaries, on evenness of wave modes, and on relationship between a period and a thickness of the waveguide. One of consequences of such dependence is the inhibition of the Bragg reflection in the waveguide having the congruent periodic boundaries. On the other hand when a frequency of the wave coincides with one of the gaps, the resonant wave can propagate only in one direction – along grooves of the periodic waveguide. This phenomenon is similar to the stripe phase in high temperature superconductors.

Besides the theoretical investigations, experimental investigations are done upon Bragg reflections (stop band), distribution of scattered power along corrugation, effect of average distance between parallel plates and distance between antennas on transmitted power and width and location of stop and pass band in the spectrum of a periodically corrugated waveguide, effect of phase shift on Bragg reflections. In addition of these experiments, gradually transferred from periodically corrugated waveguide to flat waveguide experiments are done. Then experimental investigations are evaluated.

As last, in this thesis, initial calculations to obtain dispersion equation of periodically two dimensional corrugated waveguide are done.

1.2. Previous Studies

For scientists who research electromagnetic wave propagation through various structures and its behavior because of the physical properties of the structures, periodic structures are always very interesting and attractive subject. Periodic structures supports a lot of processes like achievement of required slow wave motion or resonance condition, enhancement of filtering, band passing and rejecting, directive radiation, frequency selection. In the below paragraphs, both theoretical and practical previous investigations of periodic structures are mentioned briefly.

Wave propagation along a rectangular waveguide with slowly varying width has been investigated with the help of field theory and approximate circuit theory. In the field theory approach, two different methods of analysis have been attempted. Many properties of the modulated periodic structure, e.g., the frequency dependence of the propagation constant, group and phase velocities and the electric field axial variation for the fundamental space harmonic and its filter-like property have been investigated. The magnetic field lines on the H-plane for a typical case exhibit an expected configuration. Experimental results show close agreement with analysis. It is concluded that this structure supports the fast fundamental space harmonic. These investigations were done by Mallick, A.K. and Sanyal, G.S. Weissberg, E. studied to determination the guided wavelength in a dielectric-filled periodic structure, such as a corrugated wall or serrated waveguide. In this investigation, it is seen that the accepted traveling probe technique requires a slot in the broad wall of the guide and a groove in the dielectric material. Even if the errors introduced by these modifications could be tolerated, other effects render this technique unsuitable. One of these is surface wave effect which results in a measured wavelength higher than the one in the guide and lower than the free-space value. If the structure is dissipative, such as a serrated guide, more difficulties arise. Birdsall, C.K. and White, R.M. did experiments with open periodic structures and it is shown that a large change in transmission at the transition from allowed to forbidden regions. At the boundaries of the forbidden regions, the radial distribution of the fields of a wave impressed upon the structure changes from one corresponding to slow-wave propagation to a field distribution corresponding to radiation. At these boundaries, the local field shapes do not change very much. However, at the boundary a large decrease in transmission through the structure is found, but with little change in input VSWR; this implies a change from real characteristic impedance to about the same value of radiation resistance. This behavior suggests applications to sharp cutoff absorptive filters. W.S. C. Chang emphasized that periodic structures are used widely in integrated optics for input-output couplers, band stop filters, modulators, directional couplers, and distributed feedback lasers. An analytical discussion and review of these devices is given based upon the coupled-mode transmission-line analysis. Experimental results and performance characteristics are presented to illustrate the special features of each type of device. Finally, the usefulness of transmission-line analysis to the understanding and the design of these devices is pointed out. Rotman, W. and Oliner, A.A. investigated that the center fin in trough waveguide can be modified in a periodic fashion to alter the propagation characteristics of the guide. Two such periodic modifications, first is an array of circular holes and the second is a periodic array of teeth, have been measured fairly extensively and analyzed theoretically. These configurations are useful in connection with antenna scanning or waveguide filter applications. The array of holes produces only a mild slowing of the propagating wave, but the toothed structure, which may alternatively be described as a series of flat strips extending beyond the edge of the tin, can cause the propagating wave to vary from a very slow to a very fast wave. The periodic structures are theoretically treated by two methods, a transverse resonance procedure and a periodic cell approach. These theoretical results agree very well with each other and with the measured data. Propagation in a rectangular waveguide periodically loaded with resonant irises is studied by Navarro, M.S., Rozzi, T.E. and Yuen Tze Lo. In this contribution they treat the problem of an infinite rectangular waveguide periodically loaded by means of infinitely thin resonant irises. The method of solution breaks down the problem into two separate steps: 1) the multi port network characterization of the resonant iris; 2) the network analysis of the equivalent periodic network. The results for the resonant iris can be used for various applications, such as the design of waveguide filters and matching networks. In the limiting cases of purely capacitive or inductive irises, the results agree exactly with existing experimental and numerical values. The size of the eigen value equation to be solved for the periodic structure equals half the number of ports of the network characterization of the iris and is generally small (typically five to seven). The eigen values have good convergence properties with resect to the size of the matrix. Theoretical and experimental study of the evolution of fields in an over dimensioned waveguide with a corrugated surface is achieved by Fenelon, J.P. and Papiernik, A. To obtain answers to problems arising in many microwave applications, some labs use over dimensioned corrugated waveguides. The authors' propose is theoretical approach with eigen modes that enables to determine the values of the limiting frequencies (frequencies of π modes in the periodic structure) of an over dimensioned parallel piped cavity loaded with a thin corrugation as a function of the height of the aperture. In this approach, the electric field is represented by different analytical functions. The authors compare the theoretical results with the experimental values obtained for different apertures and periodicities, according to the value of the wavelength in comparison with the aperture and the period. Each function is in good agreement in a certain frequency range. Wave propagation in sinusoidally stratified dielectric media is investigated by Tamir, T., Wang, H.C. and Oliner, A.A. The dispersion properties and the fields of electromagnetic waves are investigated for propagation in a stratified infinite medium. The stratification is characterized by a dielectric constant which, along one coordinate, is modulated sinusoidally about an average value. A systematic and comprehensive study is presented for the case of H modes for which the pertinent wave equation is in the form of a Mathieu differential equation. The modes and dispersion characteristics are analyzed in terms of a "stability" chart, which is customary in the study of the Mathieu equation. Results are obtained for an unbounded medium and for a waveguide filled with the modulated medium. Also, the reflection occurring at an interface between free space and a semi-infinite medium of this type is examined. In addition to these rigorous results for arbitrary values of modulation, simple analytical expressions are given for all of these cases where the modulation in the dielectric is small. It is shown that the fields are then expressible in terms of the fundamental and the two nearest space harmonics. The fields within a unit cell in the stratified medium are calculated for both small and large modulation and for frequencies up through the second pass band. It is of interest that the variation of the fields is not, in general, simply related to the variation of the dielectric constant within a cell. Microcavities, photonic bandgaps and applications to lasers and optical communications are mentioned by Lee, R.K., Xu, Y. and Yariv, A. Structures with periodically modulated refractive index are frequently discussed under the classification of photonic crystals. Recently, much attention has been paid to these types of structures for a large variety of applications such as the inhibition or enhancement of spontaneous emission, ultra-low threshold lasers, compact optical circuits, light-emitting diodes with increased efficiency and novel optical waveguides. Using structures that exhibit a photonic bandgap (PBG), it has been shown that high-Q, small modal volume microcavities can be created. Advances in semiconductor fabrication technology have made it possible to make semiconductor PBG microcavities for optical wavelengths. Multimode network analysis for frequency selective characteristics of dielectric periodic structures with arbitrary profiles is investigated by Yang Li, Xu Shanjia and Wu Xianliang. In this investigation, the frequency selective reflection characteristics of dielectric periodic structures with arbitrary groove profiles for the oblique incidence of a plane wave are analyzed. Emphasis is placed on the discussion about the effect of the different groove profiles on the reflection characteristics of the millimeter wave (MMW) frequency selective surface (FSS). Some useful guidelines for the design of FSS are thus suggested. Moreover, the physical explanation of the related wave phenomenon is given. A novel photonic bandgap structure for low-pass filter of wide stopband is studied by Taesun Kim and Chulhun Seo. In this study, a novel photonic bandgap (PBG) structure is proposed for increasing the stopband of a low-pass filter without the increasing circuit size for applications in microstrip circuits. The proposed structure is connected in two parallel periodic structures which have a different center frequency of the stopband. The wide stopband is achieved by two periodic structures of two different stopbands. They also show the performance improvement of microstrip patch antenna by etching of the proposed structure in ground plane. Jakoby, B. and Vellekoop, M.J. investigated in detail FFT based analysis of periodic structures in microacoustic devices. Periodic structures utilized as transducer or reflector elements play an important role in microacoustic wave devices. Such structures can be described using approximate analytical models. However, to obtain the accuracy required for reliable device simulation, numerical methods have to be employed. In this contribution, authors present an efficient numerical approach to calculate the dispersion curves associated with microacoustic modes propagating in periodic structures; the method is demonstrated for the case of Love wave modes. The computational efficiency is related to the utilization of the FFT algorithm in a hybrid Method of Moments (MoM) / Mode-Matching analysis. From the obtained dispersion curves, characteristic parameters such as the stop band width can be obtained which can be used in a coupling-of-modes (COM) model of the structure. Yang, H.D. investigated surface-wave elimination in integrated circuit structures with artificial periodic materials. Surface-wave (or dielectric slab) modes in integrated circuit structures often result in undesired energy losses and cross talk between components. In this contribution, author investigates the feasibility of surface-wave elimination in integrated circuit structures by using planar artificial periodic (photonic band-gap) substrates. A full-wave 3-D integral-equation moment-method is employed to find the propagation constants of guided-wave modes on grounded dielectric slabs with planar periodic implants. Rectangular blocks in both a rectangular lattice and a triangular lattice are investigated. It is found that surface-waves forbidden characteristics are mostly determined by the lattice structures and insensitive to the shape and size of the periodic elements. Attempt has been made to obtain the omnidirectional wave band-gap. The limitation on complete surface-wave elimination is discussed. This contribution initiates the investigation of a class of novel integrated circuit components which have potential applications in millimeter-waves and optics. Planar periodic structures for microwave and millimeter wave circuit applications are investigated by Yongxi Qian and Itoh, T. Periodic structures, some of which are known as photonic band-gap (PBG) crystals, offer new dimensions of freedom in controlling the behavior of electromagnetic waves in modern microwave and millimeter wave circuits and antennas. This study summarizes several novel structures developed recently at the authors' group, as well as some of their applications. The structures described include: (1) Dielectric-based PBG microstrip lines; (2) PBG ground plane for microstrip lines; (3) PBG-based high-Q image guide resonator; (4) Compact 2D PBG lattice for surface wave suppression in microstrip patch antennas; and (5) Uniplanar compact PBG (UC-PBG) structure and its unique characteristics such as slow-wave effect, wide stopband, leakage suppression as well as perfect magnetic surface impedance. Liu, J., Butler, J.K., Evans, G.A. and Rosen, A. studied analysis of millimeter wave phase shifters coupled to a fixed periodic structure. The propagation characteristics of an active plasma-induced millimeter wave phase shifter coupled to a fixed periodic structure are discussed. The numerical calculation is based on an improved boundary value solution. Like a normal dielectric slab waveguide with a plasma layer, the grating waveguide displays a phase shift with the increase of the plasma density. This phase shift due to the significant change of the field distribution has an impact on the modal attenuation coefficient. It results in the scanning of the radiation beam in the vicinity of the second Bragg. Especially, at both weak and strong plasma densities when the mode losses are small, the resonances caused by the periodic structure do not appear to be weakened. The results can be used to design electronically controllable millimeter wave scanning antennas. Characterization of corrugated waveguides by modal analysis is investigated by Esteban, J. and Rebollar, J.M. A. In this study, general formulation for the characterization of corrugated waveguides is presented. The formulation is based on modal expansion in the different smooth-walled waveguides which constitute the corrugated structure and on the use of mode matching at discontinuities. The use of an admittance matrix formulation and a suitable root-finding algorithm leads to a rigorous and efficient technique. Dispersion curves are presented for corrugated waveguides of circular and rectangular cross-sections. Complex modes are obtained for deep corrugations. The effect of the finite thickness and width of teeth and slots on the dispersion behavior is shown. Amari, S., Vahldieck, R., Bornemann, J., and Leuchtmann, P. studied spectrum of corrugated and periodically loaded waveguides from classical matrix eigen values. The investigation presents a rigorous full-wave analysis of propagation in corrugated and periodically loaded waveguides. The propagation constants are determined from the classical eigenvalues of a canonical matrix eigenvalue problem instead of a determinant. The entries of the matrix are computed only once per frequency point. The entire $k_0 - \beta$ diagram of a corrugated circular waveguide, a circular waveguide periodically loaded with dielectric disks, and a rectangular waveguide periodically loaded with capacitive irises are determined and compared with results of other researchers. Excellent agreement is documented in each case. Levy, R. investigated tapered corrugated waveguide low-pass filters. Several new synthesis techniques are described for the design of tapered corrugated waveguide low-pass filters. Previous techniques are based on image-parameter methods which are both nonoptimum and difficult to apply to new specifications. The new synthesis methods give filters which can be constructed to work directly from dimensions generated by a computer. The impedance tapering implies that the terminating impedance transformers used in the image-parameter designs may be either eliminated or reduced in length. Amari, S., Vahldieck, R. and Bornemann, J. investigated accurate analysis of periodic structures with an additional symmetry in the unit cell from classical matrix eigenvalues. Dispersion diagrams of periodic structures with an additional symmetry in the unit cell are investigated by the example of a parallel-plate waveguide loaded with irises of zero thickness. The propagation constants of the Floquet modes are determined from the classical eigenvalues of a non-Hermitian matrix. Rizzoli, V. and Lipparini, A. investigated Bloch-wave analysis of stripline and microstrip-array slow-wave structures. The investigation discusses a general approach to the analysis of periodic structures essentially consisting of an array of coupled striplines or microstrips. It is shown that any such structure can be represented as a cascade of identical multiport networks of known topology, thus allowing a straightforward analysis in terms of Bloch waves. The method is equally applicable to homogeneous and nonhomogeneous dielectric (i.e., MIC) devices. Bragg reflection characteristics of millimeter waves in a periodically plasma-induced semiconductor waveguide are investigated by Matsumoto, M., Tsutsumi, M. and Kumagai, N. Theoretical analysis on the Bragg reflection characteristics of millimeter waves in a periodically plasma-induced semiconductor waveguide is presented. The plasma is assumed to be generated by light illumination. Numerical examples are given which show the dependence of the Bragg reflection characteristics on the length of the plasma-induced section and on the plasma density. Since the period can be changed by altering the illumination pattern, this type of periodic structure may be developed to tunable filters or tunable DBR oscillators for millimeter-wave region. Characterization and design of two-dimensional electromagnetic band-gap structures by use of a full-wave method for diffraction gratings is studied by Frezza, F., Pajewski, L. and Schettini, G. In this investigation, an accurate and efficient characterization of a two-dimensional (2-D) electromagnetic band-gap (EBG) structures is performed, which exploits a full-wave diffraction theory developed for one-dimensional diffraction gratings. EBG materials constituted by 2-D arrays of dielectric rods with arbitrary shape and lattice configuration are analyzed, and the transmission and reflection efficiencies are determined. The high convergence rate of the proposed technique is demonstrated. Results are presented for both TE and TM polarizations, showing the efficiencies as a function of frequency and physical parameters. Comparisons with other theoretical results reported in the literature are shown with a very good agreement, and the authors' theory is also favorably compared with available experimental data. Useful design contour plots are reported by which a very immediate and accurate visualization of the band-gap configurations can be obtained, and design formulas are also included. Finally, the behavioral differences when a periodical defect is present are also highlighted. Periodic waveguide structures with long cells are investigated by Votruba, J. In this study, a class of periodic waveguide structures with stepwise constant circular cross section is analyzed by means of Hahn's method of modal field matching along transverse planes. It allows one to resolve algebraically the implicit determinant relation between the phase shift per cell and frequency and to obtain an explicit formula. Dispersion diagrams and field distributions are also calculated and plotted and convergence properties of the method are tested. Goblick, T.J. and Bevensee, R.M. investigated variational principles and mode coupling in periodic structures. Variational techniques are used in analyzing periodic "cold" microwave structures for the angular frequency, omega, as a function of assumed phase shift per periodic cell. Two variational expressions are given: one for omega in terms of the E- and H-fields, and one for k^2 = omega$^2\mu$ epsilon in terms of the E-field. For structures with relatively light coupling between cells, the trial fields to be used with the variational expressions are composed of closed cavity modes, phase shifted by phi radians from cell to cell. Both variational expressions yield determinantal equations for k^2(phi) which agree with equations previously derived from a mode coupling point of view. One form of an equivalent lumped circuit is given to represent the structure within one of its pass bands. Curves compare the variational-mode coupling expression for k^2(phi) of a periodically lumped loaded transmission line with exact expressions.

1.3. Floquet's Theorem

In general, the field of the slow wave structure must be distributed according to Floquet's theorem for periodic boundaries. Floquet's periodicity theorem states that:

The steady-state solutions for the electromagnetic fields of a single propagating mode in a periodic structure have the property that fields in adjacent cell are related by a complex constant.

Mathematically, the theorem can be stated;

$$E(x,y,z-L) = E(x,y,z)e^{j\beta_0 L} \tag{1.3.1}$$

where $E(x,y,z)$ is a periodic function of z with period L. Since β_0 is the phase constant in the axial direction, in a slow wave structure β_0 is the phase constant of average electron velocity.

It is postulated that the solution to Maxwell's equations in a periodic structure can be written;

$$E(x,y,z) = f(x,y,z)e^{-j\beta_0 z} \tag{1.3.2}$$

where $f(x,y,z)$ is a periodic function of z with period L that is the period of slow wave structure.

For a periodic structure, equation (1.3.2) can be rewritten with z replaced by $z-L$:

$$E(x,y,z-L) = f(x,y,z-L)e^{-j\beta_0(z-L)} \tag{1.3.3}$$

Since $f(x,y,z-L)$ is a periodic function with period L, then

$$f(x,y,z-L) = f(x,y,z) \tag{1.3.4}$$

Substitution of equation (1.3.4) in (1.3.3) results in

$$E(x,y,z-L) = f(x,y,z)e^{-\beta_0 z}e^{+j\beta_0 L} \tag{1.3.5}$$

and substitution of equation (1.3.2) in (1.3.5) gives

$$E(x,y,z-L) = E(x,y,z)e^{+j\beta_0 L} \tag{1.3.6}$$

This expression is the mathematical statement of Floquet's theorem, equation (1.3.1). Therefore equation (1.3.2) does indeed satisfy Floquet's theorem.

From the theory of Fourier series, any function that is periodic, single-valued, finite and continuous may be represented by a Fourier series. Hence the field distribution function $E(x,y,z)$ may be expanded into a Fourier series of fundamental period L as

$$E(x,y,z) = \sum_{n=-\infty}^{\infty} E_n(x,y)e^{-j(2\pi n/L)z}e^{-j\beta_0 z} = \sum_{n=-\infty}^{\infty} E_n(x,y)e^{-j\beta_n z} \tag{1.3.7}$$

where

$$E_n(x,y)=\frac{1}{L}\int_0^L E(x,y,z)e^{j(2\pi n/L)z}dz \tag{1.3.8}$$

are the amplitudes of n harmonics and

$$\beta_n=\beta_0+\frac{2\pi n}{L} \tag{1.3.9}$$

is the phase constant of the nth modes, where $n=-\infty,\ldots,-2,-1,0,1,2,\ldots\infty$.

The quantities $E_n(x,y)e^{-j\beta_n z}$ are known as spatial harmonics by analogy with time-domain Fourier series. The question is whether equation (1.3.7) can satisfy the electric wave equation, $\nabla^2\vec{E}=\gamma^2\vec{E}$. Substitution of equation (1.3.7) into the wave equation results in

$$\nabla^2\left[\sum_{n=-\infty}^{\infty}E_n(x,y)e^{-j\beta_n z}\right]-\gamma^2\left[\sum_{n=-\infty}^{\infty}E_n(x,y)e^{-j\beta_n z}\right]=0 \tag{1.3.10}$$

Since the wave equation is linear, equation (1.3.10) can be written as

$$\sum_{n=-\infty}^{\infty}\left[\nabla^2 E_n(x,y)e^{-j\beta_n z}-\gamma^2 E_n(x,y)e^{-j\beta_n z}\right]=0 \tag{1.3.11}$$

It is evident from the preceding equation that if each spatial harmonic is itself a solution of the wave equation for each value of n, the summation of space harmonics also satisfies the wave equation of (1.3.10). This means that only the complete solution of equation (1.3.10) can satisfy the boundary conditions of a periodic structure.

Furthermore, equation (1.3.7) shows that the field in a periodic structure can be expanded as in an infinite series of waves, all at the same frequency but with different phase velocities, ϑ_{pn}. That is,

$$\vartheta_{pn} = \frac{\omega}{\beta_n} \equiv \frac{\omega}{\beta_0 + (2\pi n/L)} \tag{1.3.12}$$

The group velocity, ϑ_{gr}, defined by $\vartheta_{gr} = \partial\omega/\partial\beta$, is then given as

$$\vartheta_{gr} = \left[\frac{d(\beta_0 + (2\pi n/L))}{d\omega}\right]^{-1} = \frac{\partial\omega}{\partial\beta_0} \tag{1.3.13}$$

which is independent of n.

It is important to note that the phase velocity ϑ_{pn} in the axial direction decreases for higher values of positive n and β_0. So it appears possible for a microwave of suitable n to have a phase velocity less than the velocity of light. It follows that interactions between the electron beam and microwave signal are possible and thus the amplification of active microwave devices can be achieved.

$\omega - \beta$ diagrams are named as Brillouin diagrams. The second quadrant of $\omega - \beta$ diagram indicates the negative phase velocity that corresponds to the negative n. This means that the electron beam moves in the positive z direction (propagation direction) while the beam velocity coincides with the negative spatial harmonic's phase velocity. This type of tube is called a backward-wave oscillator. And forbidden regions for propagation occurs because if the axial phase velocity of any spatial harmonic exceeds the velocity of light, the structure radiates energy.

1.4. Periodic Structures

An infinite transmission line or waveguide periodically loaded with reactive elements is referred to as periodic structures. As shown in figure 1.1, periodic structures can take various forms, depending on the transmission line media being used. Often the loading elements are formed as discontinuities in the line, but in any case they can be modeled as lumped reactances across a transmission line as shown in figure 1.2. Periodic structures support slow wave (slower than the phase velocity of the unloaded line), and have pass-band and stop-band characteristics similar to filters; they find application in traveling wave tubes, masers, phase-shifters, and antennas.

1.4.1. Analysis of Infinite Periodic Structures

We begin by studying the propagation characteristics of the infinite loaded line shown in figure 1.2. Each unit cell of this line consists of a length d of transmission line with a shunt susceptance across the midpoint of the line; the susceptance b is normalized to the characteristic impedance, Z_0.

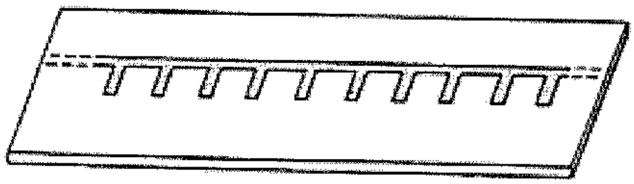

(a)

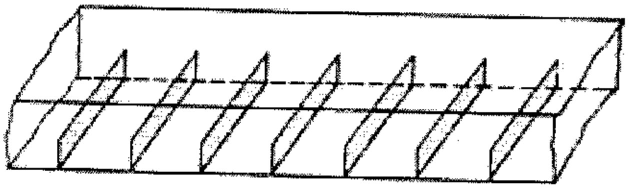

(b)

Figure 1.1. Examples of periodic structures. (a) Periodic stubs on a micro strip line (b) Periodic diagrams in a waveguide. (David M. Pozar, Microwave Engineering, 1993)

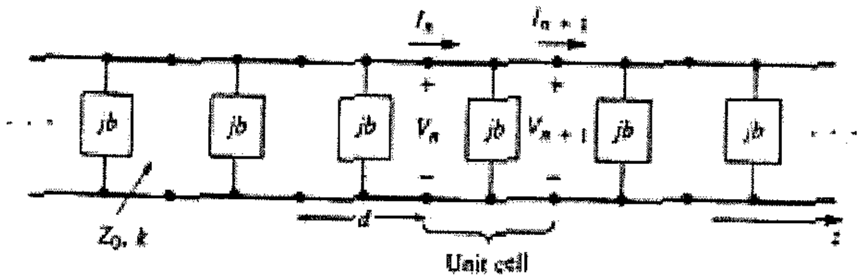

Figure 1.2. Equivalent circuit of a periodically loaded transmission line. The unloaded line has characteristic impedance Z_0 and propagation constant k. (David M. Pozar, Microwave Engineering, 1993)

If we consider the infinite line as being composed of a cascade of identical two-port networks, we can relate the voltages and currents on either side of the nth cell using the $ABCD$ matrix:

$$\begin{bmatrix} V_n \\ I_n \end{bmatrix} = \begin{bmatrix} A & B \\ C & D \end{bmatrix} \begin{bmatrix} V_{n+1} \\ I_{n+1} \end{bmatrix} \tag{1.4.1}$$

where A, B, C and D are the matrix parameters for a cascade of a transmission line section of length $d/2$, a shunt susceptance b, and another transmission line section of length $d/2$. From the table of "ABCD Parameters of some useful two port circuits" (can be seen in Appendix I) we than have, in normalized form,

$$\begin{bmatrix} A & B \\ C & D \end{bmatrix} = \begin{bmatrix} \cos\theta/2 & j\sin\theta/2 \\ j\sin\theta/2 & \cos\theta/2 \end{bmatrix} \begin{bmatrix} 1 & 0 \\ jb & 1 \end{bmatrix} \begin{bmatrix} \cos\theta/2 & j\sin\theta/2 \\ j\sin\theta/2 & \cos\theta/2 \end{bmatrix}$$
$$= \begin{bmatrix} (\cos\theta - b/2\sin\theta) & j(\sin\theta + b/2\cos\theta - b/2) \\ j(\sin\theta + b/2\cos\theta + b/2) & (\cos\theta - b/2\sin\theta) \end{bmatrix} \tag{1.4.2}$$

where $\theta = kd$, and k is the propagation constant of the unloaded line.

The reader can verify that $AD-BC=1$, as required for reciprocal networks.

Now for any wave propagating in the $+z$ direction, we must have

$$V(z)=V(0)e^{-\gamma z} \tag{1.4.3a}$$

$$I(z)=I(0)e^{-\gamma z} \tag{1.4.3b}$$

for a phase reference at $z=0$. Since the structure is infinitely long, the voltage and current at the nth terminals can differ from the voltage and current at the $n+1$ terminals only by the propagating factor, $e^{-\gamma d}$. Thus,

$$V_{n+1}=V_n e^{-\gamma d} \tag{1.4.4a}$$

$$I_{n+1}=I_n e^{-\gamma d} \tag{1.4.4b}$$

Using this result in (1.4.1) gives the following:

$$\begin{bmatrix} V_n \\ I_n \end{bmatrix}=\begin{bmatrix} A\,B \\ C\,D \end{bmatrix}\begin{bmatrix} V_{n+1} \\ I_{n+1} \end{bmatrix}=\begin{bmatrix} V_{n+1}e^{\gamma d} \\ I_{n+1}e^{\gamma d} \end{bmatrix},$$

or

$$\begin{bmatrix} A-e^{\gamma d} & B \\ C & D-e^{\gamma d} \end{bmatrix}\begin{bmatrix} V_{n+1} \\ I_{n+1} \end{bmatrix}=0 \tag{1.4.5}$$

For a nontrivial solution, the determinant of the above matrix must vanish:

$$AD+e^{2\gamma d}-(A+D)e^{\gamma d}-BC=0 \tag{1.4.6}$$

or, since $AD-BC=1$,

$$1+e^{2\gamma d}-(A+D)e^{\gamma d}=0,$$

$$e^{-\gamma d}+e^{\gamma d}=A+D,$$

$$\cosh \gamma d = \frac{A+D}{2} = \cos\theta - \frac{b}{2}\sin\theta \tag{1.4.7}$$

Where (1.4.2) was used for the values of A and D. Now if $\gamma = \alpha + j\beta$, we have that

$$\cosh \gamma d = \cosh \alpha d \cos \beta d + j \sinh \alpha d \sin \beta d = \cos\theta - \frac{b}{2}\sin\theta \tag{1.4.8}$$

Since the right-hand side of (1.4.8) is purely real, we must have either $\alpha = 0$ or $\beta = 0$.

Case 1: ($\alpha = 0$, $\beta \neq 0$) This case corresponds to a non-attenuating, propagating wave on the periodic structure, and defines the pass-band of the structure. Then (1.4.8) reduces to;

$$\cos \beta d = \cos\theta - \frac{b}{2}\sin\theta \tag{1.4.9a}$$

which can be solved for β if the magnitude of the right-hand side is less than or equal to unity. Note that there are an infinite number of values of β that can satisfy (1.4.9a).

Case 2: ($\alpha \neq 0$, $\beta = 0, \pi$) In this case the wave does not propagate, but is attenuated along the line; this defines the stop-band of the structure. Because the line is lossless, power is not dissipated, but is reflected back to the input of the line. The magnitude of (1.4.8) reduces to

$$\cosh \alpha d = \left| \cos\theta - \frac{b}{2}\sin\theta \right| \geq 1 \tag{1.4.9b}$$

which has only one solution ($\alpha > 0$) for positively traveling waves; ($\alpha < 0$) applies for negatively traveling waves. If $\cos\theta - \frac{b}{2}\sin\theta \leq -1$, (1.4.9b) is obtained from

(1.4.8) by letting $\beta = \pi$; then all the lumped loads on the line are $\lambda/2$ apart, yielding an input impedance the same as if β=0.

Thus, depending on the frequency and normalized susceptance values, the periodically loaded line will exhibit either pass-bands or stop-bands, and so can be considered as a type of filter. It is important to note that the voltage and current waves defined in (1.4.3) and (1.4.4) are only meaningful when measured at the terminals of the unit cells, and do not apply the voltages and currents that may exists at points within a unit cell. These waves are sometimes referred to as Bloch waves because of their similarity to elastic waves that propagate through periodic crystal lattices.

Besides the propagation constant of the waves on the periodically loaded line, we will also be interested in the characteristic impedance for these waves. We can define the characteristic impedance at the unit cell terminals as;

$$Z_B = Z_0 \frac{V_{n+1}}{I_{n+1}} \tag{1.4.10}$$

since V_{n+1} and I_{n+1} in the above derivation were normalized quantities. This impedance is also referred as the Bloch impedance. From (1.4.5) we have that

$$(A - e^{\gamma d})V_{n+1} + BI_{n+1} = 0\,,$$

so (1.4.10) yields

$$Z_B = \frac{-BZ_0}{A - e^{\gamma d}}$$

From (1.4.6) we can solve for $e^{\gamma d}$ in terms of A and D as follows:

$$e^{\gamma d} = \frac{(A+D) \pm \sqrt{(A+D)^2 - 4}}{2}$$

Then the Bloch impedance has two solutions given by

$$Z_B^{\pm} = \frac{-2BZ_0}{A - D \mp \sqrt{(A+D)^2 - 4}} \tag{1.4.11}$$

For symmetrical unit cells (as assumed in figure 1.2) we will always have $A = D$. In this case (1.4.11) reduces to

$$Z_B^{\pm} = \frac{\pm BZ_0}{\sqrt{A^2 - 1}} \tag{1.4.12}$$

The $\pm$ solutions correspond to the characteristic impedance for positively and negatively traveling waves, respectively. For symmetrical networks these impedances are the same except for the sign; the characteristic impedance for a negatively traveling wave turns out to be negative because we have defined I_n in figure 1.2 as always being in the positive direction.

From equation (1.4.2) we see that B is always purely imaginary. If $\alpha = 0$, $\beta \neq 0$ (pass-band), then equation (1.4.7) shows that $\cosh \gamma d = A \leq 1$ (for symmetrical networks) and equation (1.4.12) shows that Z_B will be real. If $\alpha \neq 0$, $\beta = 0$ (stop-band), then equation (1.4.7) shows that $\cosh \gamma d = A \geq 1$, and (1.4.12) shows that Z_B is imaginary. This situation is similar to that for the wave impedance of a waveguide, which is real for propagating modes and imaginary for cut-off, or evanescent modes.

1.4.2. Terminated Periodic Structures

Next consider a truncated periodic structure, terminated in a load impedance Z_L, as shown in figure 1.3. At the terminals of an arbitrary unit cell, the incident and reflected voltages and currents can be written as (assuming operation in the pass-band);

$$V_n = V_0^+ e^{-j\beta nd} + V_0^- e^{j\beta nd} \tag{1.4.13a}$$

$$I_n = I_0^+ e^{-j\beta nd} + I_0^- e^{j\beta nd} = \frac{V_0^+}{Z_B^+} e^{-j\beta nd} + \frac{V_0^-}{Z_B^-} e^{j\beta nd} \tag{1.4.13b}$$

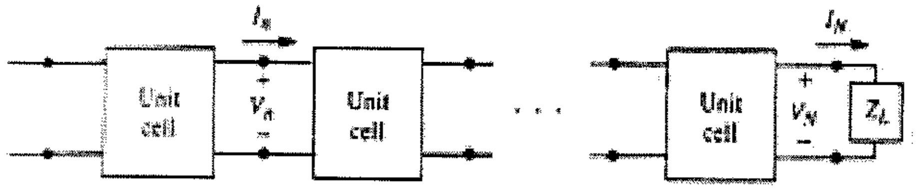

Figure 1.3. A periodic structure terminated in a normalized load impedance, Z_L. (David M. Pozar, Microwave Engineering, 1993)

where we have replaced γ_Z in (1.4.3) with $j\beta nd$, since we are only interested in terminal quantities.

Now define the following incident and reflected voltages at the nth unit cell:

$$V_n^+ = V_0^+ e^{-j\beta nd} \tag{1.4.14a}$$

$$V_n^- = V_0^- e^{j\beta nd} \tag{1.4.14b}$$

Then (1.4.13) can be written as

$$V_n = V_n^+ + V_n^- \tag{1.4.15a}$$

$$I_n = \frac{V_n^+}{Z_B^+} + \frac{V_n^-}{Z_B^-} \tag{1.4.15b}$$

At the load, where $n = N$, we have

$$V_N = V_N^+ + V_N^- = Z_L I_N = Z_L\left(\frac{V_N^+}{Z_B^+} + \frac{V_N^-}{Z_B^-}\right) \tag{1.4.16}$$

so the reflection coefficient at the load can be found as;

$$\Gamma = \frac{V_N^-}{V_N^+} = -\frac{Z_L/Z_B^+ - 1}{Z_L/Z_B^- - 1} \tag{1.4.17}$$

If the unit cell network is symmetrical ($A = D$), then $Z_B^+ = Z_B^- = Z_B$, which reduces (1.4.17) to the familiar result that

$$\Gamma = \frac{Z_L - Z_B}{Z_L + Z_B} \tag{1.4.18}$$

So to avoid reflections on the terminated periodic structure, we must have $Z_L = Z_B$, which is real for a lossless structure operating in a pass-band. If necessary, a quarter wave transformers can be used between the periodically loaded line and the load.

1.4.3. $k-\beta$ (Brillouin) Diagrams and Wave Velocities

When studying the pass-band and stop-band characteristics of periodic structure, it is useful to plot the propagation constant, β, versus the propagation constant of the unloaded line, k (or ω). Such a graph is called $k-\beta$ diagram, or Brillouin diagram.

The $k-\beta$ diagram can be plotted from (1.4.9a), which is the dispersion relation for a general periodic structure. In fact, a $k-\beta$ diagram can be used to study the dispersion characteristics of many types of microwave components and transmission lines. For instance, consider the dispersion relation for a waveguide mode:

$$\beta = \sqrt{k^2 - k_c^2}$$

or

$$k = \sqrt{\beta^2 + k_c^2} \tag{1.4.19}$$

where k_c is the cut-off wave number of the mode, k is the free space wave number, and β is the propagation constant of the mode. Relation (1.4.19) is plotted in the $k-\beta$ diagram of figure 1.4. For values of $k < k_c$, there is no real solution for β, so the mode is non-propagating. For $k > k_c$, the mode propagates, and k approaches β for large values of β (TEM propagation).

The $k-\beta$ diagram is also useful for interpreting the various wave velocities associated with a dispersive structure.

The phase velocity is;

$$\vartheta_p = \frac{\omega}{\beta} = c\frac{k}{\beta}, \tag{1.4.20}$$

which is seen to be equal to c (speed of light) times the slope of the line from the origin to the operating point on the $k-\beta$ diagram.

The group velocity is;

$$\vartheta_g = \frac{d\omega}{d\beta} = c\frac{dk}{d\beta}, \qquad (1.4.21)$$

which is the slope of the $k-\beta$ curve at the operating point. Thus, referring to figure 1.4, we see that phase velocity for a propagating waveguide mode is infinite at cut-off and approaches c (from below) as k increases.

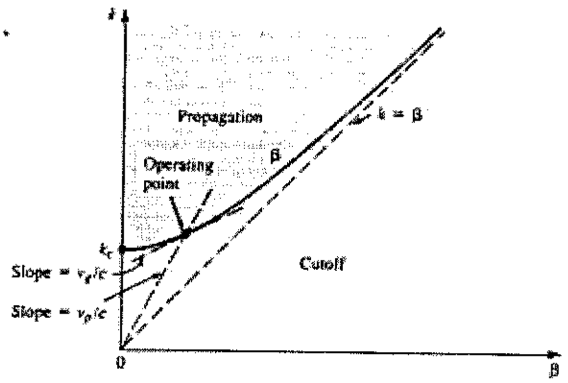

Figure 1.4. $k-\beta$ diagram for a waveguide mode. (David M. Pozar, Microwave Engineering, 1993)

1.5. Solution of Periodic Differential Equations and Their Meanings in Periodic Structures

1.5.1. Second Order Differential Equations

The most commonly occurring periodic equations are of second order. Similarly the theory of second order equations is extensive with relatively little theory having been developed for particular higher order forms. The general second order equation is;

$$\frac{d^2x}{dt^2} + \omega_0^2 x = \begin{Bmatrix} F_0 \sin\gamma t \\ 0 \end{Bmatrix} \begin{Bmatrix} Non-Homogenous, F_0 = const., \gamma = Frequency \\ Homogenous \end{Bmatrix} \qquad (1.5.1)$$

The function, $F_0 \sin \gamma t$, is generally associated with an impressed excitation. When this function is zero, equation (1.5.1) is said to be homogenous, otherwise the equation is called non-homogeneous. The major portion of the theory of periodic differential equations is addressed to the homogenous form since treatment of the non-homogeneous equation generally then follows by standard techniques.
Forced oscillations can be separated into mechanical and electrical resonances.

a) Initial Value Problems

Initial value conditions are such;

$$x(0) = 0 \text{, Displacement}$$

$$\frac{dx}{dt}(t=0) = 0 \text{, Velocity}$$

We have not external force to oscillations. In second order differential equations, we should add these two conditions to other conditions. We use initial conditions to obtain A and B.

b) General Solution

The general solution of the second order differential equations is in form that;

$$x(t) = x_c(t) + x_p(t); \tag{1.5.2}$$

$x_c(t)$: Complementary Solution

$x_p(t)$: Particular Solution

According to differential equation theory, general solution of complementary and particular parts of the second order equation can be found such:

$x_c(t) = c_1 \cos(\omega_0 t) + c_2 \sin(\omega_0 t)$, from Homogenous Equation

$x_p(t) = A\cos(\gamma t) + B\sin(\gamma t)$, from Non-Homogenous Equation

As can be seen above solutions, we have some unknown constants A, B, c_1 and c_2. We can find A and B by using initial conditions. So we have;

$$x_p(t) = \frac{F_0}{\omega_0^2 - \gamma^2}\sin(\gamma t),\ B = \frac{F_0}{\omega_0^2 - \gamma^2} \tag{1.5.3}$$

c) Total General Solution

The total general solution is in that form according to differential equation techniques;

$$x(t) = c_1 \cos\omega_0 t + c_2 \sin\omega_0 t + \frac{F_0}{\omega_0^2 - \gamma^2}\sin(\gamma t) \tag{1.5.4}$$

And again we should apply initial conditions to find c_1 and c_2. And consequently we reach below equation as total general solution;

$$x(t) = \frac{F_0}{\omega_0(\omega_0^2 - \gamma^2)}\{-\gamma\sin(\omega_0 t) + \omega_0 \sin(\gamma t)\}, \gamma \neq \omega_0 \tag{1.5.5}$$

d) In Resonance $(\gamma = \omega_0)$

If $\gamma = \omega_0$, system is in resonance. In resonance condition ($\gamma = \omega_0$); we obtain that;

$$x(t) = \frac{0}{0}\ \text{(Uncertainty)}$$

By applying L'Hopital's rule, $\frac{f'}{g'}$, we can find $x(t)$ while $\gamma = \omega_0$;

And solution will be such;

$$x(t) = \frac{F_0}{2\omega_0^2}\sin(\omega_0 t) - \frac{F_0}{2\omega_0} t\cos(\omega_0 t)\,,\ (\gamma = \omega_0) \tag{1.5.6}$$

When

Frequency of applied force = Eigen oscillation $\Rightarrow$ Resonance

In resonance case, amplitude increases.

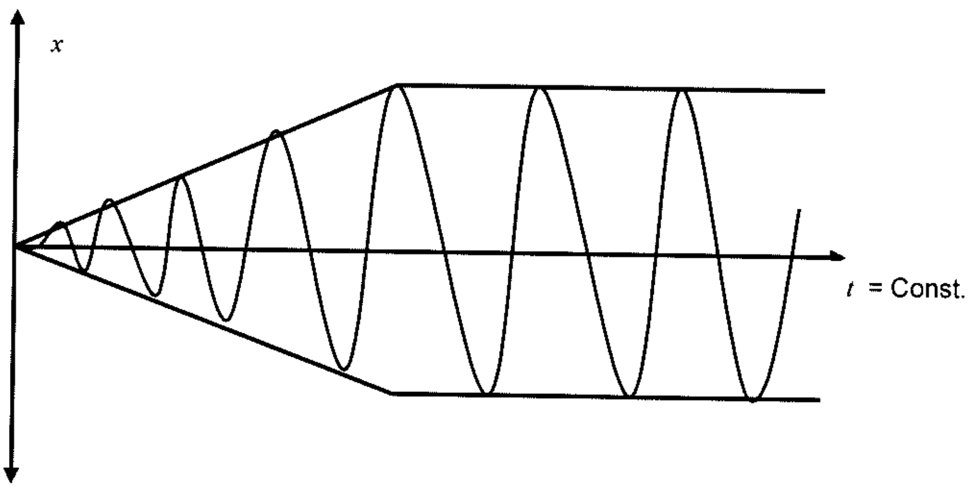

Normally any system at resonance frequency, cannot go beyond infinity.

1.5.2. Wave Propagation in a Periodic Medium

a)

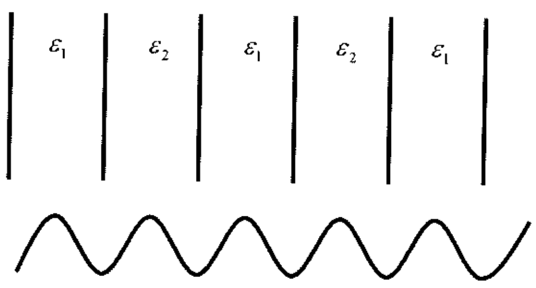

b) $n = n_0\left[1 + \mu\cos(2\chi x)\right]$, $\vartheta = \frac{c}{n}$ (*)

n : Refractive index

It is periodical dependence of refractive index

a) Wave Equation

In homogenous medium, the wave equation can be written as

$$\frac{d^2\vec{E}}{dx^2}+\omega^2\mu\varepsilon\vec{E}=0, \tag{1.5.7}$$

$$\frac{\partial^2 U}{\partial x^2}-\frac{1}{\vartheta^2}\frac{\partial^2 U}{\partial t^2}=0 \tag{1.5.8}$$

Equation (1.5.8) is the general solution for electrical or mechanical system.
We can start from this equation.

If we substitute $\frac{c}{n}$ instead of ϑ and equation (*) instead of n; we can obtain such equation:

$$\frac{\partial^2 U}{\partial x^2}-\frac{1}{c^2}\left[1+\mu\cos(2\chi x)\right]\frac{\partial^2 U}{\partial t^2}=0,\ U=A(x).e^{j\omega t} \tag{1.5.9}$$

$$\frac{d^2 A}{dx^2}+k^2\left[1+\mu\cos(2\chi x)\right]A=0,\ k^2=\frac{\omega^2}{c^2} \tag{1.5.10}$$

Any parameter in a system periodically changing x (dimension), we will have a similar equation.
Equation (1.5.10) has similar form with Mathieu equation.

In periodic differential equations, Hill and Mathieu equations take place in very large use. General form of Hill equation is,

$$\ddot{y}+(a-2q\psi(t))y=0,\ \psi(t)=\psi(t+\pi) \tag{1.5.11}$$

The function $\psi(t)$ has, by convention, a period of π and also obeys $|\psi(t)_{\max}|=1$; a is a constant parameter and $2q$ is a parameter which accounts for the magnitude of time variation.

The most widely known form of the Hill equation is the Mathieu equation in which $\psi(t)$ is sinusoidal;

$$\ddot{y}+(a-2q\cos 2t)y=0 \tag{1.5.12}$$

1.5.3. Perturbation Theory ($\mu \ll 1$)($\mu \approx 1/10$ or less)

We will use this theory to solve equation (1.5.10). Perturbation theory enables us to solve the differential equation.

In equation (1.5.10), we have A and $\omega(k)$ as unknowns.
If we expand A and ω as series, we have;

$$A(x)=\underbrace{A_0+\mu A_1}_{\text{First order solution}}+\mu^2 A_2+..........\approx A_0+\mu A_1,\ A=A_0(\mu=0) \tag{1.5.13}$$

$$\omega=\omega_0+\mu\omega_1+\mu^2\omega_2+.......... \tag{1.5.14}$$

$$k^2=(k_0+\mu k_1)^2=k_0^2+2\mu k_0 k_1+\mu^2\approx k_0^2+2\mu k_0 k_1 \tag{1.5.15}$$

For all parameters we take the part up to μ^2 because of most contributers of them.

If we substitute

$$A=A_0+\mu A_1,\ \omega=\omega_0+\mu\omega_1,\ k^2=(k_0+\mu k_1)^2=k_0^2+2\mu k_0 k_1+\mu^2\approx k_0^2+2\mu k_0 k_1;$$

in equation (1.5.10), we have;

1) μ^0 $(\mu = 0)$ term $$\frac{d^2 A_0}{dx^2} + k_0^2 A_0 = 0 \tag{1.5.16}$$

2) μ^1 term $$\frac{d^2 A_1}{dx^2} + k_0^2 A_1 = -k_0 A_0 (2k_1 + k_0 \cos(2\chi x)) \tag{1.5.17}$$

3) μ^2 term $$\frac{d^2 A_2}{dx^2} + k_0^2 A_2 = \dots\dots\dots \tag{1.5.18}$$

a) Solution of Zero Approximation

Solution of zero approximation can be written as;

$$A_0(x) = B_1 e^{jk_0 x} + B_2 e^{-jk_0 x}, \tag{1.5.19}$$

And we will substitute A_0 in second step.

b) Solution of First Approximation

Right side of equation that exists in second step is;

$$\begin{aligned} &= -k_0 B_1 \left[2k_1 e^{jk_0 x} + \frac{1}{2} k_0 e^{j(2\chi + k_0)x} + \frac{1}{2} k_0 e^{-j(2\chi - k_0)x} \right] \\ &\quad -k_0 B_2 \left[2k_1 e^{-jk_0 x} + \frac{1}{2} k_0 e^{-j(2\chi + k_0)x} + \frac{1}{2} k_0 e^{j(2\chi - k_0)x} \right] \end{aligned} \tag{1.5.20}$$

c) Analysis of Equation Obtained After the First Approximation

Case 1: $(k_0 \neq \chi)$ **Solution**

$$A_1(x) = c_1 e^{jk_0x} + c_2 e^{-jk_0x} + jk_1 x\left[B_1 e^{jk_0x} - B_2 e^{-jk_0x}\right]$$
$$+\frac{k_0^2}{8\chi(\chi+k_0)}\left[B_1 e^{j(2\chi+k_0)x} + B_2 e^{-j(2\chi+k_0)x}\right]$$
$$+\frac{k_0^2}{8\chi(\chi-k_0)}\left[B_1 e^{-j(2\chi-k_0)x} + B_2 e^{j(2\chi+k_0)x}\right] \quad (1.5.21)$$

In equation, first two parts are complementary solution from homogenous differential equation and the others are particular solution from non-homogenous differential equation that counterparts to external source.

We should take $k_1 = 0$ to verify the equation. Because oscillation that is related with t goes to infinity via x. Besides right side of the initial conditions is zero so this means in first approximation $k_1 = 0$.

If
$$k_1 = 0 \Rightarrow \omega_1 = 0,\ c = \frac{\omega}{k} \quad (1.5.22)$$

$$k^2 = k_0^2 + 2\mu k_1 \quad (1.5.23)$$

$$k^2 = k_0^2 \quad (1.5.24)$$

$$k = k_0,\ \omega = \omega_0 \quad (1.5.25)$$

Case 2: $(k_0 = \chi)$ Solution

Right side of equation is;

$$= -k_0\left[2k_1B_1 + \frac{k_0}{2}B_2\right]e^{jk_0x} - k_0\left[2k_1B_2 + \frac{k_0}{2}B_1\right]e^{-jk_0x} - \frac{k_0^2}{2}\left[B_1e^{3jk_0x} + B_2^{-3jk_0x}\right] \quad (1.5.26)$$

Only first two terms are important for us, because they arise in the resonance.

In these conditions, solution can be found;

$$x\left[2k_1B_1+\frac{k_0}{2}B_2\right]e^{jk_0x}+x\left[2k_1B_2+\frac{k_0}{2}B_1\right]e^{-jk_0x}+.......... \quad (1.5.27)$$

$$\left[2k_1B_1+\frac{k_0}{2}B_2\right]e^{jk_0x}=0 \quad (1.5.28)$$

$$\left[2k_1B_2+\frac{k_0}{2}B_1\right]e^{-jk_0x}=0 \quad (1.5.29)$$

Because of x parameter that exists in equations above, equations (1.5.28) and (1.5.29) should be zero. B_1 and B_2 are unknown quantities.

$$\begin{pmatrix} 2k_1 & \dfrac{k_0}{2} \\ \dfrac{k_0}{2} & 2k_1 \end{pmatrix}=0 \quad (1.5.30)$$

To solution of linear equation systems; the determinants of the coefficients of the unknown variables should be zero. Then;

$$4k_1^2-\frac{k_0^2}{4}=0,\ k_1^2=\frac{k_0^2}{16},\ k_1^{(1,2)}=\mp\frac{k_0}{4} \quad (1.5.31)$$

$$\omega^2=c^2k^2,\ \omega_1=ck_1,\ \omega^{\pm}=\omega_0\pm\mu\frac{ck_0}{4} \quad (1.5.32)$$

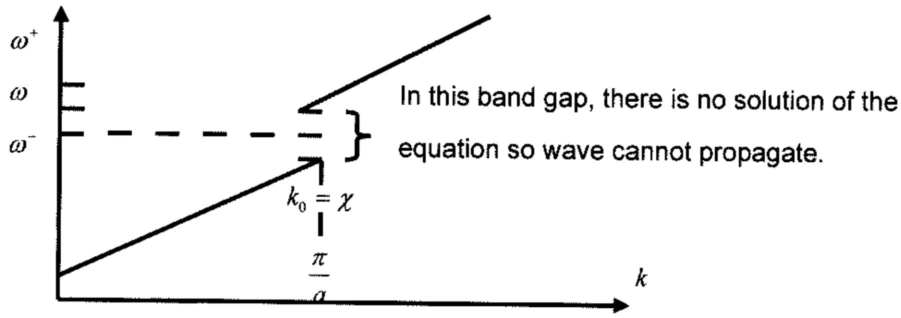

$$\Delta\omega = \omega^+ - \omega^- = \frac{\mu}{2}\omega_0 \tag{1.5.33}$$

$$2\chi = \frac{2\pi}{a},\; k_0 = \frac{2\pi}{\lambda_0} \;\Rightarrow\; \lambda_0 = 2a \rightarrow \text{Bragg Reflection} \tag{1.5.34}$$

$$\rightarrow \cos(2\chi x),\; 2\chi a = 2\pi \tag{1.5.35}$$

1.5.4. Solution of Second Approximation

Additional term is used in right side of equation in second approximation.

If we deal with $\mu^{(2)}$, we see that $k_0 = \dfrac{2\pi}{a}$.

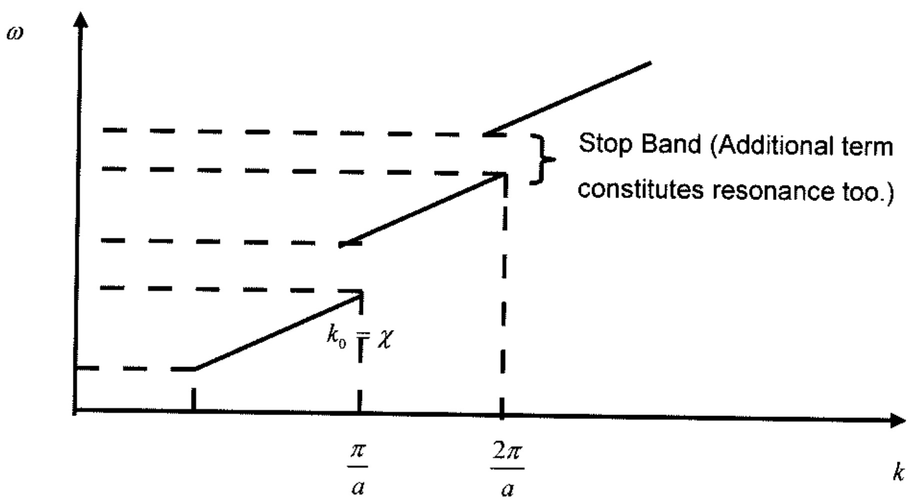

$$k_n = \frac{n\pi}{a},\ n = 1,2,3.........\tag{1.5.36}$$

In waveguide, if the frequency increases, the heat loss increases too. Because conductivity and $R_{conductivity}$ increases. By the way, if the frequency increases, loss of mode will be in effect and the power will decrease.

1.6. Analogy between Periodic Structures and Photonic Devices

Layered Structures

$f.\lambda = c$

$f, \omega = 2\pi f \quad \omega \rightarrow$

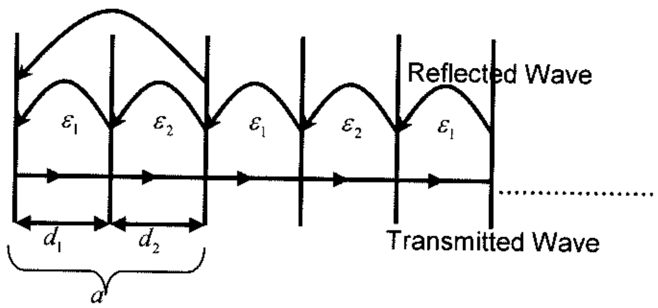

If the structure is long enough, all wave can be reflected. $\Re = \dfrac{n_2 - n_1}{n_2 + n_1}$

$$k = \frac{2\pi}{\lambda},\ \text{path} = 2a = \lambda\ \text{(Bragg reflection)}\tag{1.6.1}$$

$$\omega = 2\pi\frac{c}{\lambda} = kc,\ \ \omega = ck \rightarrow \text{Dispersion relation (curve)}\tag{1.6.2}$$

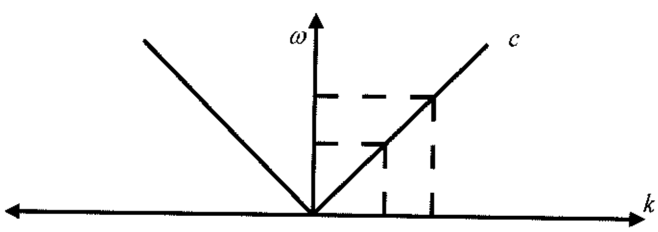

$$\beta = k_n = \frac{1}{c}\sqrt{\omega^2 - \left(\frac{n\pi}{d_{cr}}\right)^2} \rightarrow \text{For waveguide} \tag{1.6.3}$$

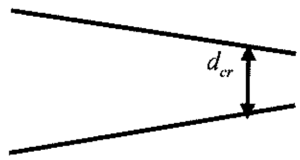

From equation (1.6.3), in waveguide at the certain critical value of thickness, d_{cr}, wave doesn't propagate.

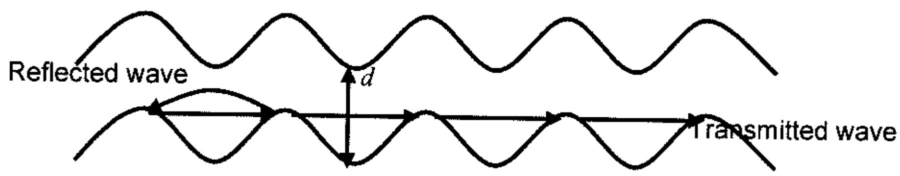

Difference of this structure is periodically changing in thickness. But in the first diagram ε is changing with periodically.

$$k_B(k_{Bragg}) = \frac{2\pi}{\lambda} = \frac{2\pi}{2a} = \frac{\pi}{a} \tag{1.6.4}$$

$k_B = \frac{\pi}{a} \Rightarrow$ Wave cannot propagate through the structure.

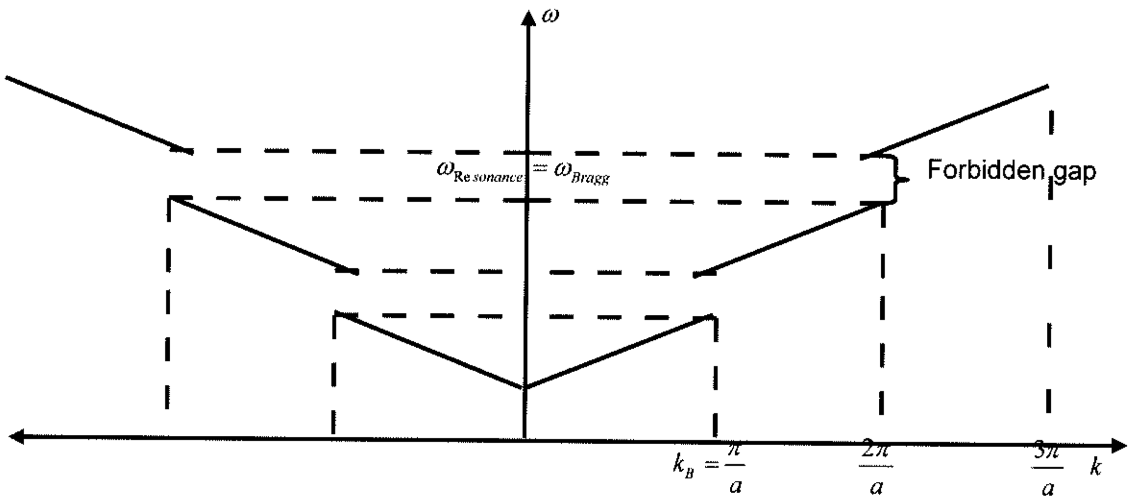

These gaps are proportional to $\frac{\Delta n}{n_{avr}}\omega_{\mathrm{Resonance}}$. ω_{Bragg} occurs at multiple of $\frac{\pi}{a}$ but we couldn't see these resonances at $\frac{2\pi}{a}$ and beyond in experiments because of attenuation.

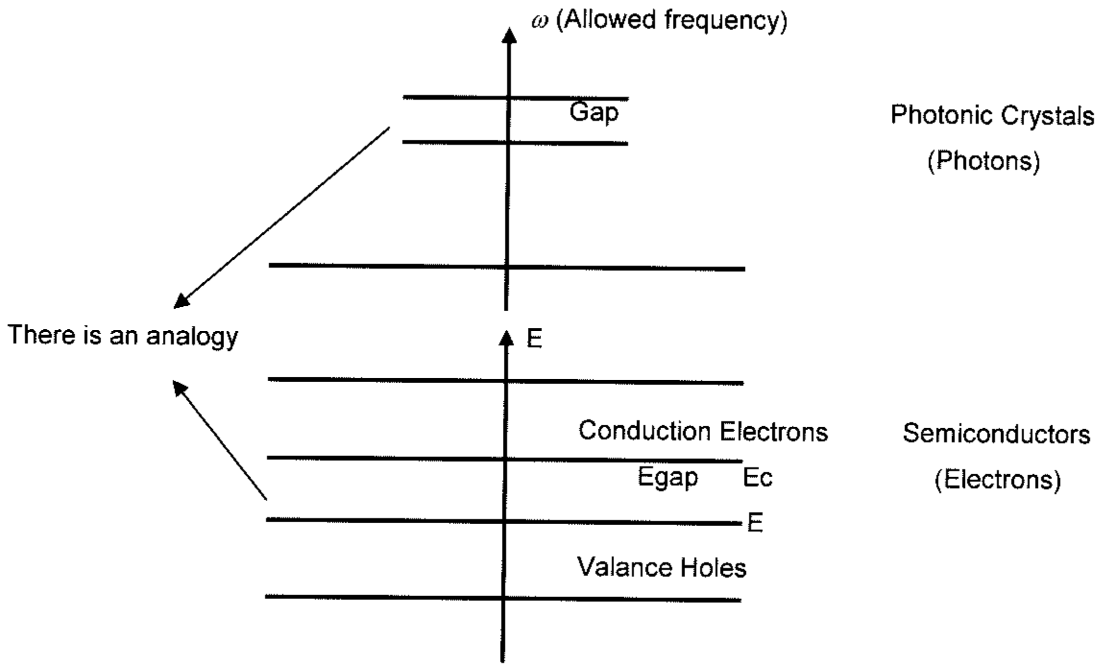

In the near time, photonic chips will be developed instead of the semiconductor chips and data will be carried by photons instead of electrons. Because the bandwidth is proportional to the operating frequency, optical devices have larger bandwidth. By using optical devices, we can transmit more data faster.

Because atoms of crystal have periodic deployment, in general crystal is used.

$$\lambda = \frac{h}{p} = \frac{h}{m\vartheta} \rightarrow \text{De Broglie wavelength} \qquad (1.6.5)$$

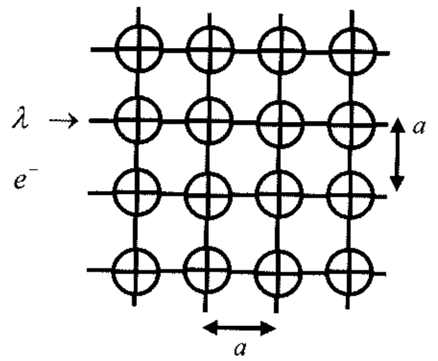

Semiconductor Crystal

(Lattice)

$$k = \frac{\pi}{a}$$

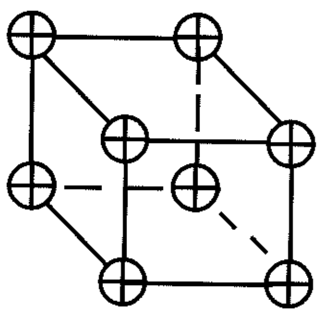

1.7. Some Applications of Periodic Structures

1.7.1. Fiber Grating Sensors

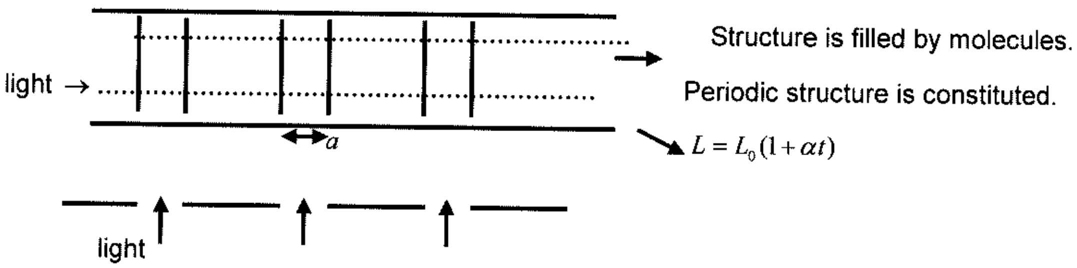

$$a = a_0(1+\alpha t)$$

ω_{Bragg} changes with t so we can measure the changing of temperature.

or pressure;

$$a = a_0(1+\alpha p)$$

1.7.2. Super Directive Antennas

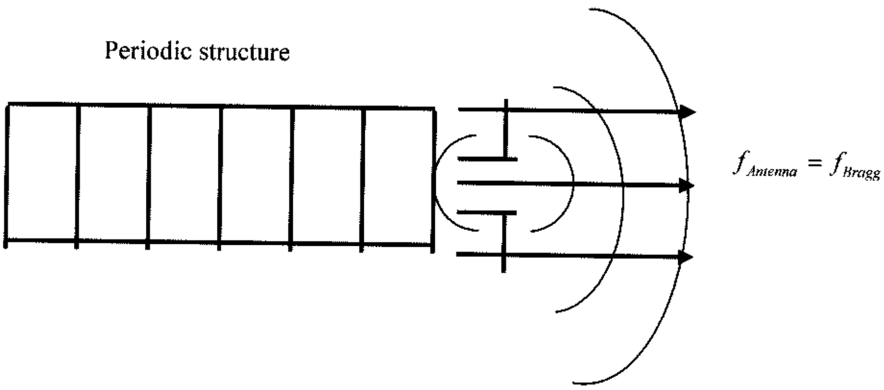

Antenna does the propagation in both directions.

When $f_{Antenna} = f_{Bragg}$, all propagation goes one direction because of reflection.

1.7.3. Distributed Bragg Reflector Laser

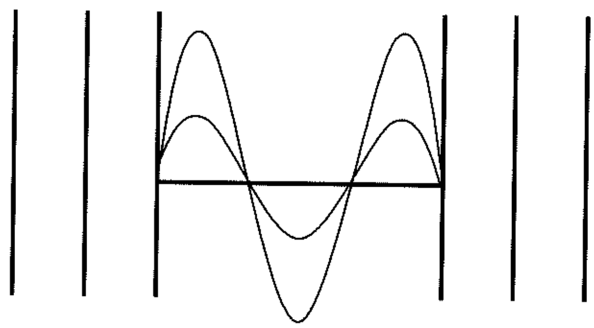

Fundamentals of laser are based on the resonance frequency.

We can obtain more level of energy by using periodic structures.

$$\Re = l\frac{d_2 - d_1}{d_2 + d_1}, \text{ Reflection coefficient}$$

2. THEORETICAL INVESTIGATIONS

2.1. Statements of the Problem for Periodically One Dimensional Corrugated Waveguides with Phase Shift between Parallel Plates

2.1.1. Initial Equations for Geometry with Phase Shift between Parallel Plates

In this theoretical part of study, electromagnetic wave propagation through a specially designed periodically one dimensional corrugated waveguide is investigated. In the theoretical section, we follow the paper by Pogrebnyak (2003, 2004). This guide is open waveguide with upper and lower boundaries as can be seen in figure 2.1. And its boundaries are conductor plates. Dielectric medium takes place in the space ($y_d(x) > y > y_{-d}(x)$) between these parallel plates. The geometry of the guide is shown detailed in Figure 2.1. Profiles of these plates are sinusoidal functions. The medium between the boundaries is assumed to be linear, homogeneous, isotropic and non-dispersive. Amplitudes of the upper and lower plate corrugation are ρ and ξ respectively, and their corresponding expressions for the profiles are $y_d(x) = d/2 + \rho\cos(qx+\theta)$ for upper plate and $y_{-d}(x) = -d/2 + \xi\cos(qx)$ for the lower one. In this geometry, $q = 2\pi/a$, and a is the period of the corrugations, d is average thickness between parallel plates and θ is the phase shift between the parallel plates. We assumed that the corrugations' amplitudes are small i.e. $\xi/d <<1$, $\rho/d <<1$ and $\xi q<<1$, $\rho q<<1$.

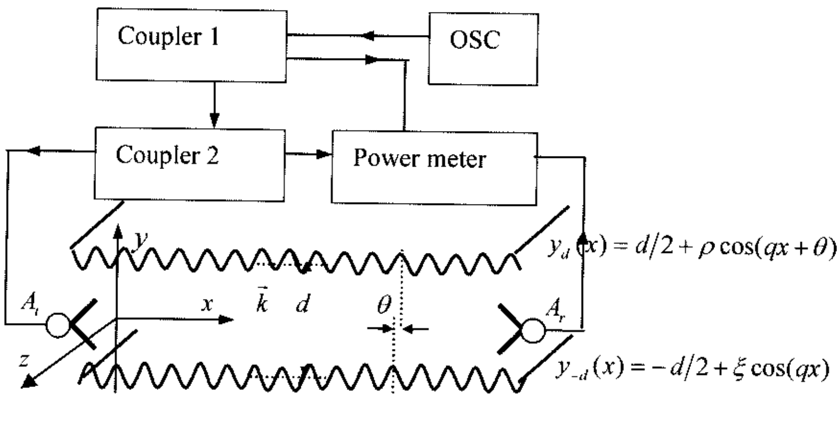

Figure 2.1. Geometry of a planar periodically one dimensional corrugated waveguide. The phase shift between two corrugated plates equals to θ.

In such structure, the electromagnetic wave propagation can be analyzed as follows. The TE wave that has the wave vector in the x- and z-components in the plane of the waveguide satisfies to two wave equations. The first wave equation, for the E_x component of the electric field, describes wave propagation along the z-axis (along the grooves). The periodicity along the x-axis doesn't affect strongly wave propagation in the z direction. In the first order approximation, we can ignore the changing of the parameters of wave propagation in z direction. In this case the eigen value problem reduces to solving of the wave equation.

In source free and losses media, Maxwell's equations can be written in differential form such;

$$\nabla \times \vec{E} = -\mu \frac{\partial \vec{H}}{\partial t} \tag{2.1.1}$$

$$\nabla \times \vec{H} = \varepsilon \frac{\partial \vec{E}}{\partial t} \tag{2.1.2}$$

$$\nabla . \vec{D} = 0 \tag{2.1.3}$$

$$\nabla . \vec{B} = 0 \tag{2.1.4}$$

The first two Maxwell's equations are uncoupled, and the wave equations are obtained as follows;

$$\nabla^2 \vec{E} = \mu\varepsilon \frac{\partial^2 \vec{E}}{\partial t^2} \tag{2.1.5}$$

$$\nabla^2 \vec{H} = \mu\varepsilon \frac{\partial^2 \vec{H}}{\partial t^2} \tag{2.1.6}$$

For time harmonic fields (time variations are of the form $e^{j\omega t}$), the wave equations can be written as;

$$\nabla^2 \vec{E} = -\omega^2 \mu\varepsilon \vec{E} = -k^2 \vec{E} \tag{2.1.7}$$

$$\nabla^2 \vec{H} = -\omega^2 \mu\varepsilon \vec{H} = -k^2 \vec{H} \tag{2.1.8}$$

In general, the wave equation can be written as;

$$\nabla^2 \varphi + k^2 \varphi = 0 \tag{2.1.9}$$

k can be written as in terms of ε, the electric permittivity of the medium, and c, velocity of light, as;

$$k^2 = \varepsilon \frac{\omega^2}{c^2} \tag{2.1.10}$$

and via explicit form of the Laplacian, the wave equation becomes in form;

$$\frac{\partial^2 \varphi}{\partial x^2} + \frac{\partial^2 \varphi}{\partial y^2} + \frac{\partial^2 \varphi}{\partial z^2} + \varepsilon \frac{\omega^2}{c^2} \varphi = 0 \tag{2.1.11}$$

and wave equation supports the boundary condition in such equation;

$$\varphi(x, y_{-d}(x), z) = \varphi(x, y_d(x), z) = 0 \tag{2.1.12}$$

Where $\varphi(x,y,z)$ stands for the z component of the electric field, E_z, of the TE wave, ω is the wave frequency, ε is the dielectric constant of the medium, c is the velocity of light. $\varphi(x,y,z)$ can be represented in Fourier Series (Floquet's Theorem) because of boundary periodicity.

$$\varphi(x,y,z)=\sum_n [a_n \cos(k_{yn}y)+b_n \sin(k_{yn}y)]e^{(j(k_x+nq)x+jk_z z)} \tag{2.1.13}$$

Where a_n and b_n are the Fourier series coefficients; k_{yn} is transverse component and k_x and k_z are the longitudinal components of the wave vector $\vec{k}$.

From the wave equation (2.1.11) and equation (2.1.13) we can reach the such relation;

$$\varepsilon\frac{\omega^2}{c^2}-(k_x+nq)^2-k_{yn}{}^2-k_z{}^2=0 \tag{2.1.14}$$

This relation is then used for finding of the dispersion relation, $\omega(\vec{k})$.

Via expressing equation (2.1.13) as a Mclaurin series at the boundaries, $y=-d/2$ and $y=d/2$, and then substituting of these equations into the boundary condition, we can reach a system of linear algebraic equations for the coefficients a_n and b_n. By solving the determinant of this system for zero, the allowed values of k_{yn} can be found, so the frequency spectrum of the waveguide can be found. For small corrugations, it is sufficient to take the first three space harmonics. It can be easily realized that a_n and b_n decrease when n increases. That's why we can restrict ourselves to the approximation of three main space harmonics with the wave numbers k_0 and $k_{\pm1}$.

Regarding the approximations mentioned above, the terms including ρ and ξ with powers of order higher than 2 may be eliminated.

For $\varphi(x,y)=\sum_n [a_n \cos(k_{yn}y)+b_n \sin(k_{yn}y)]e^{j(k_x+nq)x}$, (We are able to ignore k_z in this situation because our wave propagates in x direction and it is assumed that no variation exists along the z direction).

Expressing $\varphi(x,y)$ in Mclaurin series at $y=-d/2$ and $y=d/2$ gives;
For lower boundary,

$$\varphi(x,y)(y=-d/2)=\sum_n\Bigg[\left[a_n\cos(k_n\frac{d}{2})-b_n\sin(k_n\frac{d}{2})\right]e^{j(k_x+nq)x}$$
$$+\left[a_nk_n\sin(k_n\frac{d}{2})+b_nk_n\cos(k_n\frac{d}{2})\right]\xi\cos(qx)e^{j(k_x+nq)x}$$
$$+\left[-\frac{1}{2}a_nk_n^2\cos(k_n\frac{d}{2})+\frac{1}{2}b_nk_n^2\sin(k_n\frac{d}{2})\right]\xi^2\cos^2(qx)e^{j(k_x+nq)x}\Bigg] \quad (2.1.15)$$

And for upper boundary,

$$\varphi(x,y)(y=d/2)=\sum_n\Bigg[\left[a_n\cos(k_n\frac{d}{2})+b_n\sin(k_n\frac{d}{2})\right]e^{j(k_x+nq)x}$$
$$+\left[-a_nk_n\sin(k_n\frac{d}{2})+b_nk_n\cos(k_n\frac{d}{2})\right]\rho\cos(qx+\theta)e^{j(k_x+nq)x}$$
$$+\left[-\frac{1}{2}a_nk_n{}^2\cos(k_n\frac{d}{2})-\frac{1}{2}b_nk_n{}^2\sin(k_n\frac{d}{2})\right]\rho^2\cos^2(qx+\theta)]e^{j(k_x+nq)x}\Bigg] \quad (2.1.16)$$

At this stage we should restrict ourselves to main 3 harmonics of the wave and write 3 equations for equations (2.1.15) and (2.1.16), each harmonics corresponds to -1, 0, 1 values of n. This gives us the system of 6 algebraic equations which will lead us to analytic solution with a good approximation. Also, here two constraints should be taken into account. The first is, $\rho/d \ll 1$, $\xi/d \ll 1$ which states the comparable size of amplitudes of the corrugations of the two plates with respect to the plate separation. The second is, $\rho/a \ll 1$ and $\xi/a \ll 1$, which gives the comparable size of the amplitudes of the corrugations with respect to the wavelengths of the corrugations. The next step is putting these six equations into a matrix form and pursuing the nontrivial solution.

Consequently, the following characteristic equation is obtained (Pogrebnyak, 2004, 2003) for determination of allowed values of k_{y0} in the first Brillouin minizone;

$$\tan(k_0 d) = \frac{1}{4}(\xi^2 + \rho^2)\left[\frac{k_0 k_1}{\tan(dk_1)} + \frac{k_0 k_{-1}}{\tan(dk_{-1})}\right]$$
$$-\frac{1}{2}\xi\rho\frac{\cos\theta}{\cos(k_0 d)}\left[\frac{k_0 k_1}{\sin(k_1 d)} + \frac{k_0 k_{-1}}{\sin(k_{-1} d)}\right] \quad (2.1.17)$$

where $k_{\pm 1}$ are the wave numbers of the $n = \pm 1$ harmonics.
From equation (2.1.14), we can obtain

$$k_{\pm 1} = \sqrt{k_0^{\ 2} \mp 2k_x q - q^2} \quad (2.1.18)$$

In equations (2.1.17), (2.1.18) and below the subscript y is dropped in the wave number k_{yn}.

2.1.2. Spectrum of Cutoff Frequency for Geometry with Phase Shift between Parallel Plates

a) General Case

Method of successive approximation with respect to ξ and ρ is applied to solve the equation (2.1.17) i.e. $k_0 = k_0^{(0)} + \delta k + ...$, δk will be the incremental step in each iteration. We can start from the initial expression for smooth waveguide and we will reach the desired value for k_0 gradually. In smooth boundaries case, $\xi = 0$ and $\rho = 0$, we can see that $\tan(k_0^{(0)} d) = 0$ from equation (2.1.17), therefore;

$$k_0^{(0)} = \frac{p\pi}{d} \equiv k_{0p},\ \omega_{0p} = \frac{c}{\sqrt{\varepsilon}} \frac{p\pi}{d},\ p = 1,2,3,..... \tag{2.1.19}$$

There are well known modes and cutoff frequencies in a smooth planar waveguide. k_x which is the wave number for the wave propagation in x - direction is found by substituting equation (2.1.19) into (2.1.14). Then we have;

$$k_x = \sqrt{\varepsilon \frac{\omega^2}{c^2} - \frac{p^2 \pi^2}{d^2}} \tag{2.1.20}$$

$k_x = 0$ in the first Brilloin minizone for spectrum of cutoff frequency.
Then the wave numbers can be written as;

$$k_{+1} = k_{-1} = \sqrt{k_0^2 - q^2} \tag{2.1.21}$$

Substituting equation (2.1.21) and equation (2.1.19) into (2.1.17) yields;

$$\begin{aligned} \tan(k_0 d) = \frac{1}{4}(\xi^2 + \rho^2) \left[\frac{k_0 k_1}{\tan(dk_1)} + \frac{k_0 k_{-1}}{\tan(dk_{-1})} \right] \\ - \frac{1}{2} \xi\rho \frac{\cos\theta}{\cos(k_0 d)} \left[\frac{k_0 k_1}{\sin(k_1 d)} + \frac{k_0 k_{-1}}{\sin(k_{-1} d)} \right] \end{aligned} \tag{2.1.22}$$

$$= \frac{1}{4}(\xi^2 + \rho^2) \left[\frac{2k_0 k_1}{\tan(dk_1)} \right] - \frac{1}{2} \xi\rho \frac{\cos\theta}{\cos(k_0 d)} \left[\frac{2k_0 k_1}{\sin(k_1 d)} \right] \tag{2.1.23}$$

$$=\frac{1}{2}(\xi^2+\rho^2)\left[\frac{k_0k_1}{\tan(dk_1)}\right]-\xi\rho\frac{\cos\theta}{\cos(k_0d)}\left[\frac{k_0k_1}{\sin(k_1d)}\right] \tag{2.1.24}$$

$$\tan(k_0d)\cong d\delta k \tag{2.1.25}$$

$$\Rightarrow \delta k=\frac{\xi^2+\rho^2}{2d}.\frac{k_0k_1}{\tan(dk_1)}-\frac{\xi\rho}{d}.\frac{\cos\theta}{\cos(dk_0)}.\frac{k_0k_1}{\sin(dk_1)} \tag{2.1.26}$$

$$k_0=k_0^{(0)}+\delta k=\frac{p\pi}{d}+\frac{\xi^2+\rho^2}{2d}.\frac{k_0k_1}{\tan(dk_1)}-\frac{\xi\rho}{d}.\frac{\cos\theta}{\cos(dk_0)}.\frac{k_0k_1}{\sin(dk_1)} \tag{2.1.27}$$

$$\omega_p=\left[1+\frac{\xi^2+\rho^2}{2d}k_1\cot(dk_1)+(-1)^{p+1}\frac{\xi\rho}{d}.\frac{k_1\cos\theta}{\sin(dk_1)}\right].\omega_{0p} \tag{2.1.28}$$

And shift of the cutoff frequency can be found as;

$$\delta\omega_p=\left[\frac{\xi^2+\rho^2}{2d}k_1\cot(dk_1)+(-1)^{p+1}\frac{\xi\rho}{d}.\frac{k_1\cos\theta}{\sin(dk_1)}\right].\omega_{0p} \tag{2.1.29}$$

On the other hand, to investigate the special cases easily, equation (2.1.22) can be written as;

$$\tan(k_0d)=\frac{1}{4}(\xi^2+\rho^2)\left[\frac{2k_0k_{\pm1}}{\tan(dk_{\pm1})}\right]-\frac{1}{2}\xi\rho\frac{\cos\theta}{\cos(k_0d)}\left[\frac{2k_0k_{\pm1}}{\sin(k_{\pm1}d)}\right] \tag{2.1.30}$$

$$=\frac{1}{2}(\xi^2+\rho^2)\left[\frac{k_0k_{\pm1}}{\tan(dk_{\pm1})}\right]-\xi\rho\frac{\cos\theta}{\cos(k_0d)}\left[\frac{k_0k_{\pm1}}{\sin(k_{\pm1}d)}\right] \tag{2.1.31}$$

via using the equation (2.1.25) at this point, we can reach such equation;

$$\delta k = \frac{1}{2}\xi^2 \frac{p\pi}{d^3}\left[d\left(\frac{p^2\pi^2}{d^2} - q^2\right)^{1/2} \cot\left(d\left(\frac{p^2\pi^2}{d^2} - q^2\right)^{1/2}\right)\right]$$

$$+\frac{1}{2}\rho^2 \frac{p\pi}{d^3}\left[d\left(\frac{p^2\pi^2}{d^2} - q^2\right)^{1/2} \cot\left(d\left(\frac{p^2\pi^2}{d^2} - q^2\right)^{1/2}\right)\right]$$

$$-\xi\rho \frac{\cos(\theta)}{\cos(p\pi)} \frac{p\pi}{d^3}\left[d\left(\frac{(p^2\pi^2/d^2 - q^2)^{1/2}}{\sin(d(p^2\pi^2/d^2 - q^2)^{1/2})}\right)\right] \tag{2.1.32}$$

Let

$$d\left(\frac{p^2\pi^2}{d^2} - q^2\right)^{1/2} = x \tag{2.1.33}$$

Then

$$\delta k = \frac{1}{2}\xi^2 \frac{p\pi}{d^3}\left(\frac{x}{\tan x}\right) + \frac{1}{2}\rho^2 \frac{p\pi}{d^3}\left(\frac{x}{\tan x}\right) - \xi\rho \frac{p\pi}{d^3}\frac{\cos\theta}{\cos(p\pi)}\left(\frac{x}{\sin x}\right) \tag{2.1.34}$$

$$k_0 = k_0^{(0)} + \delta k = \frac{p\pi}{d} + \frac{1}{2}\xi^2 \frac{p\pi}{d^3}\left(\frac{x}{\tan x}\right) + \frac{1}{2}\rho^2 \frac{p\pi}{d^3}\left(\frac{x}{\tan x}\right)$$

$$-\xi\rho \frac{p\pi}{d^3}\frac{\cos\theta}{\cos(p\pi)}\left(\frac{x}{\sin x}\right) \tag{2.1.35}$$

$$\omega_p = \frac{c}{\sqrt{\varepsilon}}\left(\frac{p\pi}{d} + \frac{1}{2}\xi^2 \frac{p\pi}{d^3}\left(\frac{x}{\tan x}\right) + \frac{1}{2}\rho^2 \frac{p\pi}{d^3}\left(\frac{x}{\tan x}\right)\right.$$

$$\left. -\xi\rho \frac{\cos\theta}{\cos(p\pi)}\frac{p\pi}{d^3}\left(\frac{x}{\sin x}\right)\right) \tag{2.1.36}$$

$$\omega_p = \omega_{0p}\left(1 + \frac{\xi^2+\rho^2}{2d^2}\left(\frac{x}{\tan x}\right) - \frac{\xi\rho\cos\theta}{d^2\cos(p\pi)}\left(\frac{x}{\sin x}\right)\right) \tag{2.1.37}$$

$\Rightarrow \delta\omega_p = \Delta\omega = \omega_p - \omega_{op}$ (shift of the cutoff frequency) can be written as;

$$= \left(\frac{\xi^2 + \rho^2}{2d^2} \left(\frac{x}{\tan x} \right) - \frac{\xi \rho \cos\theta}{d^2 \cos(p\pi)} \left(\frac{x}{\sin x} \right) \right) . \omega_{0_p} \tag{2.1.38}$$

After the general case, now in the following sections several different cases are investigated. Because ω_c, the cutoff frequency, changes because of the relative changes of the physical parameters of the guide, namely the ratio between d and a or substituting some significant arguments instead of $k_{\pm 1}$ values in the characteristic equation. In each case we will determine, $\Delta\omega$, the shift amount in ω_c.

In equation (2.1.32), $p \neq 0$ is the constraint which should be satisfied for the below cases.

b) Special Cases

(i) Cutoff Frequency Shift for the Case $d >> a$

If $d >> a \Rightarrow$

$$d\sqrt{\left(\frac{p^2\pi^2}{d^2} - q^2 \right)} = d\sqrt{\left(\frac{p^2\pi^2}{d^2} - \frac{4\pi^2}{a^2} \right)} = idq \tag{2.1.39}$$

$$\delta k = \frac{1}{2}\xi^2 \frac{p\pi}{d^3}\left[\frac{idq}{\tan(idq)} \right] + \frac{1}{2}\rho^2 \frac{p\pi}{d^3}\left[\frac{idq}{\tan(idq)} \right] - \xi\rho \frac{p\pi}{d^3} \frac{\cos\theta}{\cos(p\pi)} \left[\frac{idq}{\sin(idq)} \right] \tag{2.1.40}$$

Thanks to use of hyperbolic functions' features for δk, we can reach such equation;

$$\delta k = \frac{1}{2}\xi^2 \frac{p\pi}{d^3}\left[\frac{idq}{i\tanh(dq)} \right] + \frac{1}{2}\rho^2 \frac{p\pi}{d^3}\left[\frac{idq}{i\tanh(dq)} \right]$$
$$-\xi\rho \frac{p\pi}{d^3} \frac{\cos\theta}{\cos(p\pi)} \left[\frac{idq}{i\sinh(dq)} \right] \tag{2.1.41}$$

$$\delta k=\frac{1}{2}\xi^2\frac{p\pi}{d^3}\left[\frac{d\,2\pi/a}{\tanh(d\,2\pi/a)}\right]+\frac{1}{2}\rho^2\frac{p\pi}{d^3}\left[\frac{d\,2\pi/a}{\tanh(d\,2\pi/a)}\right]-\xi\rho\frac{p\pi}{d^3}\frac{\cos\theta}{\cos(p\pi)}\left[\frac{d\,2\pi/a}{\sinh(d\,2\pi/a)}\right]$$

$$\delta k=\frac{1}{2}\xi^2\frac{p\pi}{d^3}\frac{2\pi d}{a}+\frac{1}{2}\rho^2\frac{p\pi}{d^3}\frac{2\pi d}{a} \qquad (2.1.42)$$

$$\delta k=\frac{\xi^2 p\pi^2}{d^2 a}+\frac{\rho^2 p\pi^2}{d^2 a} \qquad (2.1.43)$$

then

$$k_0=\frac{p\pi}{d}+\frac{\xi^2 p\pi^2}{d^2 a}+\frac{\rho^2 p\pi^2}{d^2 a} \qquad (2.1.44)$$

and the new cutoff frequency is;

$$\omega_c=\frac{c}{\sqrt{\varepsilon}}\left[\frac{p\pi}{d}+\frac{\xi^2 p\pi^2}{d^2 a}+\frac{\rho^2 p\pi^2}{d^2 a}\right] \qquad (2.1.45)$$

$$\omega_c=\omega_{0p}\left[1+\frac{\xi^2\pi}{da}+\frac{\rho^2\pi}{da}\right] \qquad (2.1.46)$$

Thus the amount of shift, $\Delta\omega$, can be found as;

$$\Delta\omega=\omega_c-\omega_{0p}=\omega_{0p}\left[\frac{\xi^2\pi}{da}+\frac{\rho^2\pi}{da}\right] \qquad (2.1.47)$$

(ii) Cutoff Frequency Shift for the Case $k_{\pm 1}=0$

In equation $k_{\pm 1}=\sqrt{k_0^{\,2}\mp 2k_x q-q^2}$, $k_x=0$ in cutoff frequency investigation.

If $$k_{\pm 1} = \sqrt{k_0^{\ 2} - q^2} = 0 \qquad (2.1.48)$$

Then it is easily seen that;

$$d\left(\frac{p^2\pi^2}{d^2} - q^2\right)^{1/2} = x = 0 \qquad (2.1.49)$$

When $k_{\pm 1} = 0$ value is substituted into equation (2.1.34), equation takes the form;

$$\delta k = \frac{1}{2}\xi^2 \frac{p\pi}{d^3}\left[\frac{0}{0}\right] + \frac{1}{2}\rho^2 \frac{p\pi}{d^3}\left[\frac{0}{0}\right] - \xi\rho \frac{p\pi}{d^3}\frac{\cos\theta}{\cos(p\pi)}\left[\frac{0}{0}\right] \qquad (2.1.50)$$

In this situation we have $\frac{0}{0}$ indefiniteness. So we must apply L'Hopital's rule.

After applying L'Hopital's rule upon term x, equation (2.1.34) takes form;

$$\delta k = \frac{1}{2}\xi^2 \frac{p\pi}{d^3}\left[\frac{1}{\sec^2 x}\right] + \frac{1}{2}\rho^2 \frac{p\pi}{d^3}\left[\frac{1}{\sec^2 x}\right] - \xi\rho \frac{p\pi}{d^3}\frac{\cos\theta}{\cos(p\pi)}\left[\frac{1}{\cos x}\right] \qquad (2.1.51)$$

If $x = 0 \Rightarrow$ $$\delta k = \frac{1}{2}\xi^2 \frac{p\pi}{d^3} + \frac{1}{2}\rho^2 \frac{p\pi}{d^3} - \xi\rho \frac{p\pi}{d^3}\frac{\cos\theta}{\cos(p\pi)} \qquad (2.1.52)$$

And corresponding cutoff frequency is;

$$\omega_c = \frac{c}{\sqrt{\varepsilon}}\left[\frac{p\pi}{d} + \frac{1}{2}\xi^2 \frac{p\pi}{d^3} + \frac{1}{2}\rho^2 \frac{p\pi}{d^3} - \xi\rho \frac{p\pi}{d^3}\frac{\cos\theta}{\cos(p\pi)}\right] \qquad (2.1.53)$$

$$\omega_c = \omega_{op}\left[1+\frac{1}{2}\frac{\xi^2}{d^2}+\frac{1}{2}\frac{\rho^2}{d^2}-\frac{\xi\rho}{d^2}\frac{\cos\theta}{\cos(p\pi)}\right] \tag{2.1.54}$$

And the amount of shift of the cutoff frequency is;

$$\Delta\omega = \omega_{op}\left[\frac{1}{2}\frac{\xi^2}{d^2}+\frac{1}{2}\frac{\rho^2}{d^2}-\frac{\xi\rho}{d^2}\frac{\cos\theta}{\cos(p\pi)}\right] \tag{2.1.55}$$

(iii) Cutoff Frequency Shift for the Case $k_{\pm 1} = (2n+1)\pi/2d$ **,** $n = 0,1,2,.....$

If $k_{\pm 1} = (2n+1)\pi/2d$, $n = 0,1,2,..... \Rightarrow$

$$d\left(\frac{p^2\pi^2}{d^2}-q^2\right)^{1/2} = x = d\frac{(2n+1)\pi}{2d} = \frac{(2n+1)\pi}{2}$$

It is easily realized that if this value of $k_{\pm 1}$ is substituted into equation (2.1.34), it makes the first two terms of the equation equal zero, so the remaining term is;

$$\delta k = -\xi\rho\frac{p\pi}{d^3}\frac{\cos\theta}{\cos(p\pi)}\left(\frac{(2n+1)\frac{\pi}{2}}{\cos(\pi n)}\right) \tag{2.1.56}$$

$$\delta k = \xi\rho\frac{p\pi}{d^3}(-1)^{p+1}\cos\theta\left(\frac{(2n+1)\frac{\pi}{2}}{(-1)^n}\right) \tag{2.1.57}$$

$$k_0 = \frac{p\pi}{d}+\xi\rho\frac{p\pi}{d^3}(-1)^{p+1}\cos\theta\left(\frac{(2n+1)\frac{\pi}{2}}{(-1)^n}\right) \tag{2.1.58}$$

And new cutoff frequency is;

$$\omega_c = \frac{c}{\sqrt{\varepsilon}}\left[\frac{p\pi}{d} + \xi\rho\frac{p\pi}{d^3}\cos\theta(-1)^{p+1}\left(\frac{(2n+1)\frac{\pi}{2}}{(-1)^n}\right)\right] \tag{2.1.59}$$

$$\omega_c = \omega_{0p}\left[1 + \frac{\xi\rho}{d^2}\cos\theta(-1)^{p-n+1}(2n+1)\frac{\pi}{2}\right] \tag{2.1.60}$$

And the shift of the cutoff frequency is;

$$\Delta\omega = \omega_{op}\left[\frac{\xi\rho}{d^2}\cos\theta(-1)^{p-n+1}(2n+1)\frac{\pi}{2}\right] \tag{2.1.61}$$

(iv) Cutoff Frequency Shift for the Case $k_{\pm 1} = l\pi/d$

This case is particular resonance case. This resonance case is occurred because of the relation among the integers d, a, p and l. Firstly the relation between these integers should be investigated and the interval of each of these parameters where solutions will be sought for the characteristic equation should be defined from equation (2.1.32) before the computation of $\Delta\omega$, the shift of cutoff frequency from the zero approximation, as;

$$\frac{l\pi}{d} = \sqrt{\frac{p^2\pi^2}{d^2} - q^2} \tag{2.1.62}$$

$$l = \sqrt{p^2 - \frac{q^2 d^2}{\pi^2}} \tag{2.1.63}$$

$$l = \sqrt{p^2 - \frac{4d^2}{a^2}} \tag{2.1.64}$$

$$l^2 = p^2 - \frac{4d^2}{a^2} \tag{2.1.65}$$

$$l^2 + \left[\frac{2d}{a}\right]^2 = p^2 \tag{2.1.66}$$

When the above equation is analyzed, it is realized that it is possible to obtain values when some of the variables are predetermined or possible to restrict the definite intervals for some depending on the values of the predetermined ones. For example, choosing $p = l$ makes it impossible for such geometry to appear, on the other hand taking d/a ratio great, makes it impossible for the two modes l and p to appear closely. Consequently, in order to carry out a rational analysis of the characteristic equation of (2.1.34), one build up a reasonable relation among to four integers d, a, p, l which should match the conditions of (2.1.66).

After starting the required conditions for a correct analysis above, now we can solve equation (2.1.31) in order to evaluate the shift in the cutoff frequency when $k_{\pm 1} = l\pi/d$.

For the next iteration we substitute $k_0 = (k_0^{(0)} + \delta k)$ instead of k_0 into equation (2.1.31), after this substitution equation (2.1.31) becomes;

$$\tan d(k_0^{(0)} + \delta k) = \frac{1}{2}(\xi^2 + \rho^2)(k_0^{(0)} + \delta k)\left[\frac{l\pi/d}{\tan d(k_0^{(0)^2} + 2k_0^{(0)}\delta k + \delta k^2 - q^2)^{1/2}}\right]$$

$$-\xi\rho\frac{\cos\theta}{\cos d(k_0^{(0)} + \delta k)}(k_0^{(0)} + \delta k)\left[\frac{l\pi/d}{\sin d((k_0^{(0)^2} + 2k_0^{(0)}\delta k + \delta k^2 - q^2)^{1/2})}\right] \tag{2.1.67}$$

$$d\delta k = \frac{1}{2}(\xi^2+\rho^2)k_0^{(0)}\frac{l\pi/d}{\tan d\left(\frac{l^2\pi^2}{d^2}+\frac{2p\pi}{d}\delta k\right)^{1/2}} - \xi\rho\frac{\cos\theta}{\cos d(k_0^{(0)}+\delta k)}k_0^{(0)}\frac{l\pi/d}{\sin d\left(\frac{l^2\pi^2}{d^2}+\frac{2p\pi}{d}\delta k\right)^{1/2}}$$

If the denominators are expanded with Binomial series, the expression becomes;

$$d\delta k = \frac{1}{2}(\xi^2+\rho^2)\frac{p\pi}{d}\frac{l\pi/d}{\tan l\pi\left(1+\frac{pd}{l^2\pi}\delta k\right)}$$

$$-\xi\rho\frac{\cos\theta}{\cos d(k_0^{(0)})}\frac{p\pi}{d}\frac{l\pi/d}{\sin l\pi\left(1+\frac{pd}{l^2\pi}\delta k\right)} \qquad (2.1.68)$$

$$d\delta k = \frac{1}{2}(\xi^2+\rho^2)\frac{p\pi}{d}\frac{l\pi}{d}\frac{l}{pd\delta k} + \xi\rho\cos\theta\frac{p\pi}{d}\frac{l\pi}{d}\frac{l}{pd\delta k}(-1)^{p-l+1} \qquad (2.1.69)$$

$$\delta k_0^{\ 2} = \frac{(\xi^2+\rho^2)l^2\pi^2}{2d^4} + \frac{\xi\rho\cos(\theta)l^2\pi^2(-1)^{p-l+1}}{d^4} \qquad (2.1.70)$$

$$\delta k_0^{\ 2} = \frac{l^2\pi^2}{2d^4}\left[(\xi^2+\rho^2)+2\xi\rho\cos(\theta)(-1)^{p-l+1}\right] \qquad (2.1.71)$$

$$\delta k_0 = \pm\frac{l\pi}{\sqrt{2}d^2}\left[(\xi^2+\rho^2)+2\xi\rho\cos(\theta)(-1)^{p-l+1}\right]^{1/2} \qquad (2.1.72)$$

$$k_0 = \frac{p\pi}{d} \pm \frac{l\pi}{\sqrt{2}d^2}\left[(\xi^2+\rho^2)+2\xi\rho\cos(\theta)(-1)^{p-l+1}\right]^{1/2} \qquad (2.1.73)$$

then our new cutoff frequency ω_c is;

$$\omega_c = \frac{c}{\sqrt{\varepsilon}}\left[\frac{p\pi}{d} \pm \frac{l\pi}{\sqrt{2}d^2}\left[(\xi^2+\rho^2)+2\xi\rho\cos(\theta)(-1)^{p-l+1}\right]^{1/2}\right] \qquad (2.1.74)$$

It is obvious from above equations that the case of spectrum splitting phenomenon is observed with phase shift phenomenon between parallel plates. The upper and lower bounds are symmetric with respect to ω_{0p}, the initial (zero approximation) cutoff frequency. The upper and lower cutoff frequencies are denoted as ω_c^+ and ω_c^- respectively. The region between these two bounds is called "the stop band". As a result it is possible to block and forbid this region for wave propagation by establishing the required relation among the physical parameters of the guide.

$$\omega_c^{\pm} = \omega_{0p}\left[1 \pm \frac{l}{p}\frac{1}{\sqrt{2}d}\left[(\xi^2+\rho^2)+2\xi\rho\cos(\theta)(-1)^{p-l+1}\right]^{1/2}\right] \qquad (2.1.75)$$

$$\omega_c^{+} = \omega_{0p}\left[1 + \frac{l}{p}\frac{1}{\sqrt{2}d}\left[(\xi^2+\rho^2)+2\xi\rho\cos(\theta)(-1)^{p-l+1}\right]^{1/2}\right] \qquad (2.1.76)$$

$$\omega_c^{-} = \omega_{0p}\left[1 - \frac{l}{p}\frac{1}{\sqrt{2}d}\left[(\xi^2+\rho^2)+2\xi\rho\cos(\theta)(-1)^{p-l+1}\right]^{1/2}\right] \qquad (2.1.77)$$

And appearing stop band can be written as;

$$\delta\omega = \omega_c^{+} - \omega_c^{-}$$

$$\delta\omega = 2\omega_{0p}\left[\frac{l}{p}\frac{1}{\sqrt{2}d}\left[(\xi^2+\rho^2)+2\xi\rho\cos(\theta)(-1)^{p-l+1}\right]^{1/2}\right] \qquad (2.1.78)$$

Equation (2.1.28) describes the location of a cutoff frequency with the phase shift phenomenon between parallel plates in the spectrum as a function of the geometric parameters ξ, ρ, d and a in frequency range far from resonances. Formulas

(2.1.17) and (2.1.28) are counterparts of equation (2.1.19) for the smooth waveguide. Equations (2.1.28), (2.1.29) and equation (2.1.17) indicate the non-trivial dependence of ω_p on the $k_{\pm 1}$ wave numbers and on geometric dimensions of the waveguide. Primarily it displays the resonance behavior of the system, but of not less importance is the dependence on the phase shift of the one periodic boundary with respect to another. As will be seen below, both dependencies cause new fundamental properties of wave properties of wave propagation in the waveguide.

2.1.3. Behavior of Non-Bragg Resonances (Stop Bands) for Geometry with Phase Shift between Parallel Plates

In this section the electromagnetic standing-wave phenomenon in a guide bounded by two periodically corrugated conductors with phase shift phenomenon between parallel plates is investigated. At this point, it should be explained the difference between this event and the one, which was analyzed in previous section. Although in the formulation they are seen to be similar, physically they represent two different events. First of all, in this case k_x is not equal to zero, in fact here the resonance of the wave movement in the direction that is perpendicular to the wave propagation takes place, in other words interaction of partial standing wave resonance between $n=0$ and the neighboring $n=\pm 1$ space harmonics is observed.

It is seen from equations (2.1.17), (2.1.28) and (2.1.29) that resonance (stop band) in the system occurs if;

$$k_{\pm 1} = \sqrt{k_0^{\ 2} \mp 2k_x q - q^2} = \frac{m\pi}{d} \equiv k_{1m},\ m = 1,2,3,..... \tag{2.1.79}$$

An index m designates the order number of the resonance in the system and it can be considered as the "mode" index of the $n = \pm 1$ space harmonics but in the resonance case only. From equation (2.1.79), it is seen that $m \leq p$ for the first minizone.

The Bragg resonance, $k_{x,B}^{\pm} = \pm q/2$, is a particular case of equation (2.1.79) at $m = p$. Number of resonances equal order number of the mode. For example, there are two resonances in the spectrum of the second mode ($p = 2$).

Equation (2.1.79) along with equation (2.1.19) is condition of the non-Bragg resonance between the transverse modes, and it can be written in the form;

$$k_{\pm 1} = \frac{m\pi}{d}, \; k_0^{(0)} = \frac{p\pi}{d} \qquad (2.1.80)$$

The physical meaning of the resonance (stop band) condition becomes clear if the last equations are rewritten in terms of a wavelength ($\lambda = \frac{2\pi}{k}$) of standing-wave associated with the transverse modes ($k_0^{(0)}$ and $k_{\pm 1}$) of the fundamental ($n = 0$) and the $n = \pm 1$ space harmonics.

$$k_{\pm 1} = \frac{m\pi}{d} = \frac{2\pi}{\lambda} \Rightarrow d = \frac{m\lambda}{2} \qquad (2.1.81)$$

$$k_0^{(0)} = \frac{p\pi}{d} = \frac{2\pi}{\lambda} \Rightarrow d = \frac{p\lambda}{2} \qquad (2.1.82)$$

$$d = \frac{p\lambda_0}{2} = \frac{m\lambda_1}{2} \qquad (2.1.83)$$

Equation (2.1.83) shows that the resonance occurs if the thickness of the waveguide, d, is simultaneously a multiple of half wavelengths of the standing-waves associated with the fundamental ($n = 0$) and the $n = \pm 1$ space harmonics but with different integers p and m. It is illustrated with Figure 2.2 where TE_{01} and TE_{02} field distributions for resonance cases are shown. In Figure 2.2, wave movement in the direction that is perpendicular to the wave propagation is shown as E_z.

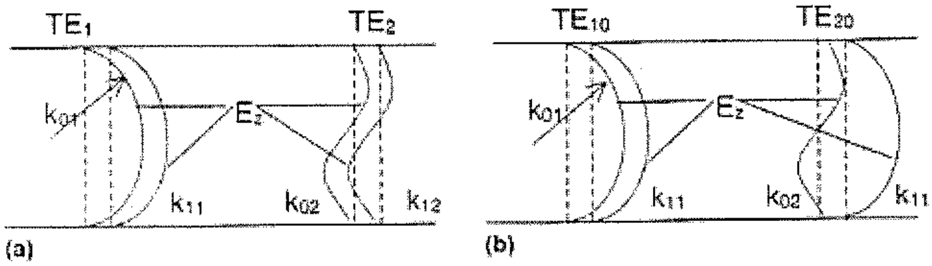

Figure 2.2. Electric field distributions for the fundamental, k_{0p}, and the first, k_{1m}, space harmonics of the TE_{10} and TE_{20} waves. (a) In a case of the Bragg resonance, distributions for both harmonics are always similar; (b) TE_{20} has different field distributions for the harmonics – this is the non-Bragg resonance. (Pogrebnyak, 2003, 2004)

It is suitable to underline here that in contrast to common consideration of interference of longitudinal traveling waves that gives rise to the Bragg reflection, equations (2.1.80), (2.1.83) are the conditions of the constructive or destructive interference of the transverse modes (standing-waves). That is why this resonance is of the non-Bragg nature.

The resonant value $k^{\pm}_{x,p,m}$ of the wave number k_x, at which the resonance condition (2.1.79)-(2.1.83) holds, can be found from equations (2.1.14) and (2.1.79);

$$\frac{m^2\pi^2}{d^2} = \frac{p^2\pi^2}{d^2} \mp 2k_x^{\pm}q - q^2 \tag{2.1.84}$$

$$k_x^{\pm} = \frac{(p^2 - m^2)\pi^2}{2qd^2} - \frac{q}{2} \tag{2.1.85}$$

$$k^{\pm}_{x,p,m} = \pm\frac{1}{2q}(k_{0p}^2 - q^2 - k_{1m}^2) \tag{2.1.86}$$

The upper sign "+" is taken for the resonant $n = +1$ harmonic and the "-" lower for the $n = -1$ harmonic. In equation (2.1.86), it is enough to consider the range $k_x > 0$ since it is obvious that;

$$k_{+1}(-|k_x|) = k_{-1}(|k_x|)$$

2.1.4. Spectrum of Subminizones for Geometry with Phase Shift between Parallel Plates

We can obtain the resonant frequency with substituting of $k_{x,p,m}^{\pm}$ into equation (2.1.14);

$$\varepsilon\frac{\omega^2}{c^2} - (k_x + nq)^2 - k_{yn} - k_z = 0 \tag{2.1.14}$$

As we know $k_z = 0$. So equation (2.1.14) becomes;

$$\varepsilon\frac{\omega^2}{c^2} - (k_x + nq)^2 - k_{yn} = 0$$

If we substitute $n = 0$ in above equation;

$$\omega^2 = \frac{c^2}{\varepsilon}({k_{x,p,m}}^2 + k_{0p}^2)$$

$$\omega_{pm} = \frac{c}{\sqrt{\varepsilon}}\left[k_{0p}^2 + \left(\frac{k_{0p}^2 - q^2 - k_{1m}^2}{2q}\right)^2\right]^{1/2} \tag{2.1.87}$$

In vicinity of resonance, the more accurate solution of equation (2.1.17) shows that this resonant frequency splits into two values as ω_{pm}^{+} and ω_{pm}^{-}. And these two values are separated by the forbidden gap $\delta\omega_{pm}$. To reach more accurate solution of resonant frequencies and stop band, below procedures are done;

$$k_{\pm 1} = \frac{m\pi}{d}, \; m = 1,2,3,..... \tag{2.1.88}$$

$$k_0 = k_0^{(0)} + \delta k = \frac{p\pi}{d} + \delta k \tag{2.1.89}$$

From equations (2.1.14) and (2.1.79)

$$k_{\pm 1} = \sqrt{\frac{p^2\pi^2}{d^2} \pm 2k_x q - q^2} \tag{2.1.90}$$

and

$$k_{x,p,m}^{\pm} = \pm\frac{q}{2}(1 + X_{p,m}) \text{ where } X_{p,m} = \frac{(m^2 - p^2)\pi^2}{(dq)^2} \tag{2.1.91}$$

Starting with the characteristic equation (2.1.17), substitution of equations (2.1.88) and (2.1.89) into equation (2.1.17) yields;

$$\tan d(k_0^{(0)} + \delta k) = \frac{1}{2}(\xi^2 + \rho^2)(k_0^{(0)} + \delta k)\left[\frac{m\pi/d}{\tan d[(k_0^{(0)^2} + 2k_0^{(0)}\delta k + \delta k^2) \pm 2k_x q - q^2]^{1/2}}\right]$$

$$-\xi\rho\frac{\cos\theta}{\cos d(k_0^{(0)} + \delta k)}(k_0^{(0)} + \delta k)\left[\frac{m\pi/d}{\sin d[(k_0^{(0)^2} + 2k_0^{(0)}\delta k + \delta k^2) \pm 2k_x q - q^2]^{1/2})}\right] \tag{2.1.92}$$

$$\tan d(k_0^{(0)}+\delta k)=\frac{1}{2}(\xi^2+\rho^2)k_0^{(0)}\frac{m\pi/d}{\tan d\left(\frac{m^2\pi^2}{d^2}+\frac{2p\pi}{d}\delta k\right)^{1/2}}$$

$$-\xi\rho\frac{\cos\theta}{\cos d(k_0^{(0)})}k_0^{(0)}\frac{m\pi/d}{\sin d\left(\frac{m^2\pi^2}{d^2}+\frac{2p\pi}{d}\delta k\right)^{1/2}} \tag{2.1.93}$$

If the denominators are expanded with Binomial series, the expression becomes;

$$d\delta k=\frac{1}{2}(\xi^2+\rho^2)\frac{p\pi}{d}\frac{m\pi/d}{\tan m\pi\left(1+\frac{pd\delta k}{m^2\pi}\right)}$$

$$-\xi\rho\frac{\cos\theta}{\cos d(k_0^{(0)})}\frac{p\pi}{d}\frac{m\pi/d}{\sin m\pi\left(1+\frac{pd\delta k}{m^2\pi}\right)} \tag{2.1.94}$$

$$d\delta k=\frac{1}{2}(\xi^2+\rho^2)\frac{p\pi}{d}\frac{m\pi}{d}\frac{m}{pd\delta k}+\xi\rho\cos\theta\frac{p\pi}{d}\frac{m\pi}{d}\frac{m}{pd\delta k}.(-1)^{p-m+1} \tag{2.1.95}$$

$$d\delta k=\frac{1}{2}\frac{m^2\pi^2}{d^3\delta k}\left[\xi^2+\rho^2+2\xi\rho\cos\theta\left(-1\right)^{p-m+1}\right] \tag{2.1.96}$$

$$\delta k^2=\frac{1}{2}\frac{m^2\pi^2}{d^4}\left[\xi^2+\rho^2+2\xi\rho\cos\theta\left(-1\right)^{p-m+1}\right] \tag{2.1.97}$$

$$\delta k=\pm\frac{1}{\sqrt{2}}\frac{m\pi}{d^2}\left[\xi^2+\rho^2+2\xi\rho\cos\theta\left(-1\right)^{p-m+1}\right]^{1/2} \tag{2.1.98}$$

Substituting the k_x value of (2.1.89) and (2.1.91) into (2.1.14) yields;

$$\varepsilon\frac{\omega^{\pm}_{p,m}{}^{2}}{c^{2}}=\frac{q^{2}}{4}\left(1+X_{p,m}\right)^{2}+\left(\frac{p\pi}{d}\pm\delta k\right)^{2} \tag{2.1.99}$$

$$\varepsilon\frac{\omega^{\pm}_{p,m}{}^{2}}{c^{2}}=\frac{q^{2}}{4}\left(1+X_{p,m}\right)^{2}+\left(\frac{p\pi}{d}\right)^{2}\pm\left(\frac{2p\pi\delta k}{d}\right) \tag{2.1.100}$$

Multiplying (2.1.100) by c^{2}/ε yields;

$$\omega^{\pm}_{p,m}{}^{2}=\frac{c^{2}q^{2}}{\varepsilon 4}\left(1+X_{p,m}\right)^{2}+\omega_{0p}^{2}\pm\frac{c^{2}}{\varepsilon}\frac{2p\pi}{d}\delta k \tag{2.1.101}$$

$$\omega^{\pm}_{p,m}{}^{2}=\frac{c^{2}q^{2}}{\varepsilon 4}\left(1+X_{p,m}\right)^{2}+\omega_{0p}^{2}$$
$$\pm\frac{c^{2}}{\varepsilon}\frac{2p\pi}{d}\frac{m\pi}{\sqrt{2}d^{2}}[\xi^{2}+\rho^{2}+2\xi\rho\cos\theta(-1)^{p-m+1}]^{1/2} \tag{2.1.102}$$

From equation (2.1.14) and equation (2.1.91) it is possible to express $\omega^{\pm}_{p,m}$ as;

$$\omega_{p,m}=\left[\omega_{0p}^{2}+\omega_{B}^{2}(1+X_{p,m})^{2}\right]^{1/2} \tag{2.1.103}$$

where $\omega_{B}=cq/(2\sqrt{\varepsilon})$ is the Bragg frequency.

By arranging equation (2.1.102), $\omega^{\pm}_{p,m}$ can be written as;

$$\omega^{\pm}_{p,m}{}^{2}=\omega_{p,m}^{2}\pm\frac{c^{2}}{\varepsilon}\frac{2p\pi}{d}\delta k \tag{2.1.104}$$

$$\omega^{\pm}_{p,m}=\sqrt{\omega_{p,m}^{2}\pm\frac{c^{2}}{\varepsilon}\frac{2p\pi}{d}\delta k} \tag{2.1.105}$$

From binomial expansion, equation (2.1.105) becomes,

$$\omega_{p,m}^{\pm} = \omega_{p,m} \pm \frac{c^2}{\varepsilon}\frac{p\pi}{d}\frac{\delta k}{\omega_{p,m}} \tag{2.1.106}$$

Then

$$\omega_{p,m}^{\pm} = \omega_{p,m} \pm \frac{c^2}{\varepsilon}\frac{p\pi}{d}\frac{1}{\omega_{p,m}}\left[\frac{1}{\sqrt{2}}\frac{m\pi}{d^2}\left[\xi^2 + \rho^2 + 2\xi\rho\cos\theta(-1)^{p-m+1}\right]^{1/2}\right] \tag{2.1.107}$$

$$\omega_{p,m}^{\pm} = \omega_{p,m} \pm \frac{1}{\omega_{p,m}}\frac{c^2}{\varepsilon}\frac{p\pi}{d}\frac{m\pi}{d}\frac{1}{d\sqrt{2}}\left[\xi^2 + \rho^2 + 2\xi\rho\cos\theta(-1)^{p-m+1}\right]^{1/2} \tag{2.1.108}$$

$$\omega_{p,m}^{\pm} = \omega_{p,m}\left[1 \pm \frac{\omega_{0p}\omega_{1m}}{\omega_{p,m}^2 d\sqrt{2}}\left[\xi^2 + \rho^2 + 2\xi\rho\cos\theta(-1)^{p-m+1}\right]^{1/2}\right] \tag{2.1.109}$$

And the stop band appears as;

$$\delta\omega = \omega_{p,m}^{+} - \omega_{p,m}^{-} = \frac{\omega_{0p}\omega_{1m}\sqrt{2}}{\omega_{p,m}d}[\xi^2 + \rho^2 + 2\xi\rho\cos\theta(-1)^{p-m+1}]^{1/2} \tag{2.1.110}$$

where
$$\omega_{0p} = \frac{ck_{0p}}{\sqrt{\varepsilon}},\ \omega_{1m} = \frac{ck_{1m}}{\sqrt{\varepsilon}} \tag{2.1.111}$$

Thus, the resonances divide the first minizone of the pth mode into subminizones. The index m shows the order number of the subminizone. A number of subminizones can be found from relation (2.1.79). Since the last gap (Bragg) takes place at $m = p$, it means that a number of subminizones equals the order number of the mode p. The number of subminizones is the same as a number of gaps, including the Bragg gap. For example, there are two subminizones in the spectrum of the second mode (p =2). The dispersion curve for this case is shown in figure 2.3.

The range, $\Delta k_{x,m}$, between two successive resonances in the k-space can be found from equation (2.1.86).

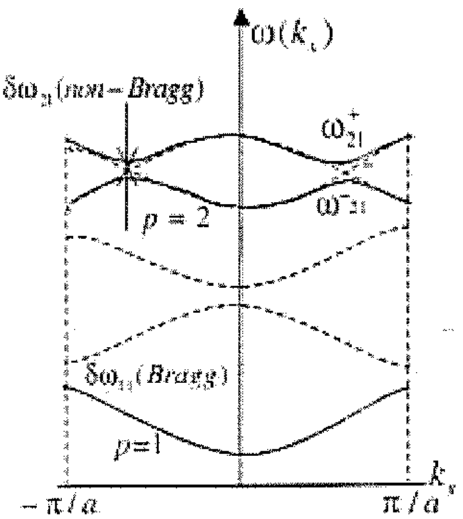

Figure 2.3. Dispersion curve $\omega(k_x)$ for the TE_{10} and TE_{20} modes in the first Brillouin zone. Non-Bragg gap $\delta\omega_{21}$ opens in the spectrum of the second mode. Corresponding field distribution is shown in Fig. 2.2b. (Pogrebnyak, 2003, 2004)

$$\Delta k_{x,m} = k^{+}_{x,p,m+1} - k^{+}_{x,p,m} = \frac{2m+1}{2q}\frac{\pi^2}{d^2} \tag{2.1.112}$$

It does not depend on the mode index p.

From equation (2.1.87) it is seen that the resonant frequency approaches to the cutoff frequency in parenthesis $(k_{0p}^2 - q^2 - k_{1m}^2)$ vanishes. Equality of this expressions to zero imposes relationship between a thickness and a period of the waveguide and mode indices p and m. It means that given cutoff frequency will be resonant under the specific geometric relationship. That is why the resonance can be named as the geometric resonance.

2.1.5. Effect of the Phase Shift between Parallel Plates on Wave Reflection

In this section of theoretical investigations, it is shown that dependency of bandwidth of the stop band on the phase shift between parallel plates. The analysis of equations (2.1.109), (2.1.110) is given here in such two cases:

(1) Case for $\theta = 0$,

(2) Case for $\theta = \pi$

1) Case for $\theta = 0$:

In this case, if $\xi = \rho$, the distance between two boundaries is constant and equals to d throughout the x-coordinate. If $\xi \neq \rho$, the deviation equals to $d \pm |\xi - \rho|$.

(a) If both p and m are even or both are odd numbers, the equations (2.1.109), and (2.1.110) for the resonant frequency and the stop band becomes;

$$\omega_{pm}^{\pm} = \omega_{pm}\left[1 \pm \frac{\omega_{0p}\omega_{1m}}{\sqrt{2}\omega_{pm}^{2}}\frac{|\xi - \rho|}{d}\right] \tag{2.1.113}$$

$$\delta\omega_{pm} = \frac{\sqrt{2}|\xi - \rho|}{d}\frac{\omega_{0p}\omega_{1m}}{\omega_{pm}} \tag{2.1.114}$$

(b) If p is even but m is odd or vice versa;

$$\omega_{pm}^{\pm} = \omega_{pm}\left[1 \pm \frac{\omega_{0p}\omega_{1m}}{\sqrt{2}\omega_{pm}^{2}}\frac{|\xi + \rho|}{d}\right] \tag{2.1.115}$$

$$\delta\omega_{pm} = \frac{\sqrt{2}\,|\xi+\rho|}{d}\frac{\omega_{0p}\omega_{1m}}{\omega_{pm}} \qquad (2.1.116)$$

2) Case for $\theta = \pi$:

In this case, distance between parallel plates varies with the x-coordinate between values $d+\xi+\rho$ and $d-\xi-\rho$.

(a) If both p and m are even or both are odd numbers, the equations for the resonant frequency and pass band, $\delta\omega_{pm}$ are given by equations (2.1.115) and (2.1.116).

(b) If p is even but m is odd or vice versa the result is the same as equations (2.1.113) and (2.1.114).

From equations (2.1.115) and (2.1.116) it can be seen easily that the pass band, $\delta\omega_{pm}$, is proportional to the perturbation $|\xi+\rho|/d$, caused by periodic corrugations. But equations (2.1.113) and (2.1.114) show that this common rule is not always valid. In the case of the $\theta = 0$, described by equations (2.1.113) and (2.1.114), all Bragg gaps ($m = p$), for every mode, vanish if $\xi = \rho$. Only the non-Bragg gaps, which have the order number m of different evenness than the mode index p, remain in the spectrum of every mode and they result into reflections. The width of these pass bands is defined by equation (2.1.110). Thus, in the waveguide having the congruent periodic boundaries, a wave propagates without Bragg reflection.

In the case $\theta = \pi$, the Bragg gaps as well as the subminizone gaps have the maximum value given by equation (2.1.110). The non-Bragg gaps, defined by the condition (2b), do not open.

Since the gaps in the spectrum correspond to the stop bands, the transmission coefficient of the waveguide into the x-direction drops to zero when a frequency of a wave coincides with the onset of the stop band.

2.1.6. Conclusion for Periodically One Dimensional Corrugated Waveguide with Phase Shift between Parallel Plates

In this thesis, it is shown that in the planar periodically corrugated waveguide, resonance interaction between transverse modes (standing-waves) occurs in a wide frequency range. Because of the interaction non-Bragg nature resonances (stop bands) occur. And these non-Bragg resonances (stop bands) divide the spectrum of the mode into the subminizones and give rise to non-Bragg reflections. The Bragg reflection corresponds to the last non-Bragg resonance (stop band) ($p = m$) in the subminizone spectrum of the mode as the stop band at the boundary of the first Brillouin zone. Number of stop bands (the same as the subminizones), including the Bragg gap, equals to the order number of the mode. For example, there are two subminizones in the spectrum of the second mode ($p = 2$). The width of stop bands depends on the phase shift, θ, between parallel periodic boundaries and mode's evenness. It varies from zero to a maximum value while one plate shifting half period of corrugation with respect to another. In a case of the congruent boundaries, the Bragg stop bands don't open, and electromagnetic wave propagates in the periodic waveguide without Bragg reflections. When the frequency of the electromagnetic wave coincides with one of the gaps, only unidirectional propagation along grooves is allowed in the waveguide. The electronic counterpart of this phenomenon arises in a periodic quantum well when the Fermi energy of a two-dimensional electron gas coincides with one of the gaps. Such a unidirectional electronic state would be similar to the stripe phase in high temperature superconductors. Electromagnetic and electronic phenomena in periodic structures are described by similar equations and they have the same wave nature.

Thus when the plates are shifted the half period of corrugation, the two-dimensional guiding structure becomes the unidirectional guide and this situation creates the photonic waveguide. Via this method, controlling and adjusting of the width of the stop band and direction of the wave propagation can be applied into different applications in optoelectronics and microwave technology.

The physical nature of the non-Bragg resonance is simple enough: the resonance occurs when a thickness of the waveguide is simultaneously a multiple of the half wavelengths of the transverse modes of the fundamental ($n = 0$) and the $n = \pm 1$ space harmonics i.e. $d = p\lambda/2 = m\lambda_1/2$. This obvious condition shows that this resonance corresponds to the constructive or destructive interference between two standing waves like it takes place in a wedge-shaped film. Since the transverse wave number $k_{y\pm 1}$ changes with k_x due to equation (2.1.79), the resonance happens at different k_x and these resonances are numerated by the index m.

2.2. Statement of the Problem for Periodically Two Dimensional Corrugated Waveguides

2.2.1. Initial Equations

In this part, wave phenomenon in planar periodically two dimensional corrugated waveguide is investigated. Because of two dimensions, there is no phase shift in our geometry. This special geometry is shown detailed in Figure 2.4.

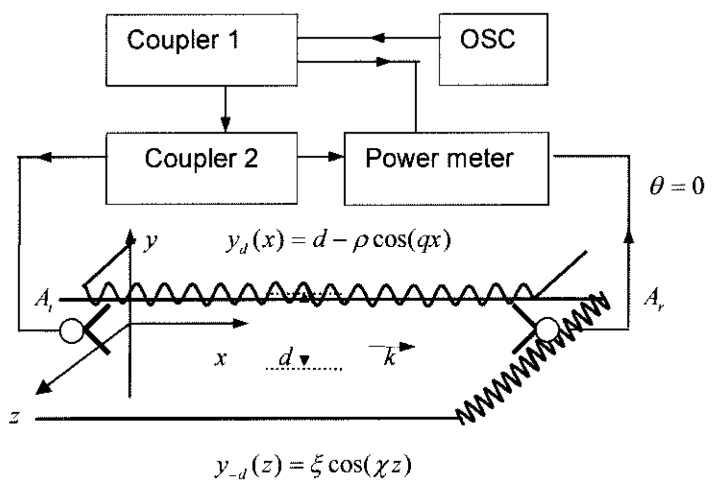

Figure 2.4. Geometry of a planar periodically two dimensional corrugated waveguide. The phase shift phenomenon isn't observed in such geometry.

In this geometry, the special waveguide has two conductor plates as its upper and lower boundaries and dielectric medium occupies the space ($y_d(x) > y > y_{-d}(z)$) between these parallel plates. As it is seen from Figure 2.4, parallel plates have sinusoidal function as their profiles. Medium between the periodic boundaries is assumed to be linear, homogenous, isotropic and non-dispersive. Amplitudes of upper and lower plate corrugations are ρ and ξ respectively and expressions of upper and lower boundaries are $y_d(x) = d - \rho\cos(qx)$ and $y_{-d}(z) = \xi\cos(\chi z)$ respectively. In this geometry, $q = 2\pi/a$, a is the period of the upper corrugation, $\chi = 2\pi/b$, b is the period of the lower corrugation, d is average thickness between parallel plates. We assumed that the corrugations have a small amplitude i.e. $\xi/d << 1$, $\rho/d << 1$ and $\xi q << 1$, $\rho q << 1$.

The wave propagation in such a structure can be analyzed as follows. The TE wave, having the x- and z- components of the wave vector in the plane of the waveguide, satisfies two wave equations. The first wave equation, for the E_x component of the electric field, describes wave propagation along the z direction. And the second wave equation, for the E_z component of the electric field, describes wave propagation along the x direction. In this case the eigen value problem reduces to solving of the two wave equations together.

For source free and lossless media, Maxwell's equations in differential form are;

$$\nabla \times \vec{E} = -\mu \nabla \times \vec{H} \tag{2.2.1}$$

$$\nabla \times \vec{H} = \varepsilon \nabla \times \vec{E} \tag{2.2.2}$$

$$\nabla . \vec{D} = 0 \tag{2.2.3}$$

$$\nabla . \vec{B} = 0 \tag{2.2.4}$$

First two of Maxwell's equations are uncoupled, the well-known wave equations are obtained as follows:

$$\nabla^2 \vec{E} = \varepsilon\mu \frac{\partial^2 \vec{E}}{\partial t^2} \tag{2.2.5}$$

$$\nabla^2 \vec{H} = \varepsilon\mu \frac{\partial^2 \vec{H}}{\partial t^2} \tag{2.2.6}$$

For time harmonic fields (time variations of the form $e^{j\omega t}$), the wave equations are:

$$\nabla^2 \vec{E} = -\omega^2 \varepsilon\mu \vec{E} = -k^2 \vec{E} \tag{2.2.7}$$

$$\nabla^2 \vec{H} = -\omega^2 \varepsilon\mu \vec{H} = -k^2 \vec{H} \tag{2.2.8}$$

In this thesis a general solution will be presented for a field component of φ, which may represent both E, electric field vector, or H, magnetic field vector.. So in general wave equation can be arranged as:

$$\nabla^2 \varphi + k^2 \varphi = 0 \tag{2.2.9}$$

where k can be written in term of ε, the dielectric permittivity of the medium, and c velocity of light as:

$$k^2 = \varepsilon \frac{\omega^2}{c^2} \tag{2.2.10}$$

and if we write the explicit form of the Laplacian, the wave equation takes the form:

$$\frac{\partial^2 \varphi}{\partial x^2} + \frac{\partial^2 \varphi}{\partial y^2} + \frac{\partial^2 \varphi}{\partial z^2} + \varepsilon \frac{\omega^2}{c^2} \varphi = 0 \tag{2.2.11}$$

And second necessary equation for the solution, boundary conditions can be written as:

$$\varphi(x, y_{-d}(z), z) = \varphi(x, y_d(x), z) = 0 \qquad (2.2.12)$$

Due to the boundary periodicity, $\varphi(x, y, z)$ can be represented in the form of a Fourier series (Floquet's theorem) as;

$$\varphi(x, y, z) = \sum_{nm} \left[a_{nm} \cos(k_{y_{nm}} y) + b_{nm} \sin(k_{y_{nm}} y) \right] e^{j(k_x + nq) + j(k_z + m\chi)z} \qquad (2.2.13)$$

where k_x, k_y, and k_z are the wave vectors in the directions of x, y and z respectively.

Substitution of equation (2.2.13) into equation (2.2.11) give us a very useful equation, which includes the relation between ω and k.

$$\varepsilon \frac{\omega^2}{c^2} - (k_x + nq)^2 - k_{y_{nm}}^2 - (k_z + m\chi)^2 = 0 \qquad (2.2.14)$$

Expressing equation (2.2.13) as a Mclaurin Series at $y = 0$ and $y = d$, the two equations of $\varphi(x, y, z)$ at the two boundaries can be written as follows:

$$\varphi(x, y, z)(y = 0) = \sum_{nm} \Big[a_{nm} e^{j(k_x + nq)x + j(k_z + m\chi)z} + b_{nm} k_{nm} e^{j(k_x + nq)x + j(k_z + m\chi)z} .(\xi \cos \chi z)$$
$$- \frac{1}{2!} a_{nm} k_{nm}^2 e^{j(k_x + nq)x + j(k_z + m\chi)z} .(\xi^2 \cos^2 \chi z) \Big] \qquad (2.2.15)$$

$$\varphi(x, y, z)(y = d) = \sum_{nm} \big[[a_{nm} \cos(k_{nm} d) + b_{nm} \sin(k_{nm} d)]$$
$$+ [-a_{nm} k_{nm} \sin(k_{nm} d) + b_{nm} k_{nm} \cos(k_{nm} d)] .(d - \rho \cos qx - d)$$

$$+\frac{1}{2!}\left[-a_{nm}k_{nm}^{2}\cos(k_{nm}d)-b_{nm}k_{nm}^{2}\sin(k_{nm}d)\right].(d-\rho\cos qx-d)^{2}\Bigg]\,e^{j(k_x+nq)x+j(k_z+m\chi)z}$$

(2.2.16)

Mathematical calculations for expressing equation (2.2.13) to Mclaurin Series at $y=0$ and $y=d$ can be seen in Appendix III.

Via expressing equation (2.2.13) as a Mclaurin series at the boundaries, $y=0$ and $y=d$, and then substituting of these equations into the boundary condition, we can reach a system of linear algebraic equations for the coefficients a_n and b_n. By solving the determinant of this system for zero, the allowed values of k_{yn} can be found, so the frequency spectrum of the waveguide can be found. For small corrugations, it is sufficient to take the first three space harmonics. It can be easily realized that a_n and b_n decrease when n increases. That's why we can restrict ourselves to the approximation of three main space harmonics with the wave numbers $k_{-1-1}, k_{-10}, k_{-11}, k_{0-1}, k_{00}, k_{01}, k_{1-1}, k_{10}$ and k_{11}.
Regarding the approximations mentioned above, the terms including ρ and ξ with powers of order higher than 2 may be eliminated.

In appendix III, IV and V, it can be seen easily the procedures to reach determinant of dispersion equation.

3. EXPERIMENTAL INVESTIGATIONS

3.1. Setup Configuration for Measurements

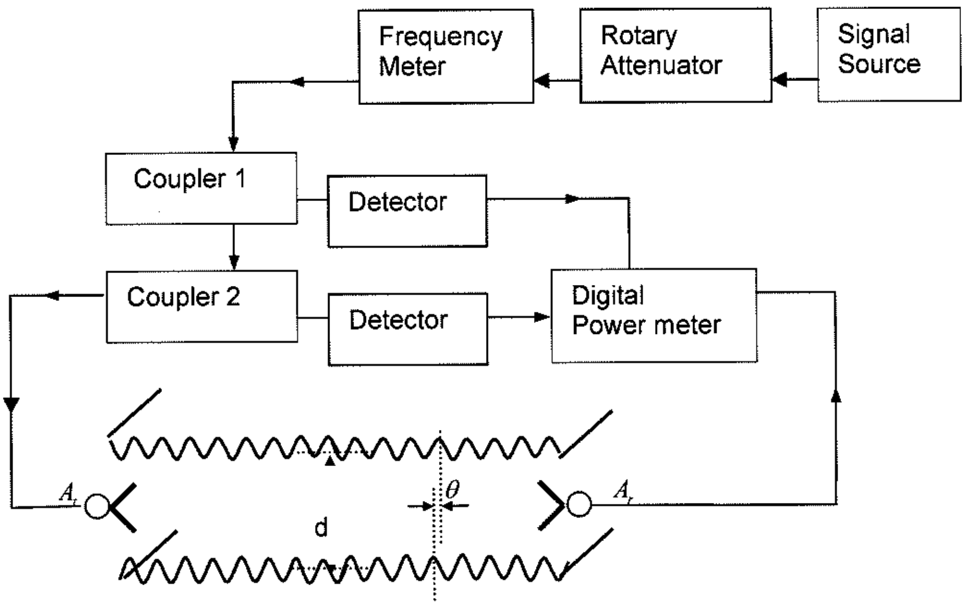

Features of Devices that was Used in Experimental Investigations

Signal Source: FMI Model: 449X / 8.2GHz-12.5GHz

Rotary Attenuator: FMI Model: 16110

Frequency Meter: FMI Model: 16072

Directional Couplers: (Coupling Value:10dB) FMI Model: 16131-10

Adapter: AGILENT Model: X281A, FMI Model:16180

Power Sensors: AGILENT Model: 8481A

Waveguide Turning: FMI Model: 16450-90RH

Horn Antennas: FMI Model: 16240-15

Digital Power Meter: AGILENT Model: E4419B

Abbreviators:

In experimental part of the thesis, features of geometry for each experimental measurement are explained under the plots.

In these explanations, we used some abbreviators which are listed below;

List of Abbreviators

d : Average distance between paralel plates
La-a : Distance between antennas
PS : Phase shift
Fcr : Critical frequency
FBragg : Bragg frequency
TP : Transmission Point
f : Frequency
$P_{incident}$: Incident power
$P_{received}$: Received power
$P_{reflected}$: Reflected power

3.2. Experimental Investigations

3.2.1. Full Corrugated Waveguide Experiments and Their Evaluations

(i) Dependency of Transmitted Power on Frequency

a) Phase Shift (θ) = π

1)

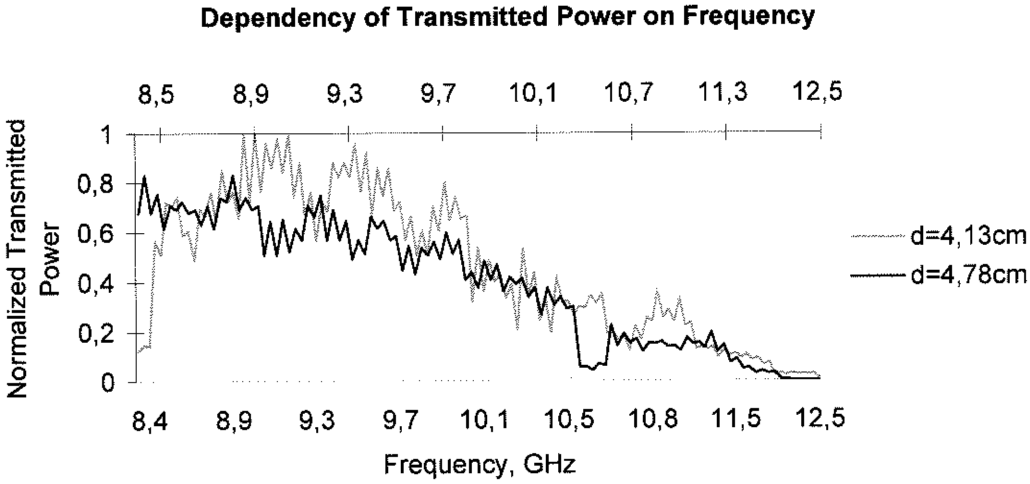

Geometry 1: d = 4,13cm, La-a = 85cm, Attenuator = 0, (Without Antennas; open waveguide).
Geometry 2: d = 4,78cm, La-a = 85cm, Attenuator = 0, (Without Antennas; open waveguide).

2)

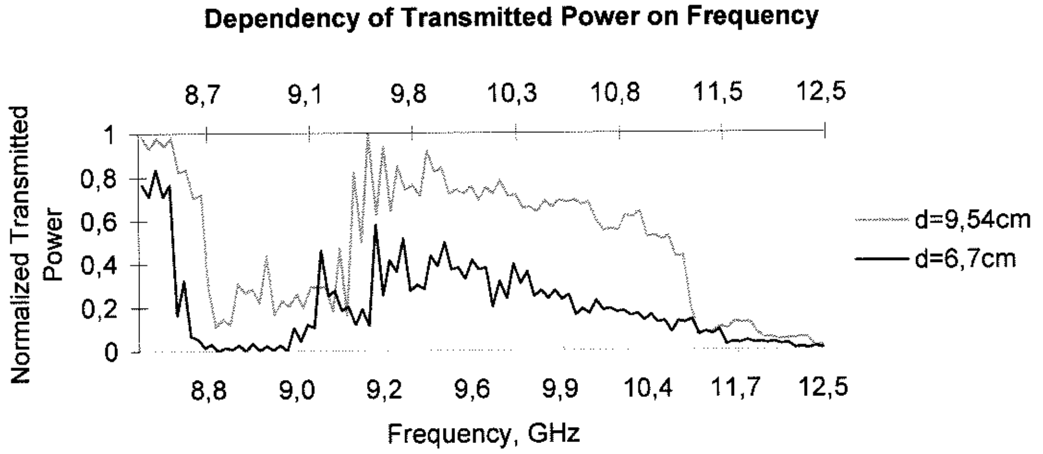

Geometry 1: d = 6,7cm, La-a = 60cm, Attenuator = 0, (Without Antennas; open waveguide).
Geometry 2: d = 9,54cm, La-a = 63cm, Attenuator = 1,56.

3)

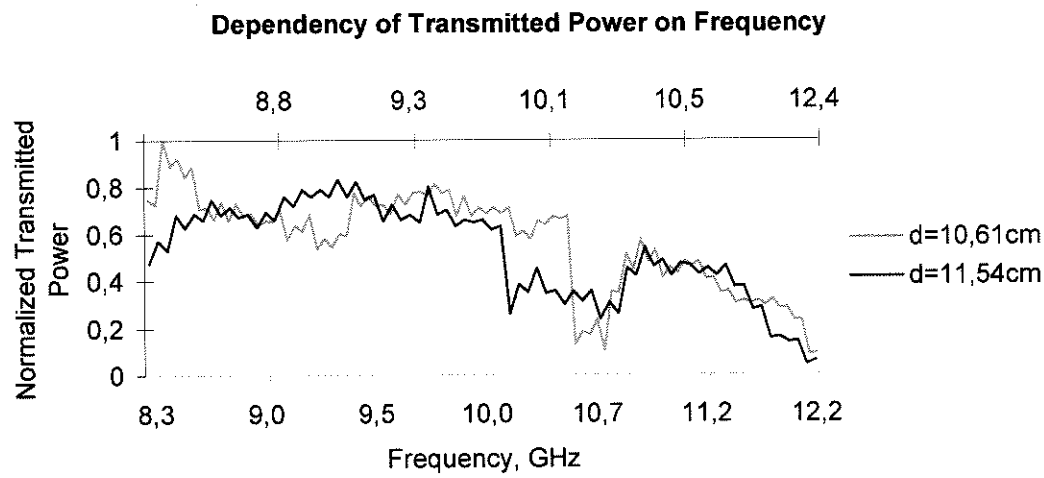

Geometry 1: d = 10,61cm, La-a = 60cm, Attenuator = 0.
Geometry 2: d = 11,54cm, La-a = 60cm, Attenuator = 0.

4)

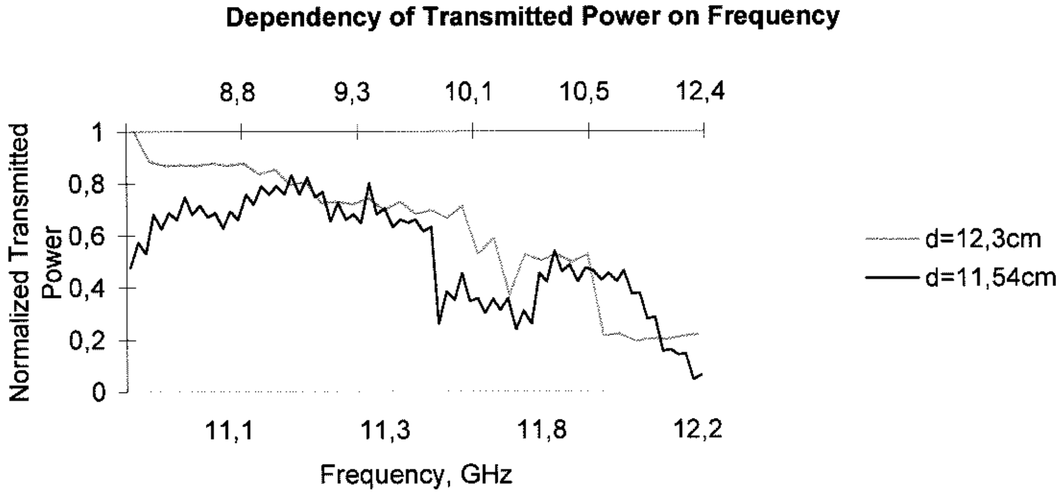

Geometry 1: d = 11,54cm, La-a = 60cm, Attenuator = 0.
Geometry 2: d = 12,3cm, La-a = 63cm, Attenuator = 1,56.

Evaluation of the Results:

To evaluate the experiments' results we should look into theoretical part of thesis at "Effect of the Phase Shift between Parallel Plates on Wave Reflection" section. In phase shift, $\theta=\pi$ case, it can be easily seen that Bragg resonances (stop bands) occur but on the contrary all non-Bragg resonances (additional stop bands) can't be observed in the spectrum of the periodically corrugated waveguide if amplitudes of corrugations equal each other. And in this section, equation (2.1.116) indicates Bragg stop band's width.

Because in our geometry, amplitudes of corrugations equal each other, according to our experiments, Bragg resonance (stop band) occured and all non-Bragg resonances (additional stop bands) wasn't observed while phase shift, $\theta=\pi$. So experimental investigations are in good agreement with theoretical investigations.

b) Phase Shift, θ, in Different Values

In our experiments, period of corrugations, 2π, equals 33mm.

1)

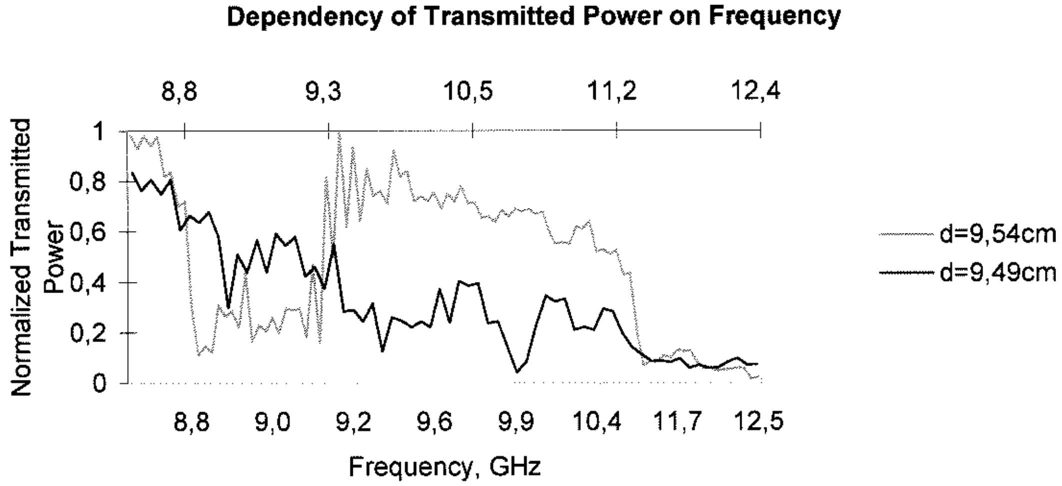

Geometry 1: d = 9,54cm, La-a = 63cm, Attenuator = 1,56, $\theta = \pi$.
Geometry 2: d = 9,49cm, La-a = 60cm, Attenuator = 1,56, $\theta = \pi$+15mm.

2)

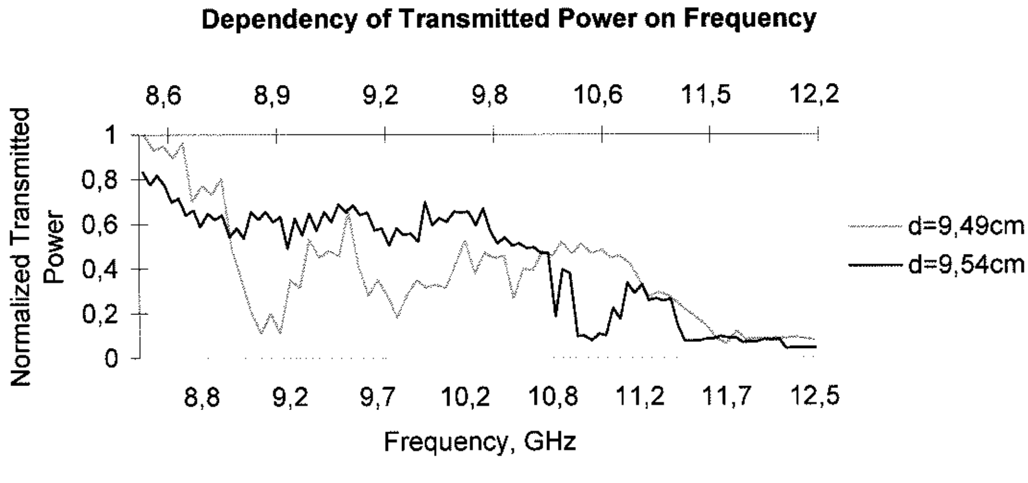

Geometry 1: d = 9,54cm, La-a = 63cm, Attenuator = 1,56, $\theta = \pi$+30mm.
Geometry 2: d = 9,49cm, La-a = 60cm, Attenuator = 1,56, $\theta = \pi$+60mm.

Evaluation of the Results:

In theoretical part of thesis at "Effect of the Phase Shift between Parallel Plates on Wave Reflection" section, it can be seen from equation (2.1.113) to equation (2.1.116) that in case phase shift, θ, equals to zero, non-Bragg resonances (additional stop bands) occur but Bragg resonances (stop bands) don't open in the spectrum of the periodically corrugated waveguide. On the contrary, in case phase shift, θ, equals to π, Bragg resonances (stop bands) occur but all non-Bragg resonances (additional stop bands) don't open in the spectrum of the periodically corrugated waveguide. These evaluations are valid while the amplitudes of the corrugations equal to each other. Besides the width of stop bands depends on the phase shift, θ, between parallel periodic boundaries and mode's evenness. It varies from zero to a maximum value while one plate shifting half period of the corrugation with respect to another. Our experimental results are in agreement with theoretical investigations.

(ii) Dependency of Transmitted Power on Frequency at New Transmission Point

1)

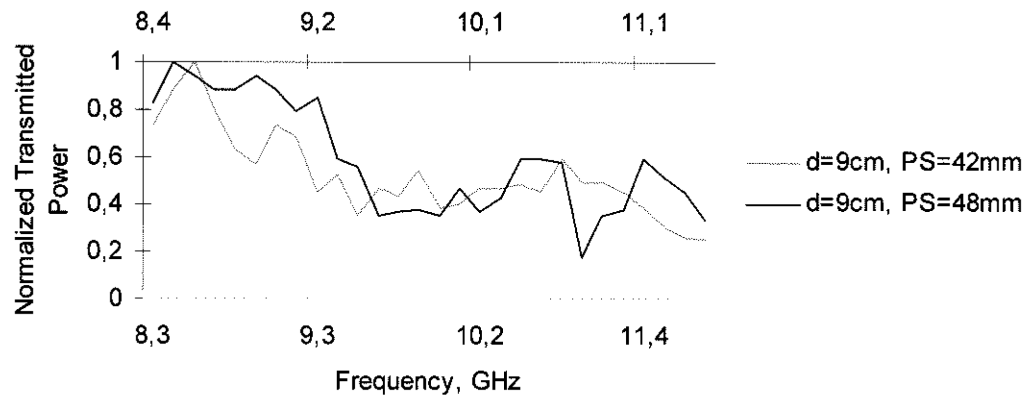

Geometry 1: d = 9cm, La-a = 56cm, Attenuator = 1,5, $\theta = \pi$+42mm, Fcr = 9,188GHz.

Geometry 2: d = 9cm, La-a = 56cm, Attenuator = 1,5, θ = π+48mm, Fcr = 8,855GHz.

2)

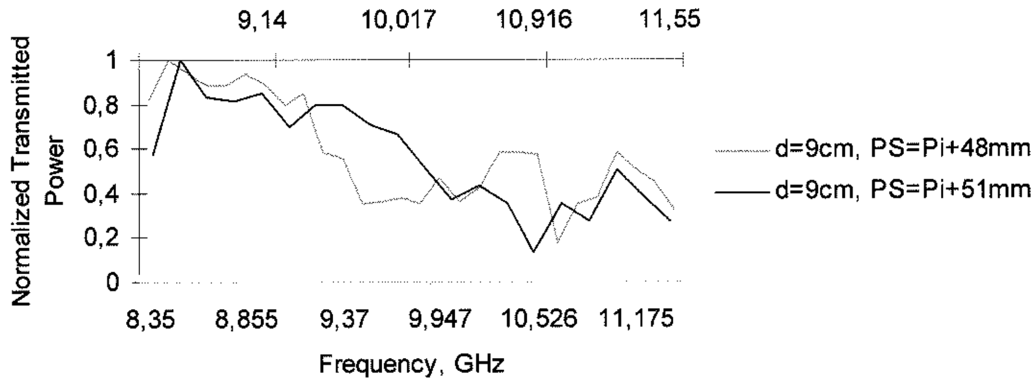

Geometry 1: d = 9cm, La-a = 56cm, Attenuator = 1,5, θ = π+48mm, Fcr = 8,855GHz.
Geometry 2: d = 9cm, La-a = 60cm, Attenuator = 1,5, θ = π+51mm. Fcr = 9,005GHz.

(iii) Dependency of Transmitted Power on Phase Shift between Parallel Plates

1)

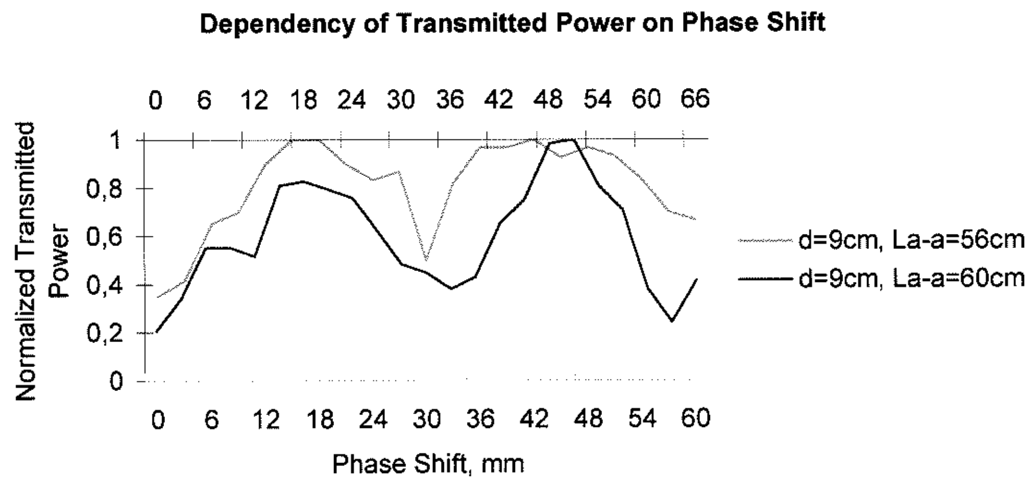

Geometry 1: d = 9cm, La-a = 56cm, Attenuator = 1,5, FBragg = 9,188GHz.
Geometry 2: d = 9cm, La-a = 60cm, Attenuator = 1,5, FBragg = 9,154GHz.

2)

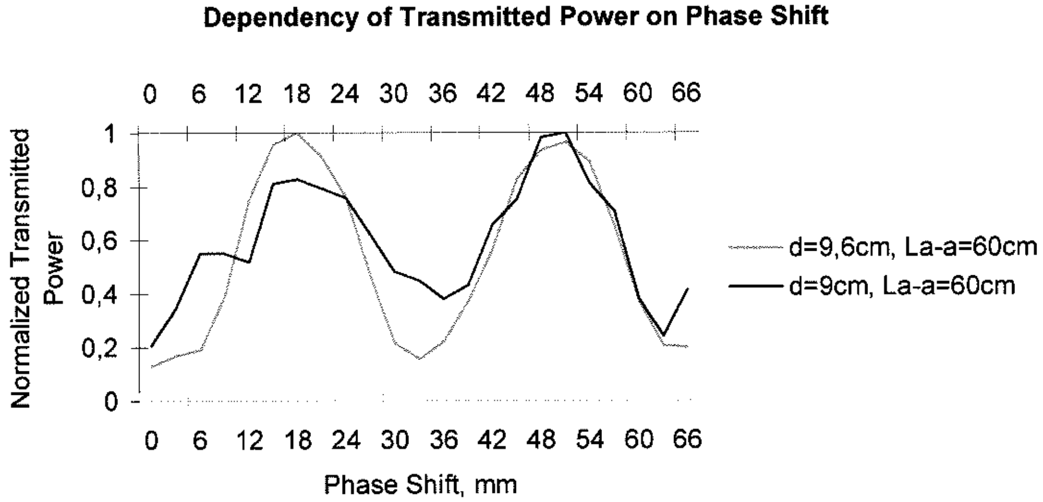

Geometry 1: d = 9cm, La-a = 60cm, Attenuator = 1,5, FBragg = 9,154GHz.
Geometry 2: d = 9,6cm, La-a = 60cm, Attenuator = 1,56, FBragg = 8,806GHz.

Evaluation of the Results

In theoretical investigations, effect of phase shift is mentioned in part 2.1.5. Effect of the Phase Shift between Parallel Plates on Wave Reflection.

Position and width of the gap (stop band) depend on the phase shift, θ, between two periodic plates and mode's evenness. It varies from zero to a maximum value while shifting one plate with respect to another on the half period of corrugation. In a case of the congruent boundaries, the Bragg gaps do not open, and an electromagnetic wave propagates in the periodic waveguide without Bragg reflections. When frequency of the electromagnetic wave coincides with one of the gaps, only unidirectional propagation along grooves is allowed in the waveguide.

It can be seen from experimental part 3.2.1.(iii) for effect of phase shift that experimental investigations approve the theoretical investigations.

(iv) Dependency of Transmitted Power and Bragg Frequency on Distance Between Antennas

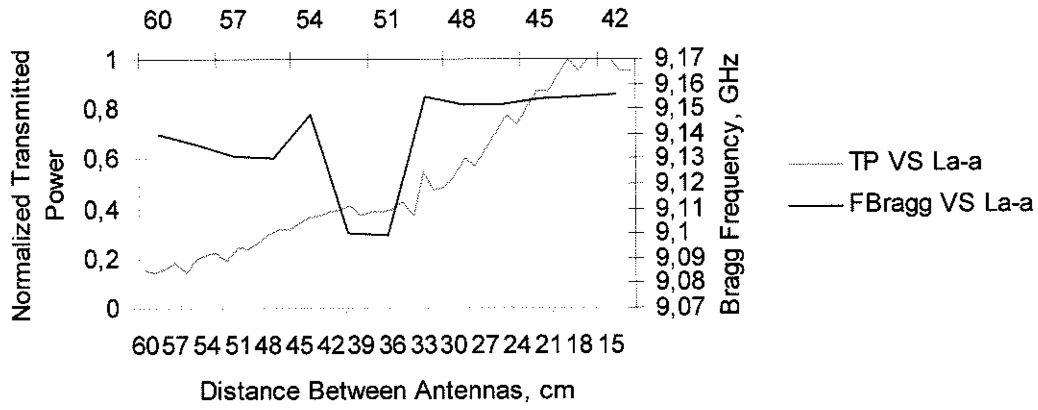

Geometry 1 (TP versus La-a): d = 9cm, Attenuator = 1,5, $\theta = \pi$, FBragg = 8,903GHz.
Geometry 2 (FBragg versus La-a): d = 9cm, Attenuator = 1,5, $\theta = \pi$.

Evaluation of the Results

Effect of La-a is investigated in both sides. One of them is effect of La-a on transmitted power and the other one is on Bragg frequency.

Theoretically if the La-a is increased, it is expected that transmitted power will decrease because of losses. It can be seen this effect of La-a in experimental part 3.2.1.(iv). And experimental results are in agreement with the theoretical indicates.

The other effect of La-a is upon Bragg frequency. Theoretically it is expected that Bragg and non-Bragg frequency aren't effected by changing of La-a. Again in experimental part 3.2.1.(iv), it can be seen that Bragg frequency isn't effected by changing of La-a.

So theoretical and experimental investigations are in agreement in these points.

(v) Dependency of Transmitted Power and Bragg Frequency on Average Thickness Between Parallel Plates

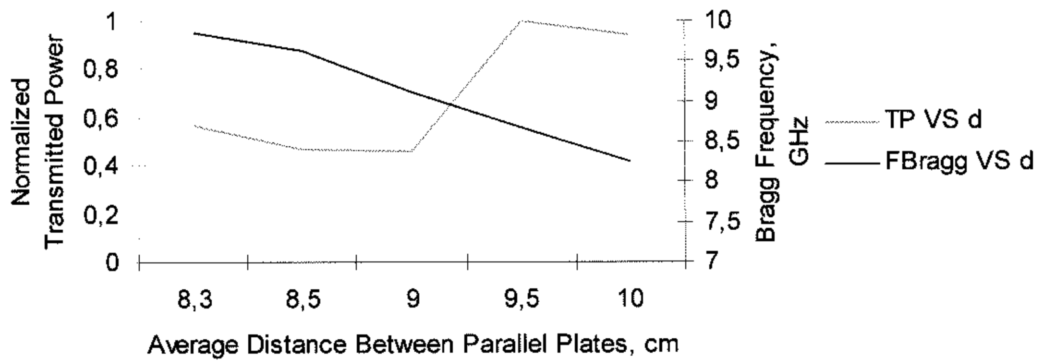

Geometry 1 (TP versus d): La-a = 60cm, Attenuator = 1,5, $\theta = \pi$.
Geometry 2 (FBragg versus d): La-a = 60cm, Attenuator = 1,5, $\theta = \pi$.

Evaluation of the Results

Effect of d can be observed in different directions. According to our experiments, firstly we can see effect of d on position of Bragg resonance (stop band) in the spectrum of the periodically corrugated waveguide and the another effect is changing of the Bragg stop band.

In theoretical part, equation (2.1.83) shows that the resonance occurs if the thickness of the waveguide, d, is simultaneously a multiple of half wavelengths of the standing-waves associated with the fundamental ($n = 0$) and the $n = \pm 1$ space harmonics but with different integers p and m. Because of this reason, resonance is also named geometric resonance.

Firstly, equation (2.1.109) (resonance frequency) shows us that if other parameters are fixed and the average distance of parallel plates, d, is changed, resonance frequency will change. If d is increased, Bragg resonance (stop band) frequency as well as the non-Bragg resonance (additional stop band) frequency will decrease. The experimental results can be seen in experimental part 3.2.1.(v)

As second effect of d, equation (2.1.110) (stop band) shows us that if other parameters are fixed and the d is changed, band gap will change. If the d is increased, band gap will decrease. And experimental results of this effect can be seen in experimental part 3.2.1.(i) and part 3.2.2.(i).a.

In experimental part 3.2.1 as you see easily, at some very small and big values of d, Bragg gap isn't seen. Also this situation is explained as condition of Bragg gap in theoretical part.

Experimental investigations of above effects support theoretical investigations.

(vi) Dependency of Scattered Power on Position of Antenna Through Corrugations

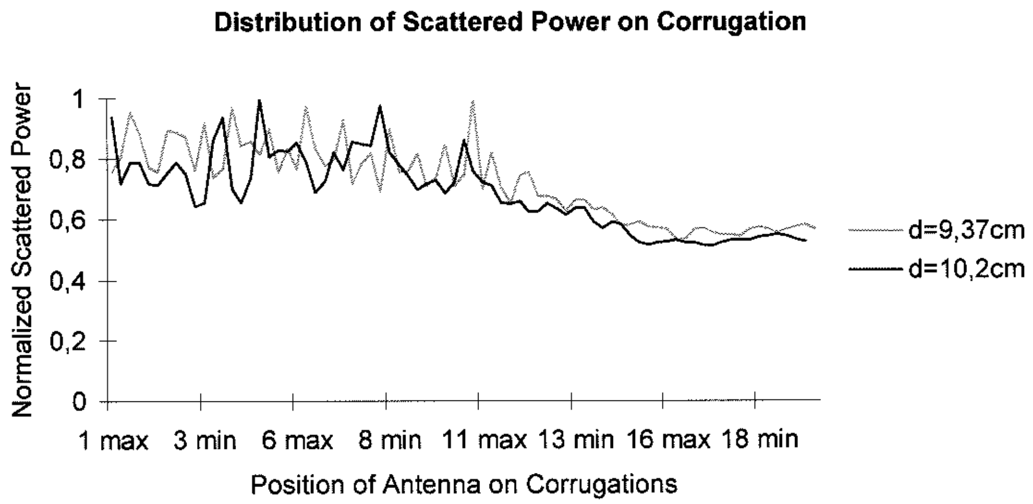

Geometry 1: d = 9,37cm, La-a = 60cm, Attenuator = 1,5, $\theta = \pi$, FBragg = 9,482GHz.
Geometry 2: d = 10,2cm, La-a = 60cm, Attenuator = 1,5, $\theta = \pi$, FBragg = 8,665GHz.

Second receiving antenna is shifted from receiving side to transmitted side.
max indicates top point of corrugation and min indicates bottom point of corrugation. So for instance, 1 max means that top point of first corrugation.

Evaluation of the Results

In our investigations, electromagnetic wave propagates through x direction. So, the periodicity along the x-axis does not affect strongly upon wave propagation into the z direction. In the first order approximation, we can neglect by change of parameters of the wave progressing into the z direction.

Scattered power experiments are done by shifting horn antenna throughout corrugation from receiving side to the transmitting side at the edge of corrugated boundary in periodically corrugated waveguide.

Theoretically, we expected that distribution of scattered power in periodically corrugated waveguide at the edge of corrugated boundary is generally sinusoidal form because of standing and pure standing waves.

It can be seen easily from experimental part 3.2.1.(vi) that distribution of scattered power is almost sinusoidal because of standing and pure standing waves and experimental results supports theoretical results.

3.2.2. Experiments with Transformation of Corrugated Waveguide to Smooth Waveguide and Their Evaluations

In this section, we investigated the changing of the position and width of the Bragg gap and distribution of scattered power while periodically corrugated waveguide is transferring to smooth waveguide incrementally. These experimental investigations are done by separating phase shift between parallel plates equals to pi and zero. And on flat waveguide. Plain stripes are added from center to both sides of corrugated waveguide while full corrugated waveguide transfers to the smooth waveguide. Our corrugated waveguide has 24 periods. Besides width of plain stripes are shown at right side of the graphics. For example 6 periods=19,2cm etc.

(i) Dependency of Transmitted Power on Frequency

a) Phase Shift (θ) = π

1)

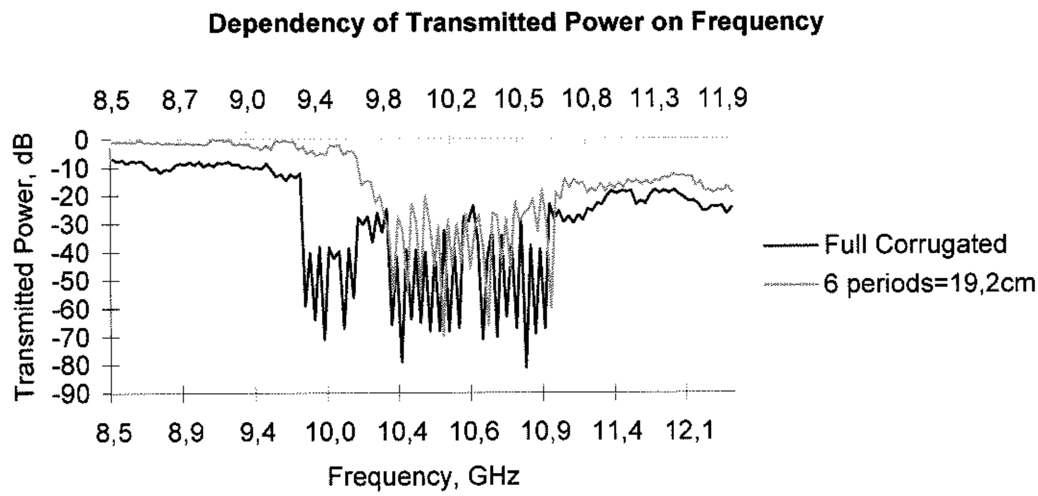

Geometry 1 (Full Corrugated): d = 5,4cm, La-a = 100,5cm, Attenuator = 0, (Without Antennas; open waveguide).
Relative Values: $P_{incident}$ = 3,14dB at f = 8,471GHz.
Geometry 2 (6 periods): d = 5,5cm, La-a = 102,5cm, Attenuator = 0.
Relative Values: $P_{received}$ = -3,60dBm, $P_{reflected}$ = -17,78dBm at f = 8,910GHz.

Plain stripes begin at 10th top from the transmitting side and end at 10th top at the receiving side.

2)

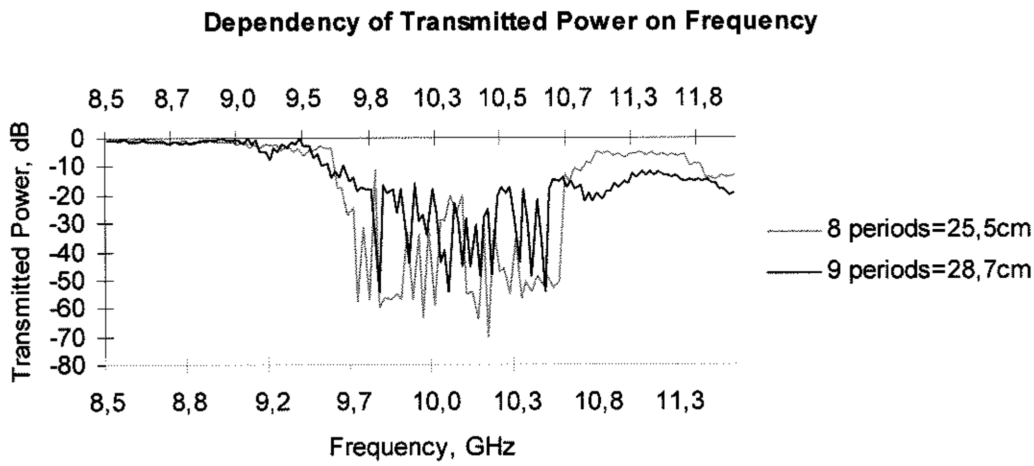

Geometry 1 (8 periods): d = 5,4cm, La-a = 102cm, Attenuator = 0.
Relative Values: $P_{received}$ = -36,4dBm at f = 8,663GHz.
Plain stripes begin at 28th cm from 1st corrugation's top at the transmitting side.
Geometry 2 (9 periods): d = 5,5cm, La-a = 102,5cm, Attenuator = 0.
Relative Values : $P_{received}$ = -4,15dBm, $P_{reflected}$ = -20,35dBm at f = 9,105GHz.
Plain stripes begin at 9th top from the transmitting side and end at 8th top at the receiving side.

3)

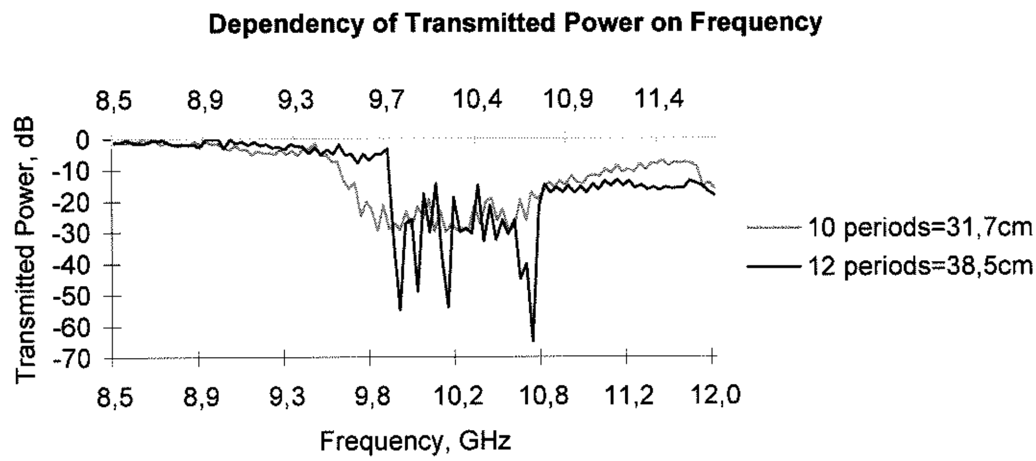

Geometry 1 (10 periods): d = 5,4cm, La-a = 102,5cm, Attenuator = 0.

Relative Values: $P_{received}$ = 214 μ W at f = 8,604GHz.
Plain stripes begin at 8th top from the transmitting side and end at 10th top at the receiving side.
Geometry 2 (12 periods): d = 5,5cm, La-a = 102,5cm, Attenuator = 0.
Relative Values: $P_{received}$ = -3,50 dBm, $P_{reflected}$ = -20,35dBm at f = 8,892GHz.
Plain stripes begin at 6th top from the transmitting side and end at 8th top at the receiving side.

4)

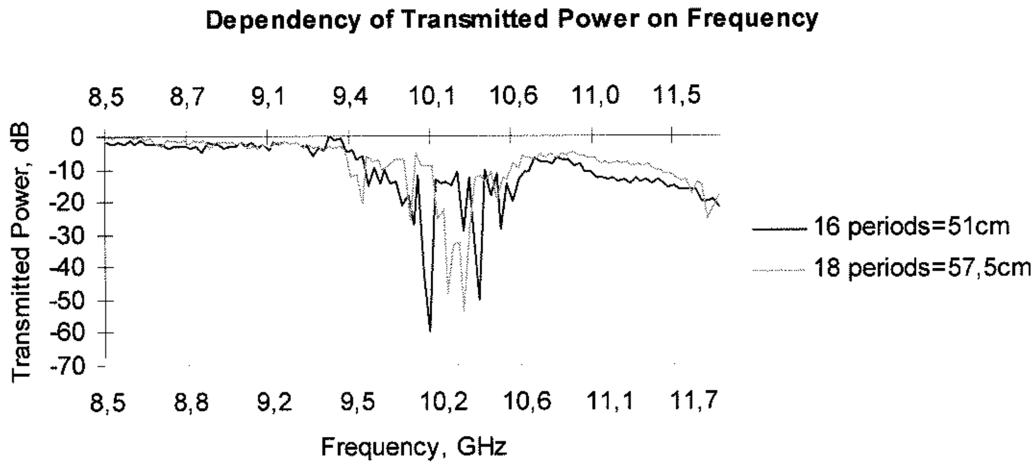

Geometry 1 (16 periods): d = 5,5cm, La-a = 102,5cm, Attenuator = 0.
Relative Values: $P_{received}$ = -3,11dBm, $P_{reflected}$ = 10,64dBm at f = 9,424GHz.
Plain stripes begin at 6th top from the transmitting side and end at 6th top at the receiving side.
Geometry 2 (18 periods): d = 5,5cm, La-a = 100cm, Attenuator = 0.
Relative Values: $P_{received}$ = -5,56dB at f = 8,535GHz.
Plain stripes begin at 6th top from the transmitting side and end at 4th top at the receiving side.

5)

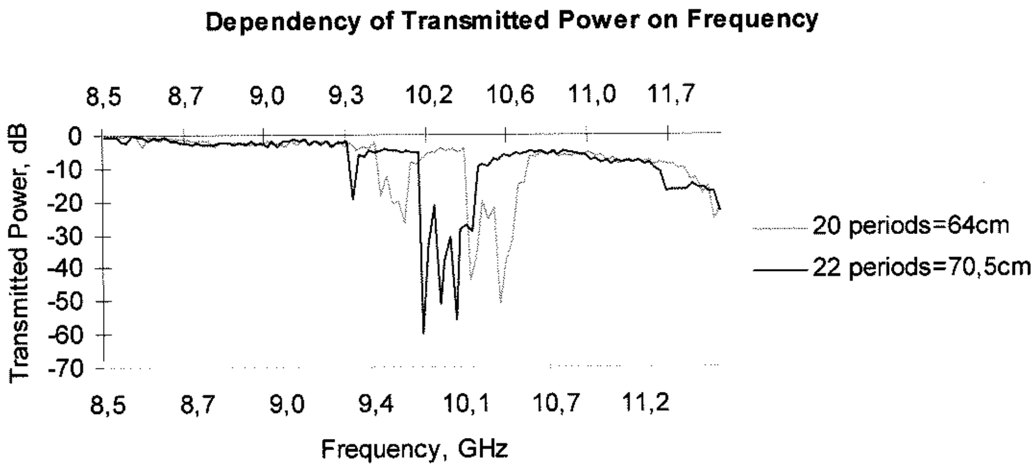

Geometry 1 (20 periods): d = 5,5cm, La-a = 100cm, Attenuator = 0.
Relative Values: $P_{received}$ = -5,35dB, $P_{reflected}$ = -19,40dB at f = 8,538GHz.
Plain stripes begin at 4th top from the transmitting side and end at 4th top at the receiving side.
Geometry 2 (22 periods): d = 5,5cm, La-a = 100cm, Attenuator = 0.
Relative Values: $P_{received}$ = -5,45dBm, $P_{reflected}$ = -18,3dBm at f = 8,564GHz.
Plain stripes begin at 2th top from the transmitting side and end at 4th top at the receiving side.

6)

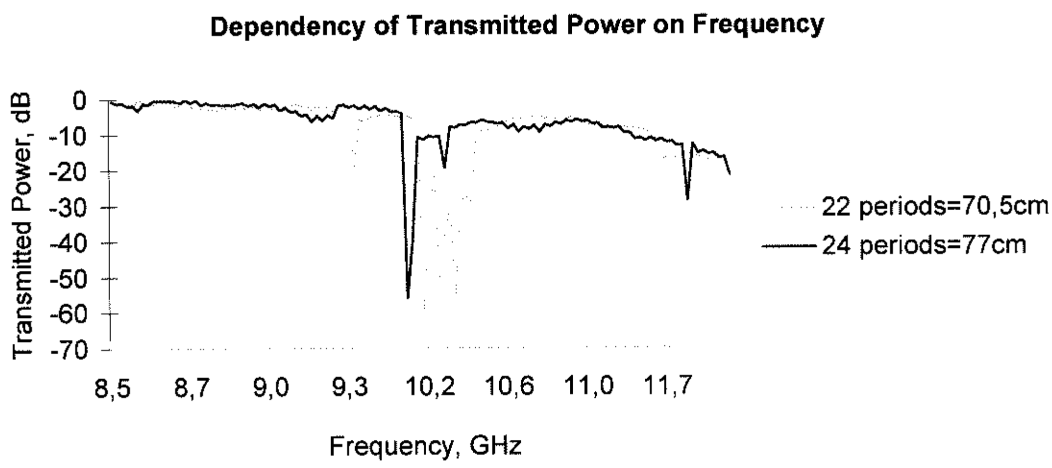

Geometry 1 (22 periods): d = 5,5cm, La-a = 100cm, Attenuator = 0.
Relative Values: $P_{received}$ = -5,45dBm, $P_{reflected}$ = -18,3dBm at f = 8,564GHz.
Plain stripes begin at 2th top from the transmitting side and end at 4th top at the receiving side.

Geometry 2 (24 periods): d = 5,5cm, La-a = 100cm, Attenuator = 0.
Relative Values: $P_{received}$ = -5,50dBm, $P_{reflected}$ = -16,65dBm at f = 8,670GHz.
Plain stripes begin at 2th top from the transmitting side and end at 2th top at the receiving side.

Evaluation of the Results

In our experiments, plain stripes are added from middle of the parallel plates into both sides of parallel plates symmetrically. Plain stripes' effects are investigated upon band gap in three directions. Firstly in geometry with phase shift, θ, between parallel plates equals to π, then equals to zero. And as last in smooth waveguide.

For phase shift, $\theta = \pi$;

According to experiments, width of Bragg band gap reduces and becomes disappear step by step while the plane stripes are added through the both sides of parallel plates symmetrically. This results are expected theoretically because when we add the plain stripes, we destroy the periodicity. So as well as non-Bragg resonance, Bragg resonance is spoiled and slowly becomes disappear.
And results in experimental part 3.2.2.(i).a are in agreement with theoretical results.

b) Phase Shift (θ) = 0

1)

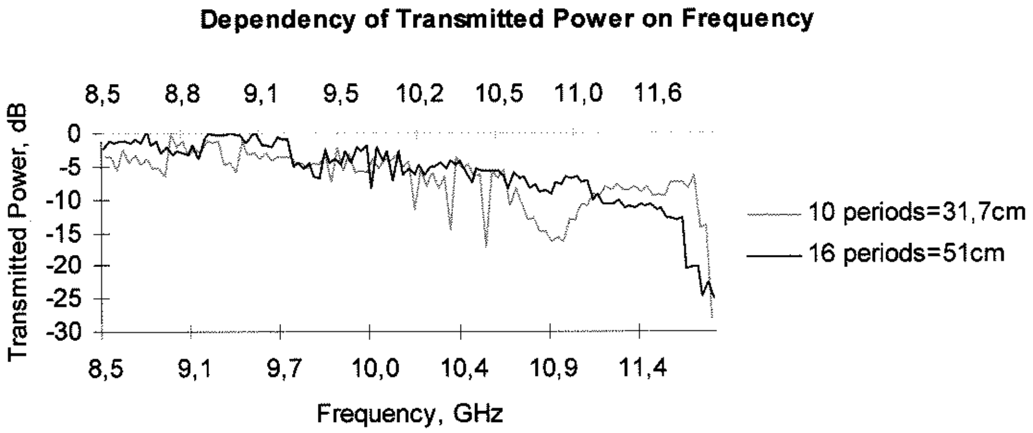

Geometry 1 (10 periods): d = 5,4cm, La-a = 102,5cm.
Relative Values: $P_{received}$ = 3,26dBm at f = 8,957GHz.
Plain stripes begin at 8th top from the transmitting side and end at 10th top at the receiving side.
Geometry 2 (16 periods): d = 5,4cm, La-a = 100cm, Attenuator = 0.
Plain stripes begin at 6th top from the transmitting side and end at 6th top at the receiving side.

2)

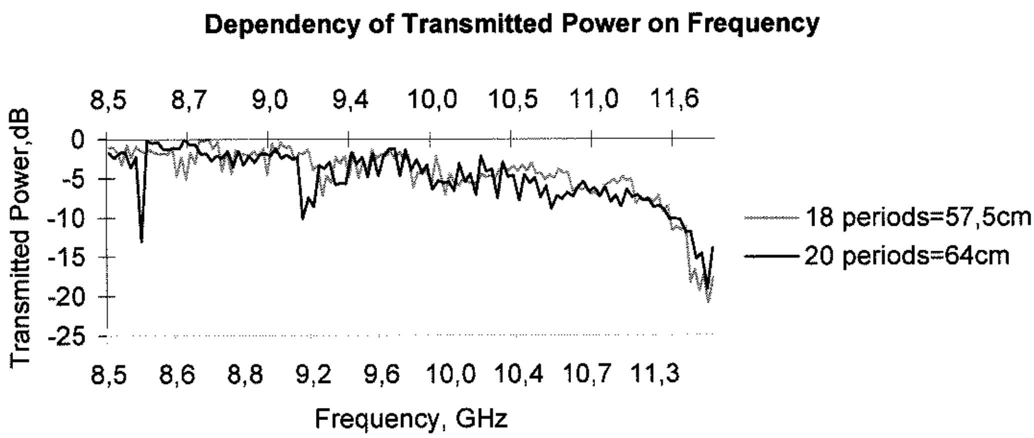

Geometry 1 (18 periods): d = 5,5cm, La-a = 100cm, Attenuator = 0.
Relative Values: $P_{received}$ = -5,10dB, $P_{reflected}$ = -14,70dB at f = 8,691GHz.

Plain stripes begin at 6th top from the transmitting side and end at 4th top at the receiving side.
Geometry 2 (20 periods): d = 5,5cm, La-a = 100cm, Attenuator = 0.
Relative Values: $P_{received}$ = -4,89dBm, $P_{reflected}$ = -16dBm at f = 8,696GHz.
Plain stripes begin at 4th top from the transmitting side and end at 4th top at the receiving side.

3)

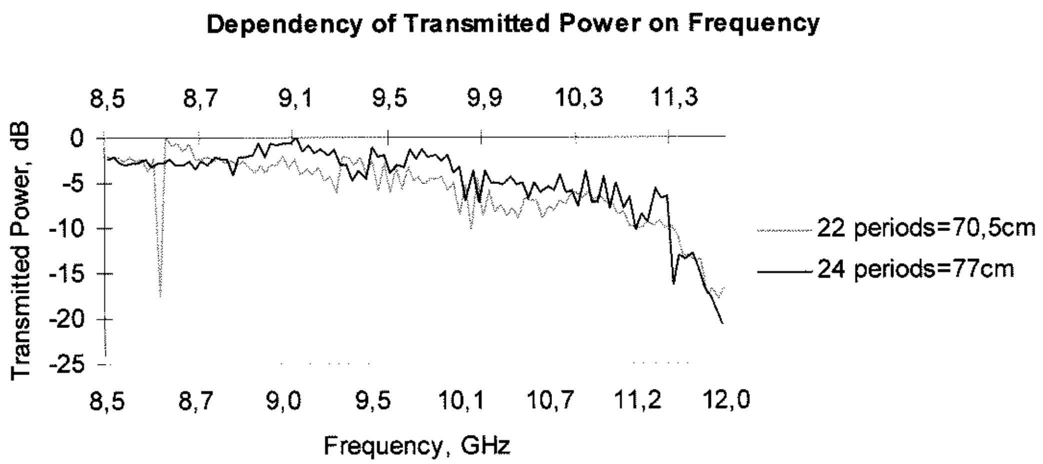

Geometry 1 (22 periods): d = 5,5cm, La-a = 100cm, Attenuator = 0.
Relative Values: $P_{received}$ = -4,13dBm, $P_{reflected}$ = -23,89dBm at f = 8,638GHz.
Plain stripes begin at 2th top from the transmitting side and end at 4th top at the receiving side.
Geometry 2 (24 periods): d = 5,5cm, La-a = 102cm, Attenuator = 0.
Relative Values: $P_{received}$ =-2,71dBm, $P_{reflected}$ = -21,84dBm at f = 9,058GHz.
Plain stripes begin at 2th top from the transmitting side and end at 2th top at the receiving side.

Evaluation of the Results

For phase shift, $\theta = 0$

As expected theoretically, in geometry that phase shift, θ, between paralel plates equals zero, no Bragg stop band was occured. In agreement with theoretical results, we couldn't observe the Bragg stop band in transferred experiments at phase shift, θ=0. When we look the experimental results in experimental part 3.2.2.(i).b, we can see easily that experimental results are in agreement with the theoretical results.

c) Flat Waveguide

1)

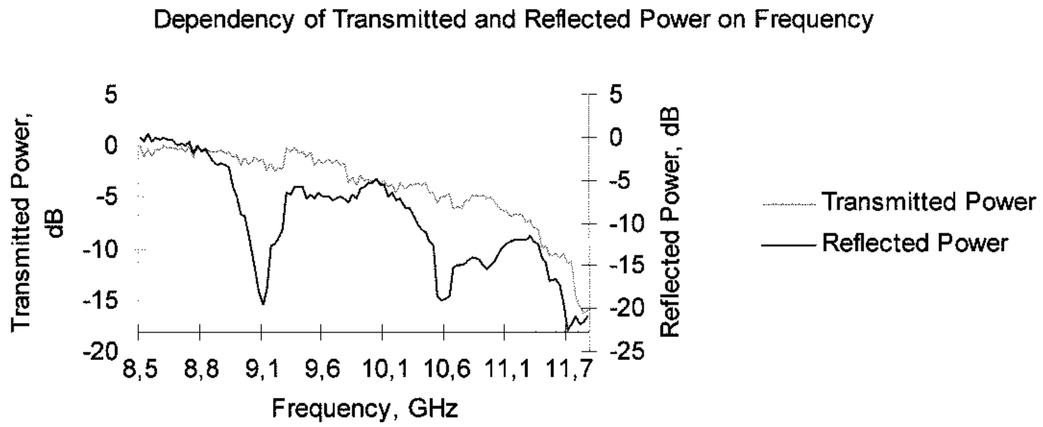

Dependency of Transmitted Power on Frequency
Geometry: d = 3,7cm, La-a = 103 cm.
Relative Values: $P_{received}$ = -6,90dBm, $P_{reflected}$ = -14,54dBm at f = 8,5GHz.
Dependency of Reflected Power on Frequency
Geometry: d = 3,7cm, La-a = 103 cm.
Relative Values: $P_{received}$ = -6,90dBm, $P_{reflected}$ = -14,54dBm at f = 8,5GHz.

2)

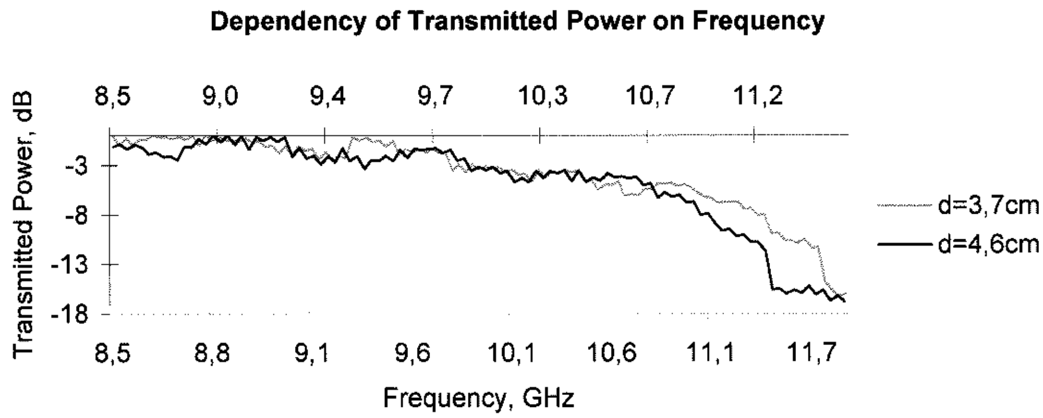

Geometry 1: d = 3,7cm, La-a = 103cm.

Relative Values: $P_{received}$ = -6,90dBm, $P_{reflected}$ = -14,54dBm at f = 8,5GHz.
Geometry 2: d = 4,6cm, La-a = 102,5cm.
Relative Values: $P_{received}$ = -4,29dBm, $P_{reflected}$ = -12,76dBm at f = 9,045GHz.

Evaluation of the Results

For Flat Waveguide;

In this geometry, because of lack of periodicity, there is no any Bragg and non-Bragg stop band. So results in experimental part 3.2.2.(i).c approve the theoretical results.

(ii) Dependency of Scattered Power on Position of Antenna Through Corrugations

Distribution of scattered power on corrugation experiments are investigated in three directions. First investigation which is separated by three parts as stop band, pass band and at boundary between stop and pass band while phase shift, θ, between paralel plates equals to zero. In Second one, phase shift, $\theta = \pi$. And last investigation is in flat waveguide.

Stop band means that measurement frequencies are in the Bragg stop band. Pass band means that measurement frequencies are out of the Bragg stop band. And boundary between stop and pass band means that measurement frequencies are at the edges of Bragg stop band.

Second receiving antenna is shifted from receiving side to the transmitting side.
max indicates top point of corrugation and min indicates bottom point of corrugation.

a) Phase Shift (θ) = π

1) Stop Band Region

1)

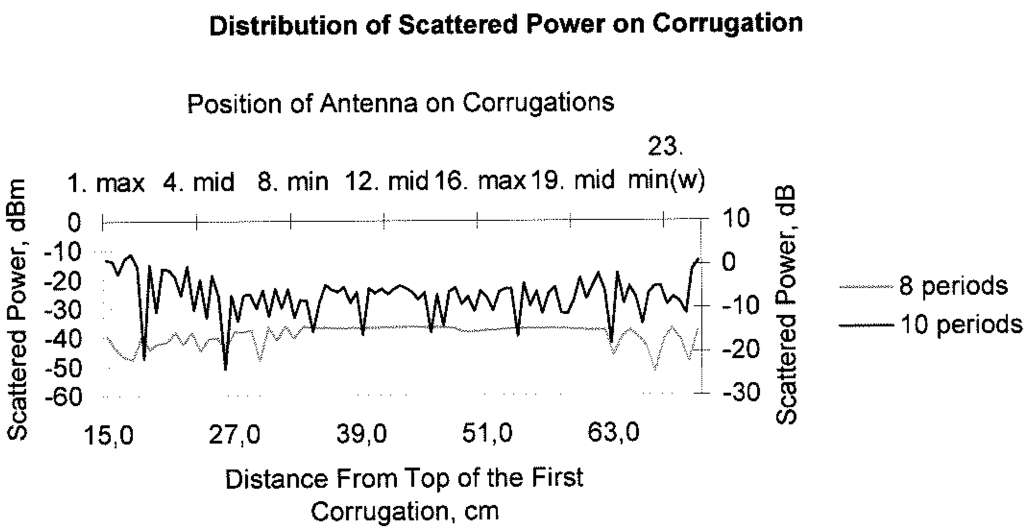

Geometry 1 (8 periods): d = 5,4cm, La-a = 102cm, Attenuator = 0, FBragg = 10,2GHz.
Plain stripes begin at 28th cm from 1st corrugation's top at the transmitting side
Geometry 2 (10 periods): d = 5,4cm, La-a = 102,5cm, F_{Bragg} = 10,122GHz.
Relative Values: $P_{received}$ = 214μW at f = 8,604GHz.
Plain stripes begin at 8th top from the transmitting side and end at 10th top at the receiving side.

2)

Distribution of Scattered Power on Corrugation

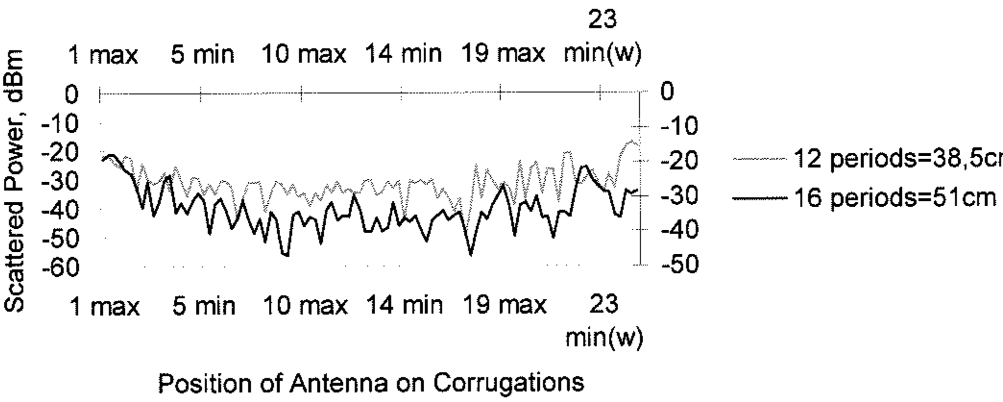

Geometry 1 (12 periods): d = 5,5cm, La-a = 102,5cm, f = 10,042GHz.
Plain stripes begin at 6th top from the transmitting side and end at 8th top at the receiving side.
Geometry 2 (16 periods): d = 5,5cm, La-a = 102,5cm, Attenuator = 0, f = 9,824GHz.
Plain stripes begin at 6th top from the transmitting side and end at 6th top at the receiving side.

3)

Distribution of Scattered Power on Corrugation

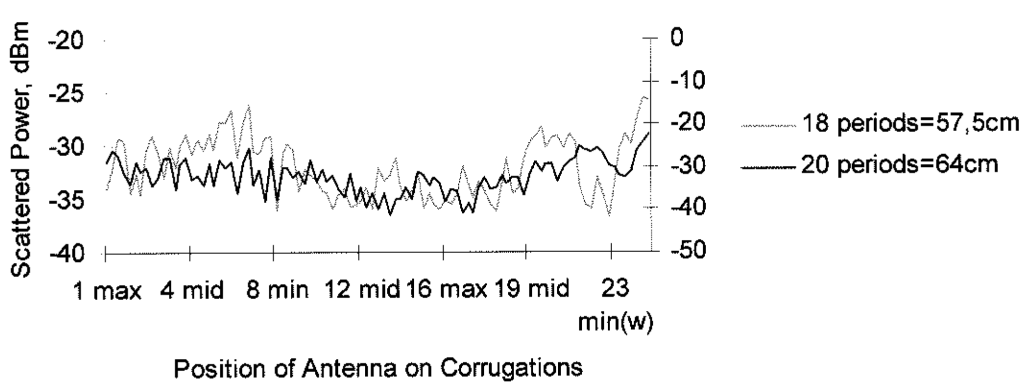

Geometry 1 (18 periods): d = 5,4cm, La-a = 100cm, Attenuator = 0, f = 10,316GHz.
Plain stripes begin at 6th top from the transmitting side and end at 4th top at the receiving side.
Geometry 2 (20 periods): d = 5,5cm, La-a = 100cm, Attenuator = 0, f = 10,346GHz.
Plain stripes begin at 4th top from the transmitting side and end at 4th top at the receiving side.

4)

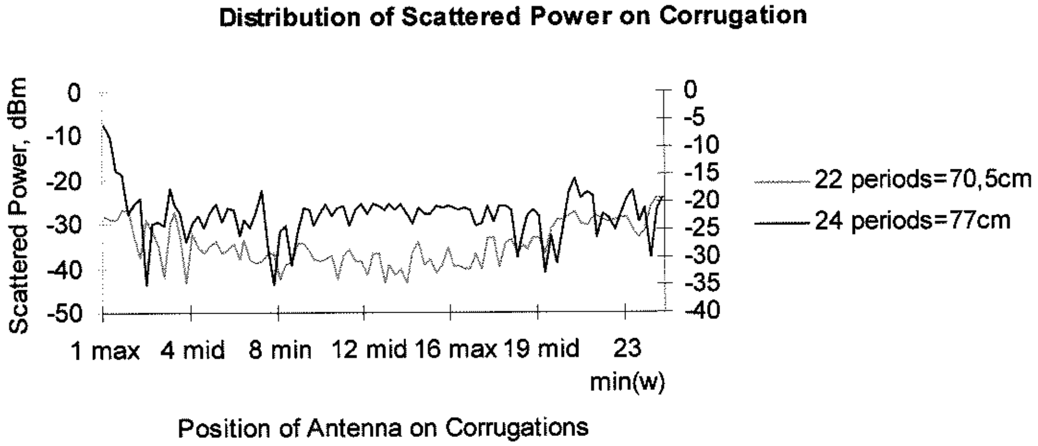

Geometry 1 (22 periods): d = 5,5cm, La-a = 100cm, Attenuator = 0, f = 10,217GHz. Plain stripes begin at 2nd top from the transmitting side and end at 4th top at the receiving side.

Geometry 2 (24 periods): d = 5,5cm, La-a = 102cm, Attenuator = 0, f = 9,5GHz. Plain stripes begin at 2nd top from the transmitting side and end at 2nd top at the receiving side.

2) Pass Band Region

1)

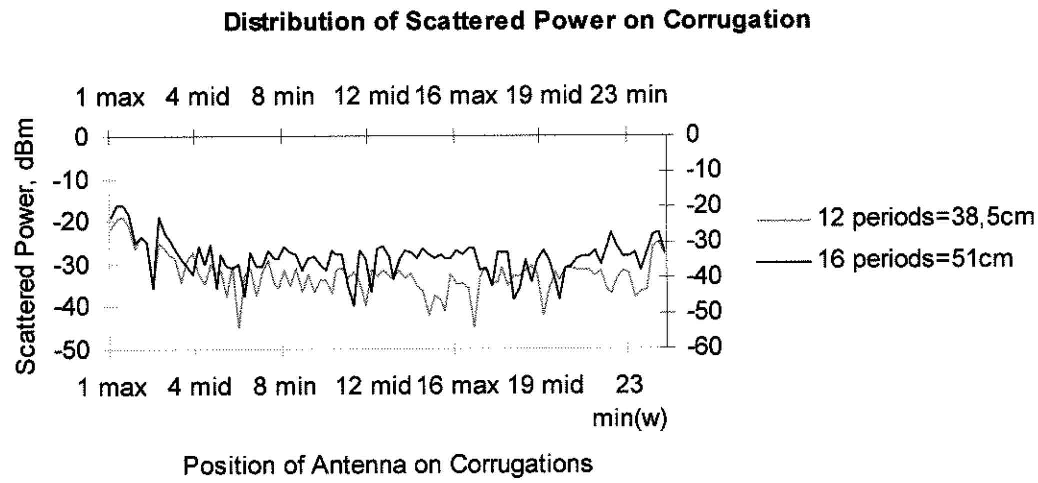

Geometry 1 (12 periods): d = 5,5cm, La-a = 102,5cm, f = 9,166GHz.
Plain stripes begin at 6th top from the transmitting side and end at 8th top at the receiving side.

Geometry 2 (16 periods): d = 5,5cm, La-a = 102,5cm, Attenuator = 0, f = 9,225GHz. Plain stripes begin at 6th top from the transmitting side and end at 6th top at the receiving side.

2)

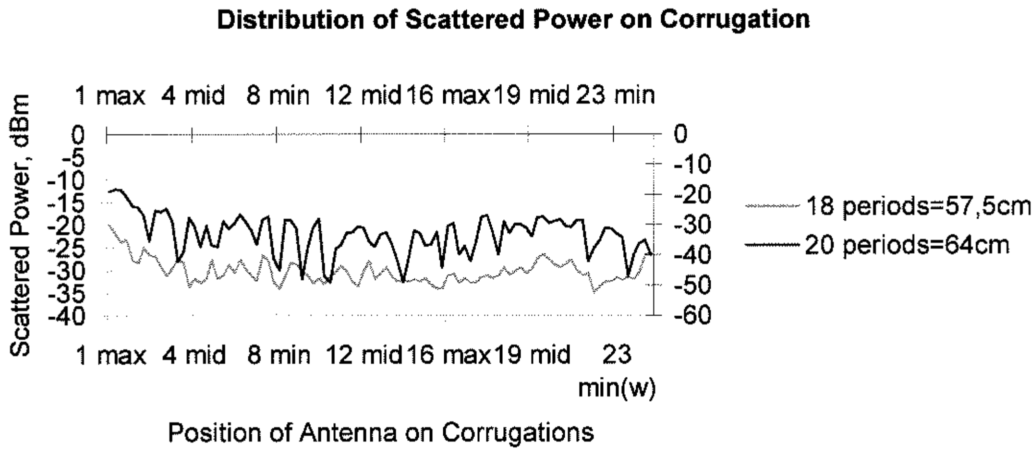

Geometry 1 (18 periods): d = 5,4cm, La-a = 100cm, Attenuator = 0, f = 8,927GHz. Plain stripes begin at 6th top from the transmitting side and end at 4th top at the receiving side.
Geometry 2 (20 periods): d = 5,5cm, La-a = 102,5cm, Attenuator = 0, f = 9,128GHz. Plain stripes begin at 4th top from the transmitting side and end at 4th top at the receiving side.

3) At Boundary between Stop and Pass Band

1)

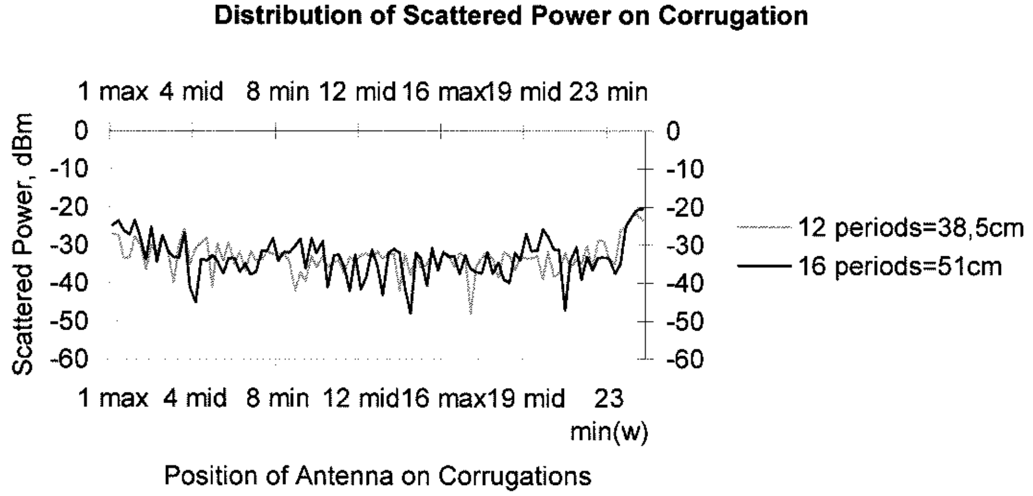

Geometry 1 (12 periods): d = 5,5cm, La-a = 102,5cm, f = 10,354GHz.
Plain stripes begin at 6th top from the transmitting side and end at 8th top at the receiving side.
Geometry 2 (16 periods): d = 5,5cm, La-a = 102,5cm, Attenuator = 0, f = 10,172GHz.
Plain stripes begin at 6th top from the transmitting side and end at 6th top at the receiving side.

2)

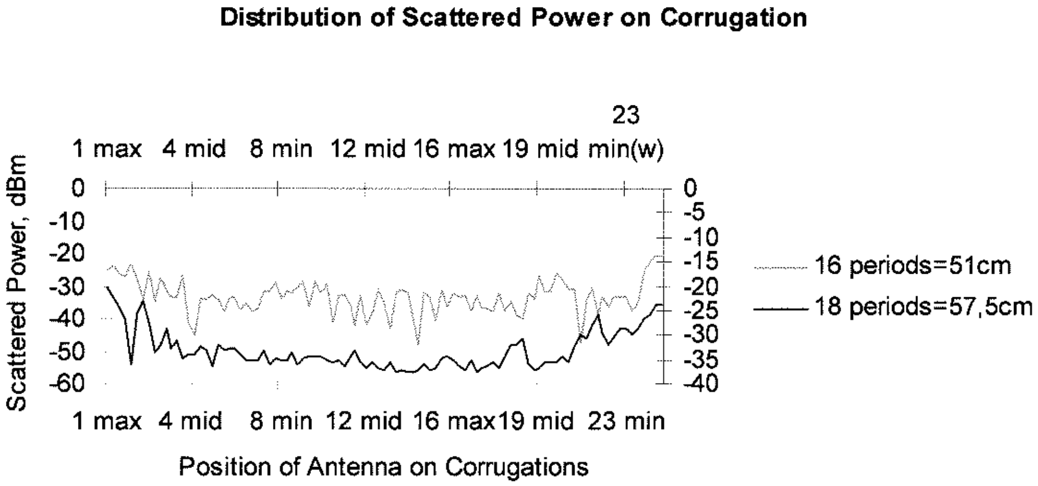

Geometry 1 (16 periods): d = 5,5cm, La-a = 102,5cm, Attenuator = 0, f = 10,172GHz.
Plain stripes begin at 6th top from the transmitting side and end at 6th top at the receiving side.
Geometry 2 (18 periods): d = 5,4cm, La-a = 100cm, Attenuator = 0, f = 9,596GHz.
Plain stripes begin at 6th top from the transmitting side and end at 4th top at the receiving side.

3)

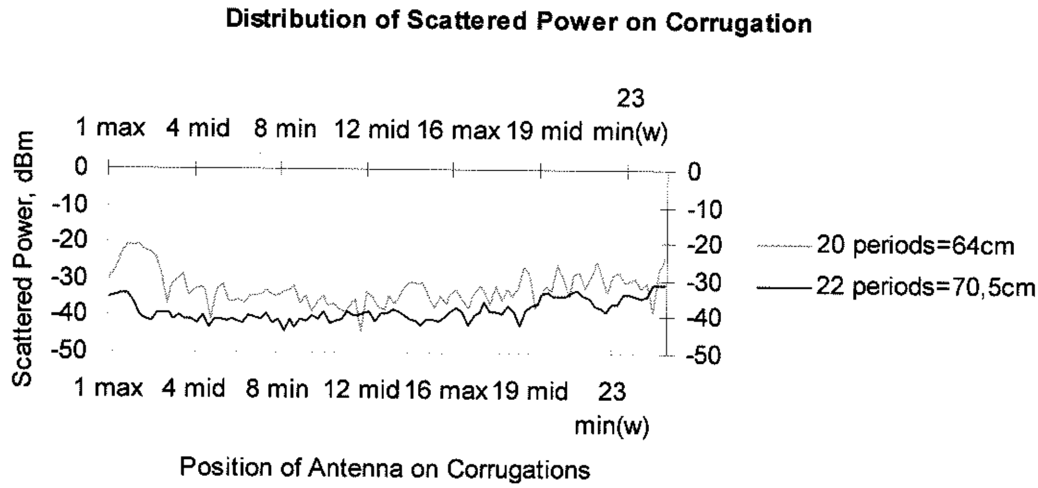

Geometry 1 (20 periods): d = 5,5cm, La-a = 100cm, Attenuator = 0, f = 9,646GHz.
Plain stripes begin at 4th top from the transmitting side and end at 4th top at the receiving side.
Geometry 2 (22 periods): d = 5,5cm, La-a = 100cm, Attenuator = 0, f = 11,217GHz.
Plain stripes begin at 2nd top from the transmitting side and end at 4th top at the receiving side.

Evaluation of the Results

As you see in experimental part 3.2.2.(ii).a, experiments were separated in three parts that were explained before. In experimental part 3.2.2.(ii).a.1, we observed the distribution of scattered power on corrugation in stop band regions. In part 3.2.2.(ii)a.2, we observed distribution of scattered power on corrugation in pass band regions and then in part 3.2.2.(ii).a.3, we observed distribution of scattered power on corrugation at boundary between stop and pass band. According to the experiments, there is no any distinctive differences between stop band, pass band and at boundary between stop and pass band in distribution of scattered power experiments.

In phase shift, θ, between parallel plates equals to π, distribution of scattered powers are almost sinusoidal because of standing and pure standing waves. Although scattered power is sinusoidal in general, middle region is more smooth than the other areas because of the plain stripes. Plain stripes spoils the periodicity so in the smooth surface, scattered power becomes more smooth.

b) Phase Shift (θ) = 0

1)

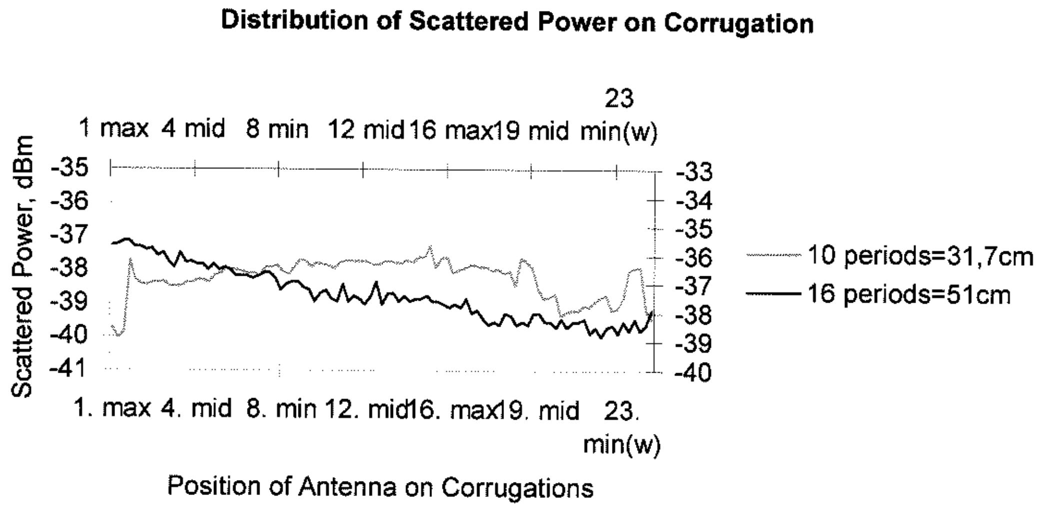

Geometry 1 (10 periods): d = 5,4cm, La-a = 102,5cm, FBragg = 10,947GHz.
Relative Values: Preceived = 3,26dBm at f = 8,957GHz.
Plain stripes begin at 8th top from the transmitting side and end at 10th top at the receiving side.
Geometry 2 (16 periods): d = 5,5cm, La-a = 100cm, Attenuator = 0.
Plain stripes begin at 6th top from the transmitting side and end at 6th top at the receiving side.

2)

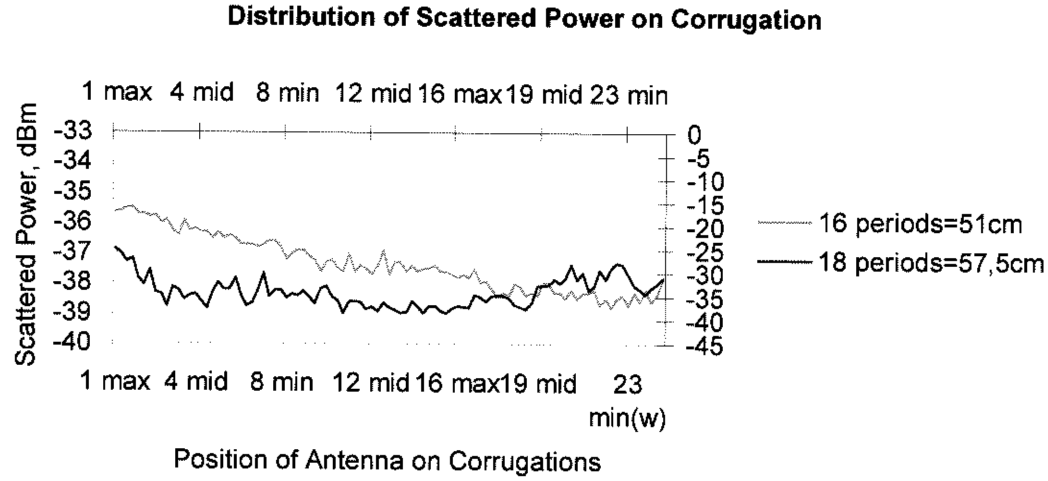

Geometry 1 (16 periods): d = 5,5cm, La-a = 100cm, Attenuator = 0.
Plain stripes begin at 6th top from the transmitting side and end at 6th top at the receiving side.
Geometry 2 (18 periods): d = 5,5cm, La-a = 100cm, Attenuator = 0, f = 9,261GHz.
Plain stripes begin at 6th top from the transmitting side and end at 4th top at the receiving side.

3)

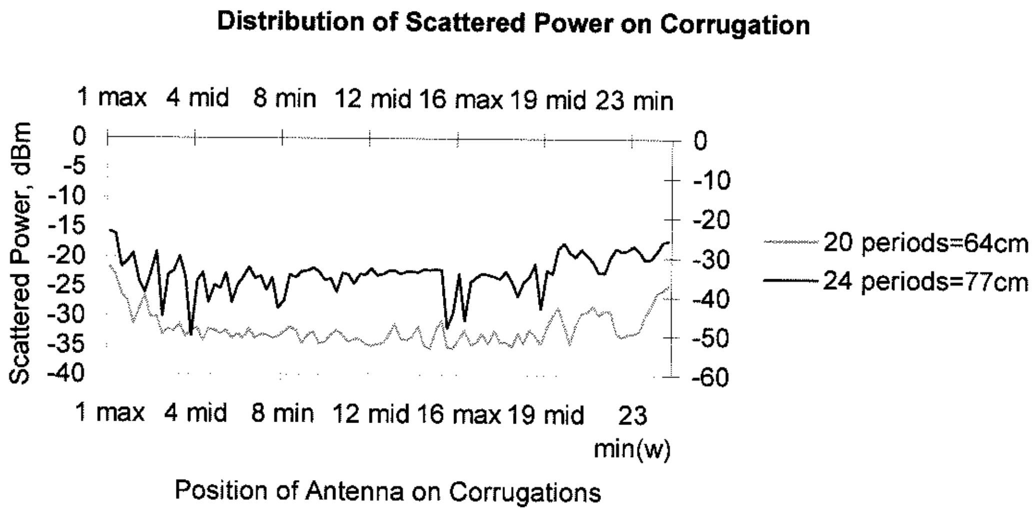

Geometry 1 (20 periods): d = 5,5cm, La-a = 100cm, Attenuator = 0, f = 9,6GHz.
Plain stripes begin at 4th top from the transmitting side and end at 4th top at the receiving side.
Geometry 2 (24 periods): d = 5,5cm, La-a = 102cm, Attenuator = 0, f = 10,1GHz.

Plain stripes begin at 2nd top from the transmitting side and end at 2nd top at the receiving side.

Evaluation of the Results

As you see in experimental part 3.2.2.(ii).b, scattered power is sinusoidal in general again. As expected, in this geometry, scattered powers are more smooth in all areas than the scattered power in phase shift, $\theta=0$ because of lack of Bragg reflections. Again in middle area scattered power is more smooth than the one in other ares because of plain stripes. As it can be seen easily, experimental results are in agreement with theoretical results.

c) Flat Waveguide

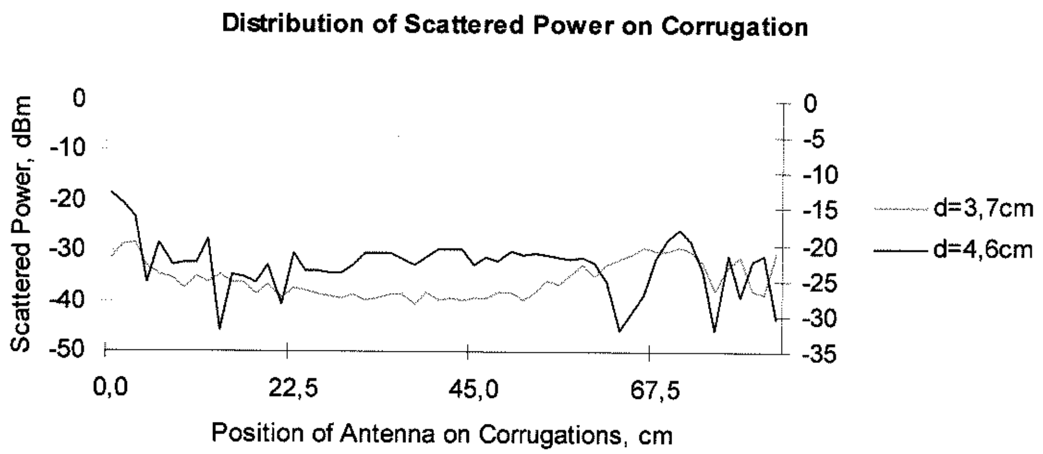

Geometry: d = 3,7cm, La-a = 103cm, f = 9,87GHz.
Geometry: d = 4,6cm, La-a = 102,5cm f = 10,5GHz, Attenuator = 0.

Evaluation of the Results

For Flat Waveguide

As you see in experimental part 3.2.2.(ii).c, distribution of scattered power is sinusoidal, in general, in according to features of plane waveguide.

All scattered power experiments are in agreement with the theoretical investigations.

REFERENCES

AMARI, S.; VAHLDIECK, R.; BORNEMANN, J.; Accurate analysis of periodic structures with an additional symmetry in the unit cell from classical matrix eigen values, Microwave Theory and Techniques, IEEE Transactions on, Volume: 46, Issue: 10, Oct. 1998, Pages: 1513-1515.

AMARI, S.; VAHLDIECK, R.; BORNEMANN, J.; LEUCHTMANN, P.;Spectrum of corrugated and periodically loaded waveguides from classical matrix eigen-values, Microwave Theory and Techniques, IEEE Transactions on, Volume: 48, Issue: 3, March 2000, Pages: 453-460.

BIRDSALL, C.K.; White, R.M.; Experiments with the Forbidden Regions of Open Periodic Structures: Application to Absorptive Filters Microwave Theory and Techniques, IEEE Transactions on, Volume: 12, Issue: 2, Mar 1964, Pages:197 – 202.

BRILLOUIN L. Brillouin, L., 1946, Wave Propagation in Periodic Structures. New York: Mc Graw-Hill. Reprinted by Dover (2^{nd} ed.), 1953, New York.

CHANG-WON Lee, Hyon Son, 1999, Periodically Slotted Dielectrically Filled Parallel-Plane Waveguide as a Leaky-Wave Antenna: E-Polarization Case. IEEE Transactions on Antennas and Propagation, vol: 47, no: 1, pp: 171.

DAVID M. POZAR, 1990, Microwave Engineering, Addison-Wesley Publishing Company.

ELACHI, C., 1976, Wave in Active and Passive Periodic Structures, A review. Proc. IEEE (64), 1966-1698.

ELACHI C. and YEH C., 1974, Mode Conversion in Periodically Disturbed Thin-Film Waveguides, J. Appl. Phys., (45), 8, 3493-3499.

ESTEBAN, J.; REBOLLAR, J.M.; Characterization of corrugated waveguides by modal analysis, Microwave Theory and Techniques, IEEE Transactions on, Volume: 39, Issue: 6, June1991, Pages: 937-943.

FENELON, J. P.; PAPIERNIK, A.; Theoretical and experimental study of the evolution of fields in an over dimensioned waveguide with a corrugated surface, Microwave Theory and Techniques, IEEE Transactions on, Volume: 39, Issue: 10, Oct. 1991 Pages: 1773-1779.

FREZZA, F.; PAJEWSKI, L.; SCHETTINI, G.; Characterization and design of two dimensional electromagnetic band-gap structures by use of a full-wave method for diffraction gratings, Microwave Theory and Techniques, IEEE Transactions on, Volume: 51, Issue: 3, March 2003, Pages: 941-951.

GOBLICK, T. J.; BEVENSEE, R. M.; Variational Principles and Mode Coupling in Periodic Structures, Microwave Theory and Techniques, IEEE Transactions on, Volume: 8, Issue: 5, Sep 1960, Pages: 500-509.

JAKOBY B., VELLEKOOP M. J., 2000, FFT-Based Analysis of Periodic Structures in Micro-acoustic Devices. IEEE Transactions on Ultrasonics Ferroelectrics and Frequency Control, vol: 47, no: 3, pp: 651-656.

KIM T., Seo C., 2000, A Novel Photonic Band gap Structure for Low-Pass Filter of Wide Stop band. IEEE Microwave and Guided Wave Letters, vol: 10, no: 1, pp: 13-15.

LEE R. K., XU Y., YARIV A., 1999, Micro-cavities, Photonic Band Gaps and Applications to Lasers and Optical Communications. LEOS'99. IEEE lasers and Electro-Optics Society 1999 12th Annual Meeting, vol: 1, pp: 54-55.

LEVY, R.; Tapered Corrugated Waveguide Low-pass Filters, Microwave Theory and Techniques, IEEE Transactions on, Volume: 21, Issue: 8, Aug 1973, Pages: 526-532.

LI Wei, LIT J. W. Y., 1997, Phase-Shifted Bragg Grating Filters with Symmetrical Structures. Light wave Technology, Journal of, vol: 15, no: 8, pp: 1405-1410.

LIU J., BUTLER J. K., EVANS G. A., ROSEN A., 1996, Analysis of Millimeter Wave Phase Shifters Coupled to a Fixed Periodic Structure. Microwave Theory and Techniques, IEEE Transactions on, vol: 44, no: 8, pp: 1416-1423.

MALLICK, A. K.; SANYAL, G. S.; Electromagnetic Wave Propagation in a Rectangular Waveguide with Sinusoidally Varying Width, Microwave Theory and Techniques, IEEE Transactions on, Volume: 26, Issue: 4, Apr 1978, Pages: 243 – 249.

MARCUSE D., 1972, Light Transmission Optics, Van Nostrand Reinhold, New York.

MATSUMOTO, M.; TSUTSUMI, M.; KUMAGAI, N.; Bragg Reflection Characteristics of Millimeter Waves in a Periodically Plasma-Induced Semiconductor Waveguide, Microwave Theory and Techniques, IEEE Transactions on, Volume: 34, Issue: 4, Apr 1986, Pages: 406-411.

NAVARRO, M.S.; ROZZI, T.E.; YUEN TZE LO; Propagation in a Rectangular Waveguide Periodically Loaded with Resonant Irises, Microwave Theory and Techniques, IEEE Transactions on, Volume: 28, Issue: 8, Aug 1980, Pages: 857– 865.

POGREBNYAK V. A., 1998, Electromagnetic Standing Wave resonances in a Dielectric Waveguide with a Periodically Irregular Boundary, Phys. Review E., (58), 5, 5261-5264.

POGREBNYAK V. A., YAKOVENKO V. M., and YAKOVENKO I. V., 1995, Surface Electronic States at the Boundary between Two Media, Phys. Lett. A., 209, 103.

POGREBNYAK V. A., 2003, Non-Bragg Reflections in a Periodic Waveguide. Optic Communications 232 (2004) 201-207.

POGREBNYAK V. A., Geometric resonance in a periodic waveguide, Journal of Applied Physics, vol: 94, No:10, pp: 6979-6981, 2003.

RICHARDS J.A., 1983, Analysis of Periodic Time-Varying Systems, Springer-Verlag.

RIZZOLI, V.; LIPPARINI, A.; Bloch-Wave Analysis of Strip-line - and Micro-strip-Array Slow–Wave Structures, Microwave Theory and Techniques, IEEE Transactions on, Volume: 29, Issue: 2, Feb 1981, Pages: 143-150.

ROTMAN, W.; OLINER, A.A.; Periodic Structures in Trough Waveguide, Microwave Theory and Techniques, IEEE Transactions on, Volume: 7, Issue: 1, Jan 1959, Pages: 134 – 142.

SAMUEL Y. LIAO, 1985, Microwave Devices and Circuits. Prentice-Hall, Inc., Englewood Cliffs, New Jersey, 07632.

SOLIMENO S., CROSIGNANI B., and DIPORTO P., 1986, Guiding, Diffraction, and Confinement of Optical Radiation, Academic, New York.

TAMIR T., H. C. WANG, A. A. OLINER, 1964, Wave Propagation in Sinusoidally Stratified Dielectric Media, IEEE Trans. Microwave Theory Tech., MTT (12), 323-335.

VOTRUBA, J.; Periodic waveguide structures with long cells Microwave Theory and Techniques, IEEE Transactions on, Volume: 48, Issue: 10, Oct. 2000, Pages: 1717-1724.

WEISSBERG, E.; Experimental Determination of Wavelength in Dielectric-Filled Periodic Structures (Correspondence), Microwave Theory and Techniques, IEEE Transactions on, Volume: 7, Issue: 4, Oct 1959, Pages: 480 – 481.

W.S. C. CHANG; Periodic Structures and Their Application in Integrated Optics, Microwave Theory and Techniques, IEEE Transactions on, Volume: 21, Issue: 12, Dec 1973, Pages: 775 – 785.

YAKUBOVICH V. A.; STARZHINSKI V. M., 1975, Linear Differential Equations with Periodic Coefficients, Vol. 1 and 2, Wiley, New York. (Translated from Russian).

YANG HYD., 2000, Surface-Wave Elimination in Integrated Circuit Structures with Artificial Periodic Materials. Electromagnetics, vol: 20, no: 2, pp: 125-130.

YANG Li, XU Shanjia, WU Xianliang, Editor(s): LIANO F. J., 1998, Multimode Network Analysis for Frequency Selective Characteristics of Dielectric Periodic Structures with Arbitrary Profiles. Microwave and Millimeter Wave Technology Proceedings, 1998. ICMMT'98. 1998 International Conference on, pp: 1049-1052.

YONGXI Qian, ITOH T., 1999, Planar Periodic Structures for Microwave and Millimeter Wave Circuit Applications. Microwave Symposium Digest, 1999 IEEE MTTT-S International, vol: 4, pp: 1533-1536.

ZENGERLE R., LEMINGER O., 1995, Phase-Shifted Bragg-Grating Filters with Improved Transmission Characteristics. Light wave Technology, Journal of, vol: 13, no: 12, pp: 2354-2358.

AUTOBIOGRAHY

I was born on 15 April 1979 in Antalya. I had my primary education in Antalya between years 1985-1990. I had my secondary school education between years 1990-1993. Then I continued my high school education in Karatay Super High School with one year English preparation course between years 1993-1997. After high school I entered Electrical and Electronics Department of University of Çukurova in 1998. I graduated from the university in 2002. And I continued Master program at Electrical and Electronics Engineering Department of University of Çukurova between years 2002-2005. I worked on periodic structures especially subject of "Investigation of Stop and Pass Bands in the Spectrum of a Periodically Corrugated Waveguide" with Prof. Dr. Victor Pogrebnyak.

APPENDIXES

APPENDIX I

Transmission ($ABCD$) Matrix and Table of the $ABCD$ Parameters of Some Useful Two Port Circuits

The Z, Y and S parameter representations can be used to characterize a microwave network with an arbitrary number of ports, but in practice many microwave networks consist of a cascade connection of two or more two-port networks. In this case it is convenient to define a 2 X 2 transmission, or $ABCD$ matrix, for each two- port network. We will then see that the $ABCD$ matrix of the cascade connection of two or more two-port networks can be easily found by multiplying the $ABCD$ matrices of the individual two-ports.

The $ABCD$ matrix is defined for a two-port network in terms of the total voltages and currents as shown in figure 6.1.a and the following

$$V_1 = AV_2 + BI_2 \tag{6.1}$$

$$I_1 = CV_2 + DI_2 \tag{6.2}$$

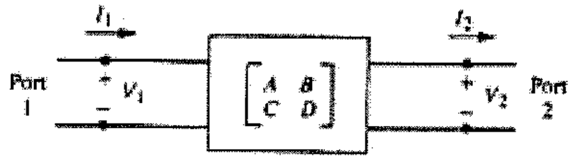

(a)

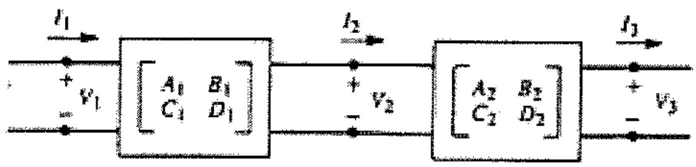

(b)

Figure 6.1. (a) A two-port network; (b) A cascade connection of two-port networks. (David M. Pozar, Microwave Engineering, 1993)

In matrix form as;

$$\begin{bmatrix} V_1 \\ I_1 \end{bmatrix} = \begin{bmatrix} A\,B \\ C\,D \end{bmatrix} \begin{bmatrix} V_2 \\ I_2 \end{bmatrix} \tag{6.3}$$

In the cascade connection of two two-port networks shown in Figure 5.1b, we have that;

$$\begin{bmatrix} V_1 \\ I_1 \end{bmatrix} = \begin{bmatrix} A_1\,B_1 \\ C_1\,D_1 \end{bmatrix} \begin{bmatrix} V_2 \\ I_2 \end{bmatrix} \tag{6.4a}$$

$$\begin{bmatrix} V_2 \\ I_2 \end{bmatrix} = \begin{bmatrix} A_2\,B_2 \\ C_2\,D_2 \end{bmatrix} \begin{bmatrix} V_3 \\ I_3 \end{bmatrix} \tag{6.4b}$$

Substituting equation (6.4b) into (6.4a) gives;

$$\begin{bmatrix} V_1 \\ I_1 \end{bmatrix} = \begin{bmatrix} A_1\,B_1 \\ C_1\,D_1 \end{bmatrix} \begin{bmatrix} A_2\,B_2 \\ C_2\,D_2 \end{bmatrix} \begin{bmatrix} V_3 \\ I_3 \end{bmatrix} \tag{6.5}$$

Table 6.1. Table of ABCD Parameters of Some Useful Two Port Circuits

Circuit	ABCD Parameters	
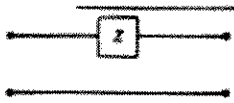	$A = 1$ $C = 0$	$B = Z$ $D = 1$
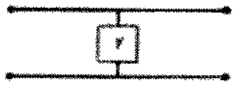	$A = 1$ $C = Y$	$B = 0$ $D = 1$
	$A = \cos \beta\ell$ $C = jY_0 \sin \beta\ell$	$B = jZ_0 \sin \beta\ell$ $D = \cos \beta\ell$
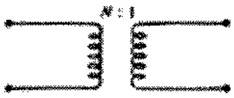	$A = N$ $C = 0$	$B = 0$ $D = \frac{1}{N}$
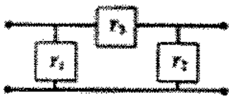	$A = 1 + \frac{Y_2}{Y_3}$ $C = Y_1 + Y_2 + \frac{Y_1 Y_2}{Y_3}$	$B = \frac{1}{Y_3}$ $D = 1 + \frac{Y_1}{Y_3}$
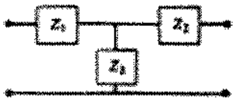	$A = 1 + \frac{Z_1}{Z_3}$ $C = \frac{1}{Z_3}$	$B = Z_1 + Z_2 + \frac{Z_1 Z_2}{Z_3}$ $D = 1 + \frac{Z_2}{Z_3}$

(David M. Pozar, Microwave Engineering, 1993)

APPENDIX II

Taylor, Mclaurin Series and Expressing $\varphi(x,y)$ in Mclaurin Series at Boundaries for Periodically One Dimensional Corrugated Waveguide

$$P(x,y) = f(a) + \frac{f'(a)}{1!}(x-a) + ... + \frac{f^{n}(a)}{n!}(x-a)^{n}$$

$$= \sum_{n=0}^{\infty} \frac{f^{n}(a)}{n!}(x-a)^{n} \rightarrow \text{Taylor Series at } x = a.$$

$$= \sum_{n=0}^{\infty} \frac{f^{n}(0)}{n!}.x^{n} \rightarrow \text{Mclaurin Series.}$$

For Lower Boundary ($y = -d/2 + \xi\cos(qx)$), ($k_{yn} = k_n$)

$$\varphi\left(x, -\frac{d}{2}\right) = \sum_{n}\left[a_n \cos\left(-k_n \frac{d}{2}\right) + b_n \sin\left(-k_n \frac{d}{2}\right)\right].e^{j(k_x + nq)x}$$

$$\varphi'(x,y) = \sum_{n}\left[-a_n k_n \sin(k_n y) + b_n k_n \cos(k_n y)\right].e^{j(k_x + nq)x}$$

$$\varphi'(x, -\frac{d}{2}) = \sum_{n}\left[-a_n k_n \sin\left(-k_n \frac{d}{2}\right) + b_n k_n \cos\left(-k_n \frac{d}{2}\right)\right].e^{j(k_x + nq)x}$$

$$\varphi''(x,y) = \sum_{n}\left[-a_n k_n^{2} \cos(k_n y) - b_n k_n^{2} \sin(k_n y)\right].e^{j(k_x + nq)x}$$

$$\varphi''(x, -\frac{d}{2}) = \sum_{n}\left[-a_n k_n^{2} \cos\left(-k_n \frac{d}{2}\right) - b_n k_n^{2} \sin\left(-k_n \frac{d}{2}\right)\right].e^{j(k_x + nq)x}$$

$$\varphi(x,y)(-d/2)=\varphi\left(x,-\frac{d}{2}\right)+\varphi^{'}\left(x,-\frac{d}{2}\right)\left(y-\left(-\frac{d}{2}\right)\right)+\frac{1}{2}!\varphi^{''}\left(x,-\frac{d}{2}\right)\left(y-\left(-\frac{d}{2}\right)\right)^{2}$$

$$=\sum_{n}\left[a_n\cos\left(-k_n\frac{d}{2}\right)+b_n\sin\left(-k_n\frac{d}{2}\right)\right]e^{j(k_x+nq)x}$$
$$+\sum_{n}\left[-a_nk_n\sin\left(-k_n\frac{d}{2}\right)+b_nk_n\cos\left(-k_n\frac{d}{2}\right)\right]e^{j(k_x+nq)x}.\left(y+\frac{d}{2}\right)$$
$$+\frac{1}{2!}\sum_{n}\left[-a_nk_n^{2}\cos\left(-k_n\frac{d}{2}\right)-b_nk_n^{2}\sin\left(-k_n\frac{d}{2}\right)\right]e^{j(k_x+nq)x}.\left(y+\frac{d}{2}\right)^{2}$$

$$\varphi(x,y)(y=-d/2)=\sum_{n}\left[a_n\cos\left(k_n\frac{d}{2}\right)-b_n\sin\left(k_n\frac{d}{2}\right)\right]e^{j(k_x+nq)x}$$
$$+\sum_{n}\left[a_nk_n\sin\left(k_n\frac{d}{2}\right)+b_nk_n\cos\left(k_n\frac{d}{2}\right)\right]e^{j(k_x+nq)x}.\left(-\frac{d}{2}+\xi\cos(qx)+\frac{d}{2}\right)$$
$$+\frac{1}{2!}\sum_{n}\left[-a_nk_n^{2}\cos\left(k_n\frac{d}{2}\right)+b_nk_n^{2}\sin\left(k_n\frac{d}{2}\right)\right]e^{j(k_x+nq)x}.\left(-\frac{d}{2}+\xi\cos(qx)+\frac{d}{2}\right)^{2}$$

$$\varphi(x,y)\downarrow_{y=-\frac{d}{2}}=\sum_{n}\left[a_n\cos\left(k_n\frac{d}{2}\right)-b_n\sin\left(k_n\frac{d}{2}\right)\right]e^{j(k_x+nq)x}$$
$$+\sum_{n}\left[a_nk_n\sin\left(k_n\frac{d}{2}\right)+b_nk_n\cos\left(k_n\frac{d}{2}\right)\right].e^{j(k_x+nq)x}.(\xi\cos(qx))$$
$$+\frac{1}{2!}\sum_{n}\left[-a_nk_n^{2}\cos\left(k_n\frac{d}{2}\right)+b_nk_n^{2}\sin\left(k_n\frac{d}{2}\right)\right]e^{j(k_x+nq)x}.(\xi\cos(qx))^{2}$$

$$\varphi(x,y)(y=-d/2)=\sum_{n}\left[\left[a_n\cos\left(k_n\frac{d}{2}\right)-b_n\sin\left(k_n\frac{d}{2}\right)\right].e^{j(k_x+nq)x}\right.$$
$$+\left[a_nk_n\sin\left(k_n\frac{d}{2}\right)+b_nk_n\cos\left(k_n\frac{d}{2}\right)\right].\xi\cos(qx).e^{j(k_x+nq)x}$$
$$\left.+\left[-\frac{1}{2}a_nk_n^{2}\cos\left(k_n\frac{d}{2}\right)+\frac{1}{2}b_nk_n^{2}\sin\left(k_n\frac{d}{2}\right)\right].\xi^{2}.\cos^{2}(qx).e^{j(k_x+nq)x}\right] \qquad (6.6)$$

For Upper Boundary ($y = d/2 + \rho\cos(qx+\theta)$), ($k_{yn} = k_n$)

$$\varphi\left(x,\frac{d}{2}\right) = \sum_n \left[a_n \cos\left(k_n \frac{d}{2}\right) + b_n \sin\left(k_n \frac{d}{2}\right)\right].e^{j(k_x+nq)x}$$

$$\varphi^{'}(x,y) = \sum_n \left[-a_n k_n \sin(k_n y) + b_n k_n \cos(k_n y)\right].e^{j(k_x+nq)x}$$

$$\varphi^{'}\left(x,\frac{d}{2}\right) = \sum_n \left[-a_n k_n \sin\left(k_n \frac{d}{2}\right) + b_n k_n \cos\left(k_n \frac{d}{2}\right)\right].e^{j(k_x+nq)x}$$

$$\varphi^{''}(x,y) = \sum_n [-a_n k_n^{\,2} \cos(k_n y) - b_n k_n^{\,2} \sin(k_n y)].e^{j(k_x+nq)x}$$

$$\varphi^{''}\left(x,\frac{d}{2}\right) = \sum_n \left[-a_n k_n^{\,2} \cos\left(k_n \frac{d}{2}\right) - b_n k_n^{\,2} \sin\left(k_n \frac{d}{2}\right)\right].e^{j(k_x+nq)x}$$

$$\varphi(x,y)(y=d/2) = \varphi\left(x,\frac{d}{2}\right) + \varphi^{'}\left(x,\frac{d}{2}\right)\left(y-\frac{d}{2}\right) + \frac{1}{2}!\varphi^{''}\left(x,\frac{d}{2}\right)\left(y-\frac{d}{2}\right)^2$$

$$= \sum_n \left[a_n \cos\left(k_n \frac{d}{2}\right) + b_n \sin\left(k_n \frac{d}{2}\right)\right]e^{j(k_x+nq)x}$$

$$+\sum_n \left[-a_n k_n \sin\left(k_n \frac{d}{2}\right) + b_n k_n \cos\left(k_n \frac{d}{2}\right)\right]e^{j(k_x+nq)x}.\left(y-\frac{d}{2}\right)$$

$$+\frac{1}{2!}\sum_n \left[-a_n k_n^{\,2} \cos\left(k_n \frac{d}{2}\right) - b_n k_n^{\,2} \sin\left(k_n \frac{d}{2}\right)\right]e^{j(k_x+nq)x}.\left(y-\frac{d}{2}\right)^2$$

$$\varphi(x,y)(y=d/2) = \sum_n \left[a_n \cos\left(k_n \frac{d}{2}\right) + b_n \sin\left(k_n \frac{d}{2}\right)\right]e^{j(k_x+nq)x}$$

$$+\sum_n \left[-a_n k_n \sin\left(k_n \frac{d}{2}\right) + b_n k_n \cos\left(k_n \frac{d}{2}\right)\right]e^{j(k_x+nq)x}.\rho\cos(qx+\theta)$$

$$+\frac{1}{2!}\sum_n \left[-a_n k_n^{\,2} \cos\left(k_n \frac{d}{2}\right) - b_n k_n^{\,2} \sin\left(k_n \frac{d}{2}\right)\right]e^{j(k_x+nq)x}.\rho^2\cos^2(qx+\theta)$$

$$\varphi(x,y)(y=d/2)=\sum_n\Bigg[[a_n\cos(k_n\frac{d}{2})+b_n\sin(k_n\frac{d}{2})].e^{j(k_x+nq)x}$$

$$+[-a_nk_n\sin(k_n\frac{d}{2})+b_nk_n\cos(k_n\frac{d}{2})]\rho\cos(qx+\theta).e^{j(k_x+nq)x}$$

$$+[-\frac{1}{2}a_nk_n^2\cos(k_n\frac{d}{2})-\frac{1}{2}b_nk_n^2\sin(k_n\frac{d}{2})].\rho^2\cos^2(qx+\theta)].e^{j(k_x+nq)x}\Bigg] \quad (6.7)$$

APPENDIX III

Expressing $\varphi(x,y)$ in Mclaurin Series at Boundaries for Periodically Two Dimensional Corrugated Waveguide

For Lower Boundary (y=0), ($k_{y_{nm}} = k_{nm}$)

$$\varphi(x,0,z) = \sum_{nm} \left[a_{nm} \cos(k_{nm}0) + b_{nm} \sin(k_{nm}0) \right] e^{j(k_x+nq)x+j(k_z+m\chi)z}$$

$$\varphi'(x,y,z) = \sum_{nm} \left[-a_{nm}k_{nm} \sin(k_{nm}y) + b_{nm}k_{nm} \cos(k_{nm}y) \right] e^{j(k_x+nq)x+j(k_z+m\chi)z}$$

$$\varphi'(x,0,z) = \sum_{nm} \left[-a_{nm}k_{nm} \sin(k_{nm}0) + b_{nm}k_{nm} \cos(k_{nm}0) \right] e^{j(k_x+nq)x+j(k_z+m\chi)z}$$

$$\varphi''(x,y,z) = \sum_{nm} \left[-a_{nm}k_{nm}^2 \cos(k_{nm}y) - b_{nm}k_{nm}^2 \sin(k_{nm}y) \right] e^{j(k_x+nq)x+j(k_z+m\chi)z}$$

$$\varphi''(x,0,z) = \sum_{nm} \left[-a_{nm}k_{nm}^2 \cos(k_{nm}0) - b_{nm}k_{nm}^2 \sin(k_{nm}0) \right] e^{j(k_x+nq)x+j(k_z+m\chi)z}$$

$$\varphi(x,y,z)(y=0) = \varphi(x,0,z) + \varphi'(x,0,z)(y-0) + \frac{1}{2!}\varphi''(x,0,z)(y-0)^2$$

$$\varphi(x,y,z)(y=0) = \sum_{nm} \Big[a_{nm} e^{j(k_x+nq)x+j(k_z+m\chi)z} + b_{nm}k_{nm} e^{j(k_x+nq)x+j(k_z+m\chi)z} .(\xi \cos \chi z)$$
$$- \frac{1}{2!} a_{nm}k_{nm}^2 e^{j(k_x+nq)x+j(k_z+m\chi)z} .(\xi^2 \cos^2 \chi z) \Big] \qquad (6.8)$$

For Upper Boundary ($y = d$), ($k_{y_{nm}} = k_{nm}$)

$$\varphi(x,d,z) = \sum_{nm}\left[a_{nm}\cos(k_{nm}d) + b_{nm}\sin(k_{nm}d)\right]e^{j(k_x+nq)x+j(k_z+m\chi)z}$$

$$\varphi'(x,y,z) = \sum_{nm}\left[-a_{nm}k_{nm}\sin(k_{nm}y) + b_{nm}k_{nm}\cos(k_{nm}y)\right]e^{j(k_x+nq)x+j(k_z+m\chi)z}$$

$$\varphi''(x,y,z) = \sum_{nm}\left[-a_{nm}k_{nm}^2\cos(k_{nm}y) - b_{nm}k_{nm}^2\sin(k_{nm}y)\right]e^{j(k_x+nq)x+j(k_z+m\chi)z}$$

$$\begin{aligned}\varphi(x,y,z)(y=d) = \sum_{nm}\Big[&\left[a_{nm}\cos(k_{nm}d) + b_{nm}\sin(k_{nm}d)\right] \\ &+\left[-a_{nm}k_{nm}\sin(k_{nm}d) + b_{nm}k_{nm}\cos(k_{nm}d)\right].(d-\rho\cos qx - d) \\ &+\frac{1}{2!}\left[-a_{nm}k_{nm}^2\cos(k_{nm}d) - b_{nm}k_{nm}^2\sin(k_{nm}d)\right].(d-\rho\cos qx - d)^2\Big]\,e^{j(k_x+nq)x+j(k_z+m\chi)z}\end{aligned} \tag{6.9}$$

Constituting System of Linear Algebraic Equations for Coefficients and Calculations for Matrix of Dispersion Equation

For Lower Boundary

$n = -1,\ m = -1$

$$\begin{aligned}\varphi(x,y,z)(y=0) = a_{-1-1}e^{j(k_x-q)x+j(k_z-\chi)z} + b_{-1-1}k_{-1-1}e^{j(k_x-q)x+j(k_z-\chi)z}.(\xi\cos\chi z) \\ -\frac{1}{2}a_{-1-1}k_{-1-1}^2e^{j(k_x-q)x+j(k_z-\chi)z}.(\xi^2\cos^2\chi z)\end{aligned}$$

$n = -1, \ m = 0$

$$\varphi(x,y,z)(y=0) = a_{-10}e^{j(k_x-q)x+j(k_z)z} + b_{-10}k_{-10}e^{j(k_x-q)x+j(k_z)z}.(\xi\cos\chi z)$$
$$-\frac{1}{2}a_{-10}k_{-10}^2e^{j(k_x-q)x+j(k_z)z}.(\xi^2\cos^2\chi z)$$

$n = -1, \ m = 1$

$$\varphi(x,y,z)(y=0) = a_{-11}e^{j(k_x-q)x+j(k_z+\chi)z} + b_{-11}k_{-11}e^{j(k_x-q)x+j(k_z+\chi)z}.(\xi\cos\chi z)$$
$$-\frac{1}{2}a_{-11}k_{-11}^2e^{j(k_x-q)x+j(k_z+\chi)z}.(\xi^2\cos^2\chi z)$$

$n = 0, \ m = -1$

$$\varphi(x,y,z)(y=0) = a_{0-1}e^{j(k_x)x+j(k_z-\chi)z} + b_{0-1}k_{0-1}e^{j(k_x)x+j(k_z-\chi)z}.(\xi\cos\chi z)$$
$$-\frac{1}{2}a_{0-1}k_{0-1}^2e^{j(k_x)x+j(k_z-\chi)z}.(\xi^2\cos^2\chi z)$$

$n = 0, \ m = 0$

$$\varphi(x,y,z)(y=0) = a_{00}e^{j(k_x)x+j(k_z)z} + b_{00}k_{00}e^{j(k_x)x+j(k_z)z}.(\xi\cos\chi z)$$
$$-\frac{1}{2}a_{00}k_{00}^2e^{j(k_x)x+j(k_z)z}.(\xi^2\cos^2\chi z)$$

$n = 0, \ m = 1$

$$\varphi(x,y,z)(y=0) = a_{01}e^{j(k_x)x+j(k_z+\chi)z} + b_{01}k_{01}e^{j(k_x)x+j(k_z+\chi)z}.(\xi\cos\chi z)$$
$$-\frac{1}{2}a_{01}k_{01}^2e^{j(k_x)x+j(k_z+\chi)z}.(\xi^2\cos^2\chi z)$$

$n=1,\ m=-1$

$$\varphi(x,y,z)(y=0)=a_{1-1}e^{j(k_x+q)x+j(k_z-\chi)z}+b_{1-1}k_{1-1}e^{j(k_x+q)x+j(k_z-\chi)z}.(\xi\cos\chi z)$$
$$-\frac{1}{2}a_{1-1}k_{1-1}^2e^{j(k_x+q)x+j(k_z-\chi)z}.(\xi^2\cos^2\chi z)$$

$n=1,\ m=0$

$$\varphi(x,y,z)(y=0)=a_{10}e^{j(k_x+q)x+j(k_z)z}+b_{10}k_{10}e^{j(k_x+q)x+j(k_z)z}.(\xi\cos\chi z)$$
$$-\frac{1}{2}a_{10}k_{10}^2e^{j(k_x+q)x+j(k_z)z}.(\xi^2\cos^2\chi z)$$

$n=1,\ m=1$

$$\varphi(x,y,z)(y=0)=a_{11}e^{j(k_x+q)x+j(k_z+\chi)z}+b_{11}k_{11}e^{j(k_x+q)x+j(k_z+\chi)z}.(\xi\cos\chi z)$$
$$-\frac{1}{2}a_{11}k_{11}^2e^{j(k_x+q)x+j(k_z+\chi)z}.(\xi^2\cos^2\chi z)$$

If we substitute the $\dfrac{e^{j\chi z}+e^{-j\chi z}}{2}$ instead of $\cos\chi z$;

$n=-1,\ m=-1$

$$\varphi=a_{-1-1}e^{j(k_x-q)x+j(k_z-\chi)z}+b_{-1-1}k_{-1-1}e^{j(k_x-q)x+j(k_z-\chi)z}.\frac{\xi}{2}(e^{j\chi z}+e^{-j\chi z})$$
$$-a_{-1-1}k_{-1-1}^2e^{j(k_x-q)x+j(k_z-\chi)z}.\frac{\xi^2}{8}(e^{j2\chi z}+e^{-j2\chi z}+2)$$

$n=-1,\ \ m=0$

$$\varphi = a_{-10}e^{j(k_x-q)x+j(k_z)z} + b_{-10}k_{-10}e^{j(k_x-q)x+j(k_z)z}.\frac{\xi}{2}(e^{j\chi z}+e^{-j\chi z})$$
$$-a_{-10}k_{-10}^2e^{j(k_x-q)x+j(k_z)z}.\frac{\xi^2}{8}(e^{j2\chi z}+e^{-j2\chi z}+2)$$

$n=-1,\ \ m=1$

$$\varphi = a_{-11}e^{j(k_x-q)x+j(k_z+\chi)z} + b_{-11}k_{-11}e^{j(k_x-q)x+j(k_z+\chi)z}.\frac{\xi}{2}(e^{j\chi z}+e^{-j\chi z})$$
$$-a_{-11}k_{-11}^2e^{j(k_x-q)x+j(k_z+\chi)z}.\frac{\xi^2}{8}(e^{j2\chi z}+e^{-j2\chi z}+2)$$

$n=0,\ \ m=-1$

$$\varphi = a_{0-1}e^{j(k_x)x+j(k_z-\chi)z} + b_{0-1}k_{0-1}e^{j(k_x)x+j(k_z-\chi)z}.\frac{\xi}{2}(e^{j\chi z}+e^{-j\chi z})$$
$$-a_{0-1}k_{0-1}^2e^{j(k_x)x+j(k_z-\chi)z}.\frac{\xi^2}{8}(e^{j2\chi z}+e^{-j2\chi z}+2)$$

$n=0,\ \ m=0$

$$\varphi = a_{00}e^{j(k_x)x+j(k_z)z} + b_{00}k_{00}e^{j(k_x)x+j(k_z)z}.\frac{\xi}{2}(e^{j\chi z}+e^{-j\chi z})$$
$$-a_{00}k_{00}^2e^{j(k_x)x+j(k_z)z}.\frac{\xi^2}{8}(e^{j2\chi z}+e^{-j2\chi z}+2)$$

$n=0,\ \ m=1$

$$\varphi = a_{01}e^{j(k_x)x+j(k_z+\chi)z} + b_{01}k_{01}e^{j(k_x)x+j(k_z+\chi)z}.\frac{\xi}{2}(e^{j\chi z}+e^{-j\chi z})$$
$$-a_{01}k_{01}^2 e^{j(k_x)x+j(k_z+\chi)z}.\frac{\xi^2}{8}(e^{j2\chi z}+e^{-j2\chi z}+2)$$

$n=1,\ \ m=-1$

$$\varphi = a_{1-1}e^{j(k_x+q)x+j(k_z-\chi)z} + b_{1-1}k_{1-1}e^{j(k_x+q)x+j(k_z-\chi)z}.\frac{\xi}{2}(e^{j\chi z}+e^{-j\chi z})$$
$$-a_{1-1}k_{1-1}^2 e^{j(k_x+q)x+j(k_z-\chi)z}.\frac{\xi^2}{8}(e^{j2\chi z}+e^{-j2\chi z}+2)$$

$n=1,\ \ m=0$

$$\varphi = a_{10}e^{j(k_x+q)x+j(k_z)z} + b_{10}k_{10}e^{j(k_x+q)x+j(k_z)z}.\frac{\xi}{2}(e^{j\chi z}+e^{-j\chi z})$$
$$-a_{10}k_{10}^2 e^{j(k_x+q)x+j(k_z)z}.\frac{\xi^2}{8}(e^{j2\chi z}+e^{-j2\chi z}+2)$$

$n=1,\ \ m=1$

$$\varphi = a_{11}e^{j(k_x+q)x+j(k_z+\chi)z} + b_{11}k_{11}e^{j(k_x+q)x+j(k_z+\chi)z}.\frac{\xi}{2}(e^{j\chi z}+e^{-j\chi z})$$
$$-a_{11}k_{11}^2 e^{j(k_x+q)x+j(k_z+\chi)z}.\frac{\xi^2}{8}(e^{j2\chi z}+e^{-j2\chi z}+2)$$

If we rearrange the exponential terms;

$n=-1,\ m=-1$

$$\varphi = a_{-1-1}e^{j(k_x-q)x+j(k_z-\chi)z} + b_{-1-1}k_{-1-1}e^{j(k_x-q)x+j(k_z-\chi)z}.\frac{\xi}{2}e^{j\chi z} + b_{-1-1}k_{-1-1}e^{j(k_x-q)x+j(k_z-\chi)z}.\frac{\xi}{2}e^{-j\chi z}$$
$$-a_{-1-1}k_{-1-1}^2e^{j(k_x-q)x+j(k_z-\chi)z}.\frac{\xi^2}{8}e^{j2\chi z} - a_{-1-1}k_{-1-1}^2e^{j(k_x-q)x+j(k_z-\chi)z}.\frac{\xi^2}{8}e^{-j2\chi z} - a_{-1-1}k_{-1-1}^2e^{j(k_x-q)x+j(k_z-\chi)z}.\frac{\xi^2}{4})$$

$$\varphi = a_{-1-1}e^{j(k_x-q)x+j(k_z-\chi)z} + b_{-1-1}k_{-1-1}e^{j(k_x-q)x+j(k_z)z}.\frac{\xi}{2} + b_{-1-1}k_{-1-1}e^{j(k_x-q)x+j(k_z-2\chi)z}.\frac{\xi}{2}$$
$$-a_{-1-1}k_{-1-1}^2e^{j(k_x-q)x+j(k_z+\chi)z}.\frac{\xi^2}{8} - a_{-1-1}k_{-1-1}^2e^{j(k_x-q)x+j(k_z-3\chi)z}.\frac{\xi^2}{8} - a_{-1-1}k_{-1-1}^2e^{j(k_x-q)x+j(k_z-\chi)z}.\frac{\xi^2}{4})$$

$n=-1,\ m=0$

$$\varphi = a_{-10}e^{j(k_x-q)x+j(k_z)z} + b_{-10}k_{-10}e^{j(k_x-q)x+j(k_z)z}.\frac{\xi}{2}e^{j\chi z} + b_{-10}k_{-10}e^{j(k_x-q)x+j(k_z)z}.\frac{\xi}{2}e^{-j\chi z}$$
$$-a_{-10}k_{-10}^2e^{j(k_x-q)x+j(k_z)z}.\frac{\xi^2}{8}e^{j2\chi z} - a_{-10}k_{-10}^2e^{j(k_x-q)x+j(k_z)z}.\frac{\xi^2}{8}e^{-j2\chi z} - a_{-10}k_{-10}^2e^{j(k_x-q)x+j(k_z)z}.\frac{\xi^2}{4})$$

$$\varphi = a_{-10}e^{j(k_x-q)x+j(k_z)z} + b_{-10}k_{-10}e^{j(k_x-q)x+j(k_z+\chi)z}.\frac{\xi}{2} + b_{-10}k_{-10}e^{j(k_x-q)x+j(k_z-\chi)z}.\frac{\xi}{2}$$
$$-a_{-10}k_{-10}^2e^{j(k_x-q)x+j(k_z+2\chi)z}.\frac{\xi^2}{8} - a_{-10}k_{-10}^2e^{j(k_x-q)x+j(k_z-2\chi)z}.\frac{\xi^2}{8} - a_{-10}k_{-10}^2e^{j(k_x-q)x+j(k_z)z}.\frac{\xi^2}{4})$$

$n=-1,\ m=1$

$$\varphi = a_{-11}e^{j(k_x-q)x+j(k_z+\chi)z} + b_{-11}k_{-11}e^{j(k_x-q)x+j(k_z+\chi)z}.\frac{\xi}{2}e^{j\chi z} + b_{-11}k_{-11}e^{j(k_x-q)x+j(k_z+\chi)z}.\frac{\xi}{2}e^{-j\chi z}$$
$$-a_{-11}k_{-11}^2e^{j(k_x-q)x+j(k_z+\chi)z}.\frac{\xi^2}{8}e^{j2\chi z} - a_{-11}k_{-11}^2e^{j(k_x-q)x+j(k_z+\chi)z}.\frac{\xi^2}{8}e^{-j2\chi z} - a_{-11}k_{-11}^2e^{j(k_x-q)x+j(k_z+\chi)z}.\frac{\xi^2}{4})$$

$$\varphi = a_{-11}e^{j(k_x-q)x+j(k_z+\chi)z} + b_{-11}k_{-11}e^{j(k_x-q)x+j(k_z+2\chi)z}.\frac{\xi}{2} + b_{-11}k_{-11}e^{j(k_x-q)x+j(k_z)z}.\frac{\xi}{2}$$
$$-a_{-11}k_{-11}^2e^{j(k_x-q)x+j(k_z+3\chi)z}.\frac{\xi^2}{8} - a_{-11}k_{-11}^2e^{j(k_x-q)x+j(k_z-\chi)z}.\frac{\xi^2}{8} - a_{-11}k_{-11}^2e^{j(k_x-q)x+j(k_z+\chi)z}.\frac{\xi^2}{4})$$

$n=0,\ \ m=-1$

$$\varphi=a_{0-1}e^{j(k_x)x+j(k_z-\chi)z}+b_{0-1}k_{0-1}e^{j(k_x)x+j(k_z-\chi)z}.\frac{\xi}{2}e^{j\chi z}+b_{0-1}k_{0-1}e^{j(k_x)x+j(k_z-\chi)z}.\frac{\xi}{2}e^{-j\chi z}$$
$$-a_{0-1}k_{0-1}^2e^{j(k_x)x+j(k_z-\chi)z}.\frac{\xi^2}{8}e^{j2\chi z}-a_{0-1}k_{0-1}^2e^{j(k_x)x+j(k_z-\chi)z}\frac{\xi^2}{8}.e^{-j2\chi z}-a_{0-1}k_{0-1}^2e^{j(k_x)x+j(k_z-\chi)z}\frac{\xi^2}{4})$$

$$\varphi=a_{0-1}e^{j(k_x)x+j(k_z-\chi)z}+b_{0-1}k_{0-1}e^{j(k_x)x+j(k_z)z}.\frac{\xi}{2}+b_{0-1}k_{0-1}e^{j(k_x)x+j(k_z-2\chi)z}.\frac{\xi}{2}$$
$$-a_{0-1}k_{0-1}^2e^{j(k_x)x+j(k_z+\chi)z}.\frac{\xi^2}{8}-a_{0-1}k_{0-1}^2e^{j(k_x)x+j(k_z-3\chi)z}\frac{\xi^2}{8}-a_{0-1}k_{0-1}^2e^{j(k_x)x+j(k_z-\chi)z}\frac{\xi^2}{4})$$

$n=0,\ \ m=0$

$$\varphi=a_{00}e^{j(k_x)x+j(k_z)z}+b_{00}k_{00}e^{j(k_x)x+j(k_z)z}.\frac{\xi}{2}e^{j\chi z}+b_{00}k_{00}e^{j(k_x)x+j(k_z)z}.\frac{\xi}{2}e^{-j\chi z}$$
$$-a_{00}k_{00}^2e^{j(k_x)x+j(k_z)z}.\frac{\xi^2}{8}e^{j2\chi z}-a_{00}k_{00}^2e^{j(k_x)x+j(k_z)z}.\frac{\xi^2}{8}e^{-j2\chi z}-a_{00}k_{00}^2e^{j(k_x)x+j(k_z)z}.\frac{\xi^2}{4})$$

$$\varphi=a_{00}e^{j(k_x)x+j(k_z)z}+b_{00}k_{00}e^{j(k_x)x+j(k_z+\chi)z}.\frac{\xi}{2}+b_{00}k_{00}e^{j(k_x)x+j(k_z-\chi)z}.\frac{\xi}{2}$$
$$-a_{00}k_{00}^2e^{j(k_x)x+j(k_z+2\chi)z}.\frac{\xi^2}{8}-a_{00}k_{00}^2e^{j(k_x)x+j(k_z-2\chi)z}.\frac{\xi^2}{8}-a_{00}k_{00}^2e^{j(k_x)x+j(k_z)z}.\frac{\xi^2}{4})$$

$n=0,\ \ m=1$

$$\varphi=a_{01}e^{j(k_x)x+j(k_z+\chi)z}+b_{01}k_{01}e^{j(k_x)x+j(k_z+\chi)z}.\frac{\xi}{2}e^{j\chi z}+b_{01}k_{01}e^{j(k_x)x+j(k_z+\chi)z}.\frac{\xi}{2}e^{-j\chi z}$$
$$-a_{01}k_{01}^2e^{j(k_x)x+j(k_z+\chi)z}.\frac{\xi^2}{8}e^{j2\chi z}-a_{01}k_{01}^2e^{j(k_x)x+j(k_z+\chi)z}.\frac{\xi^2}{8}e^{-j2\chi z}-a_{01}k_{01}^2e^{j(k_x)x+j(k_z+\chi)z}.\frac{\xi^2}{4})$$

$$\varphi = a_{01}e^{j(k_x)x+j(k_z+\chi)z} + b_{01}k_{01}e^{j(k_x)x+j(k_z+2\chi)z}.\frac{\xi}{2} + b_{01}k_{01}e^{j(k_x)x+j(k_z)z}.\frac{\xi}{2}$$
$$-a_{01}k_{01}^2e^{j(k_x)x+j(k_z+3\chi)z}.\frac{\xi^2}{8} - a_{01}k_{01}^2e^{j(k_x)x+j(k_z-\chi)z}.\frac{\xi^2}{8} - a_{01}k_{01}^2e^{j(k_x)x+j(k_z+\chi)z}.\frac{\xi^2}{4})$$

$n=1,\ m=-1$

$$\varphi = a_{1-1}e^{j(k_x+q)x+j(k_z-\chi)z} + b_{1-1}k_{1-1}e^{j(k_x+q)x+j(k_z-\chi)z}.\frac{\xi}{2}e^{j\chi z} + b_{1-1}k_{1-1}e^{j(k_x+q)x+j(k_z-\chi)z}.\frac{\xi}{2}e^{-j\chi z}$$
$$-a_{1-1}k_{1-1}^2e^{j(k_x+q)x+j(k_z-\chi)z}.\frac{\xi^2}{8}e^{j2\chi z} - a_{1-1}k_{1-1}^2e^{j(k_x+q)x+j(k_z-\chi)z}.\frac{\xi^2}{8}e^{-j2\chi z} - a_{1-1}k_{1-1}^2e^{j(k_x+q)x+j(k_z-\chi)z}.\frac{\xi^2}{4})$$

$$\varphi = a_{1-1}e^{j(k_x+q)x+j(k_z-\chi)z} + b_{1-1}k_{1-1}e^{j(k_x+q)x+j(k_z)z}.\frac{\xi}{2} + b_{1-1}k_{1-1}e^{j(k_x+q)x+j(k_z-2\chi)z}.\frac{\xi}{2}$$
$$-a_{1-1}k_{1-1}^2e^{j(k_x+q)x+j(k_z+\chi)z}.\frac{\xi^2}{8} - a_{1-1}k_{1-1}^2e^{j(k_x+q)x+j(k_z-3\chi)z}.\frac{\xi^2}{8} - a_{1-1}k_{1-1}^2e^{j(k_x+q)x+j(k_z-\chi)z}.\frac{\xi^2}{4})$$

$n=1,\ m=0$

$$\varphi = a_{10}e^{j(k_x+q)x+j(k_z)z} + b_{10}k_{10}e^{j(k_x+q)x+j(k_z)z}.\frac{\xi}{2}e^{j\chi z} + b_{10}k_{10}e^{j(k_x+q)x+j(k_z)z}.\frac{\xi}{2}e^{-j\chi z}$$
$$-a_{10}k_{10}^2e^{j(k_x+q)x+j(k_z)z}.\frac{\xi^2}{8}e^{j2\chi z} - a_{10}k_{10}^2e^{j(k_x+q)x+j(k_z)z}.\frac{\xi^2}{8}e^{-j2\chi z} - a_{10}k_{10}^2e^{j(k_x+q)x+j(k_z)z}.\frac{\xi^2}{4})$$

$$\varphi = a_{10}e^{j(k_x+q)x+j(k_z)z} + b_{10}k_{10}e^{j(k_x+q)x+j(k_z+\chi)z}.\frac{\xi}{2} + b_{10}k_{10}e^{j(k_x+q)x+j(k_z-\chi)z}.\frac{\xi}{2}$$
$$-a_{10}k_{10}^2e^{j(k_x+q)x+j(k_z+2\chi)z}.\frac{\xi^2}{8} - a_{10}k_{10}^2e^{j(k_x+q)x+j(k_z-2\chi)z}.\frac{\xi^2}{8} - a_{10}k_{10}^2e^{j(k_x+q)x+j(k_z)z}.\frac{\xi^2}{4})$$

$n = 1, \ m = 1$

$$\varphi = a_{11}e^{j(k_x+q)x+j(k_z+\chi)z} + b_{11}k_{11}e^{j(k_x+q)x+j(k_z+\chi)z}.\frac{\xi}{2}e^{j\chi z} + b_{11}k_{11}e^{j(k_x+q)x+j(k_z+\chi)z}.\frac{\xi}{2}e^{-j\chi z}$$
$$-a_{11}k_{11}^2e^{j(k_x+q)x+j(k_z+\chi)z}.\frac{\xi^2}{8}e^{j2\chi z} - a_{11}k_{11}^2e^{j(k_x+q)x+j(k_z+\chi)z}.\frac{\xi^2}{8}e^{-j2\chi z} - a_{11}k_{11}^2e^{j(k_x+q)x+j(k_z+\chi)z}.\frac{\xi^2}{4})$$

$$\varphi = a_{11}e^{j(k_x+q)x+j(k_z+\chi)z} + b_{11}k_{11}e^{j(k_x+q)x+j(k_z+2\chi)z}.\frac{\xi}{2} + b_{11}k_{11}e^{j(k_x+q)x+j(k_z)z}.\frac{\xi}{2}$$
$$-a_{11}k_{11}^2e^{j(k_x+q)x+j(k_z+3\chi)z}.\frac{\xi^2}{8} - a_{11}k_{11}^2e^{j(k_x+q)x+j(k_z-\chi)z}.\frac{\xi^2}{8} - a_{11}k_{11}^2e^{j(k_x+q)x+j(k_z+\chi)z}.\frac{\xi^2}{4})$$

For Upper Boundary

$n = -1, \ m = -1$

$$\varphi = [a_{-1-1}\cos(k_{-1-1}d) + b_{-1-1}\sin(k_{-1-1}d)]e^{j(k_x-q)x+j(k_z-\chi)z}$$
$$+[a_{-1-1}k_{-1-1}\sin(k_{-1-1}d) - b_{-1-1}k_{-1-1}\cos(k_{-1-1}d)]\frac{\rho}{2}e^{j(k_x)x+j(k_z-\chi)z}$$
$$+[a_{-1-1}k_{-1-1}\sin(k_{-1-1}d) - b_{-1-1}k_{-1-1}\cos(k_{-1-1}d)]\frac{\rho}{2}e^{j(k_x-2q)x+j(k_z-\chi)z}$$
$$-[a_{-1-1}k_{-1-1}^2\cos(k_{-1-1}d) + b_{-1-1}k_{-1-1}^2\sin(k_{-1-1}d)]\frac{\rho^2}{8}e^{j(k_x+q)x+j(k_z-\chi)z}$$
$$-[a_{-1-1}k_{-1-1}^2\cos(k_{-1-1}d) + b_{-1-1}k_{-1-1}^2\sin(k_{-1-1}d)]\frac{\rho^2}{8}e^{j(k_x-3q)x+j(k_z-\chi)z}$$
$$-[a_{-1-1}k_{-1-1}^2\cos(k_{-1-1}d) + b_{-1-1}k_{-1-1}^2\sin(k_{-1-1}d)]\frac{\rho^2}{4}e^{j(k_x-q)x+j(k_z-\chi)z}$$

$n = -1,\ \ m = 0$

$$
\begin{aligned}
\varphi &= [a_{-10}\cos(k_{-10}d) + b_{-10}\sin(k_{-10}d)]e^{j(k_x-q)x+j(k_z\chi)z} \\
&+[a_{-10}k_{-10}\sin(k_{-10}d) - b_{-10}k_{-10}\cos(k_{-10}d)]\frac{\rho}{2}e^{j(k_x)x+j(k_z)z} \\
&+[a_{-10}k_{-10}\sin(k_{-10}d) - b_{-10}k_{-10}\cos(k_{-10}d)]\frac{\rho}{2}e^{j(k_x-2q)x+j(k_z)z} \\
&-[a_{-10}k_{-10}^2\cos(k_{-10}d) + b_{-10}k_{-10}^2\sin(k_{-10}d)]\frac{\rho^2}{8}e^{j(k_x+q)x+j(k_z)z} \\
&-[a_{-10}k_{-10}^2\cos(k_{-10}d) + b_{-10}k_{-10}^2\sin(k_{-10}d)]\frac{\rho^2}{8}e^{j(k_x-3q)x+j(k_z)z} \\
&-[a_{-10}k_{-10}^2\cos(k_{-10}d) + b_{-10}k_{-10}^2\sin(k_{-10}d)]\frac{\rho^2}{4}e^{j(k_x-q)x+j(k_z)z}
\end{aligned}
$$

$n = -1,\ \ m = 1$

$$
\begin{aligned}
\varphi &= [a_{-11}\cos(k_{-11}d) + b_{-11}\sin(k_{-11}d)]e^{j(k_x-q)x+j(k_z+\chi)z} \\
&+[a_{-11}k_{-11}\sin(k_{-11}d) - b_{-11}k_{-11}\cos(k_{-11}d)]\frac{\rho}{2}e^{j(k_x)x+j(k_z+\chi)z} \\
&+[a_{-11}k_{-11}\sin(k_{-11}d) - b_{-11}k_{-11}\cos(k_{-11}d)]\frac{\rho}{2}e^{j(k_x-2q)x+j(k_z+\chi)z} \\
&-[a_{-11}k_{-11}^2\cos(k_{-11}d) + b_{-11}k_{-11}^2\sin(k_{-11}d)]\frac{\rho^2}{8}e^{j(k_x+q)x+j(k_z+\chi)z} \\
&-[a_{-11}k_{-11}^2\cos(k_{-11}d) + b_{-11}k_{-11}^2\sin(k_{-11}d)]\frac{\rho^2}{8}e^{j(k_x-3q)x+j(k_z+\chi)z} \\
&-[a_{-11}k_{-11}^2\cos(k_{-11}d) + b_{-11}k_{-11}^2\sin(k_{-11}d)]\frac{\rho^2}{4}e^{j(k_x-q)x+j(k_z+\chi)z}
\end{aligned}
$$

$n = 0,\ \ m = -1$

$$
\begin{aligned}
\varphi &= [a_{0-1}\cos(k_{0-1}d) + b_{0-1}\sin(k_{0-1}d)]e^{j(k_x)x+j(k_z-\chi)z} \\
&+[a_{0-1}k_{0-1}\sin(k_{0-1}d) - b_{0-1}k_{0-1}\cos(k_{0-1}d)]\frac{\rho}{2}e^{j(k_x+q)x+j(k_z-\chi)z} \\
&+[a_{0-1}k_{0-1}\sin(k_{0-1}d) - b_{0-1}k_{0-1}\cos(k_{0-1}d)]\frac{\rho}{2}e^{j(k_x-q)x+j(k_z-\chi)z} \\
&-[a_{0-1}k_{0-1}^2\cos(k_{0-1}d) + b_{0-1}k_{0-1}^2\sin(k_{0-1}d)]\frac{\rho^2}{8}e^{j(k_x+2q)x+j(k_z-\chi)z} \\
&-[a_{0-1}k_{0-1}^2\cos(k_{0-1}d) + b_{0-1}k_{0-1}^2\sin(k_{0-1}d)]\frac{\rho^2}{8}e^{j(k_x-2q)x+j(k_z-\chi)z} \\
&-[a_{0-1}k_{0-1}^2\cos(k_{0-1}d) + b_{0-1}k_{0-1}^2\sin(k_{0-1}d)]\frac{\rho^2}{4}e^{j(k_x)x+j(k_z-\chi)z}
\end{aligned}
$$

$n = 0,\ \ m = 0$

$$
\begin{aligned}
\varphi &= [a_{00}\cos(k_{00}d) + b_{00}\sin(k_{00}d)]e^{j(k_x)x+j(k_z)z} \\
&+[a_{00}k_{00}\sin(k_{00}d) - b_{00}k_{00}\cos(k_{00}d)]\frac{\rho}{2}e^{j(k_x+q)x+j(k_z)z} \\
&+[a_{00}k_{00}\sin(k_{00}d) - b_{00}k_{00}\cos(k_{00}d)]\frac{\rho}{2}e^{j(k_x-q)x+j(k_z)z} \\
&-[a_{00}k_{00}^2\cos(k_{00}d) + b_{00}k_{00}^2\sin(k_{00}d)]\frac{\rho^2}{8}e^{j(k_x+2q)x+j(k_z)z} \\
&-[a_{00}k_{00}^2\cos(k_{00}d) + b_{00}k_{00}^2\sin(k_{00}d)]\frac{\rho^2}{8}e^{j(k_x-2q)x+j(k_z)z} \\
&-[a_{00}k_{00}^2\cos(k_{00}d) + b_{00}k_{00}^2\sin(k_{00}d)]\frac{\rho^2}{4}e^{j(k_x)x+j(k_z)z}
\end{aligned}
$$

$n=0, \quad m=1$

$$\begin{aligned}
\varphi &= [a_{01}\cos(k_{01}d)+b_{01}\sin(k_{01}d)]e^{j(k_x)x+j(k_z+\chi)z} \\
&+[a_{01}k_{01}\sin(k_{01}d)-b_{01}k_{01}\cos(k_{01}d)]\frac{\rho}{2}e^{j(k_x+q)x+j(k_z+\chi)z} \\
&+[a_{01}k_{01}\sin(k_{01}d)-b_{01}k_{01}\cos(k_{01}d)]\frac{\rho}{2}e^{j(k_x-q)x+j(k_z+\chi)z} \\
&-[a_{01}k_{01}^2\cos(k_{01}d)+b_{01}k_{01}^2\sin(k_{01}d)]\frac{\rho^2}{8}e^{j(k_x+2q)x+j(k_z+\chi)z} \\
&-[a_{01}k_{01}^2\cos(k_{01}d)+b_{01}k_{01}^2\sin(k_{01}d)]\frac{\rho^2}{8}e^{j(k_x-2q)x+j(k_z+\chi)z} \\
&-[a_{01}k_{01}^2\cos(k_{01}d)+b_{01}k_{01}^2\sin(k_{01}d)]\frac{\rho^2}{4}e^{j(k_x)x+j(k_z+\chi)z}
\end{aligned}$$

$n=1, \quad m=-1$

$$\begin{aligned}
\varphi &= [a_{1-1}\cos(k_{1-1}d)+b_{1-1}\sin(k_{1-1}d)]e^{j(k_x+q)x+j(k_z-\chi)z} \\
&+[a_{1-1}k_{1-1}\sin(k_{1-1}d)-b_{1-1}k_{1-1}\cos(k_{1-1}d)]\frac{\rho}{2}e^{j(k_x+2q)x+j(k_z-\chi)z} \\
&+[a_{1-1}k_{1-1}\sin(k_{1-1}d)-b_{1-1}k_{1-1}\cos(k_{1-1}d)]\frac{\rho}{2}e^{j(k_x)x+j(k_z-\chi)z} \\
&-[a_{1-1}k_{1-1}^2\cos(k_{1-1}d)+b_{1-1}k_{1-1}^2\sin(k_{1-1}d)]\frac{\rho^2}{8}e^{j(k_x+3q)x+j(k_z-\chi)z} \\
&-[a_{1-1}k_{1-1}^2\cos(k_{1-1}d)+b_{1-1}k_{1-1}^2\sin(k_{1-1}d)]\frac{\rho^2}{8}e^{j(k_x-q)x+j(k_z-\chi)z} \\
&-[a_{1-1}k_{1-1}^2\cos(k_{1-1}d)+b_{1-1}k_{1-1}^2\sin(k_{1-1}d)]\frac{\rho^2}{4}e^{j(k_x+q)x+j(k_z-\chi)z}
\end{aligned}$$

$n=1,\ m=0$

$$
\begin{aligned}
\varphi &= [a_{10}\cos(k_{10}d)+b_{10}\sin(k_{10}d)]e^{j(k_x+q)x+j(k_z)z} \\
&+[a_{10}k_{10}\sin(k_{10}d)-b_{10}k_{10}\cos(k_{10}d)]\frac{\rho}{2}e^{j(k_x+2q)x+j(k_z)z} \\
&+[a_{10}k_{10}\sin(k_{10}d)-b_{10}k_{10}\cos(k_{10}d)]\frac{\rho}{2}e^{j(k_x)x+j(k_z)z} \\
&-[a_{10}k_{10}^2\cos(k_{10}d)+b_{10}k_{10}^2\sin(k_{10}d)]\frac{\rho^2}{8}e^{j(k_x+3q)x+j(k_z)z} \\
&-[a_{10}k_{10}^2\cos(k_{10}d)+b_{10}k_{10}^2\sin(k_{10}d)]\frac{\rho^2}{8}e^{j(k_x-q)x+j(k_z)z} \\
&-[a_{10}k_{10}^2\cos(k_{10}d)+b_{10}k_{10}^2\sin(k_{10}d)]\frac{\rho^2}{4}e^{j(k_x+q)x+j(k_z)z}
\end{aligned}
$$

$n=1,\ m=1$

$$
\begin{aligned}
\varphi &= [a_{11}\cos(k_{11}d)+b_{11}\sin(k_{11}d)]e^{j(k_x+q)x+j(k_z+\chi)z} \\
&+[a_{11}k_{11}\sin(k_{11}d)-b_{11}k_{11}\cos(k_{11}d)]\frac{\rho}{2}e^{j(k_x+2q)x+j(k_z+\chi)z} \\
&+[a_{11}k_{11}\sin(k_{11}d)-b_{11}k_{11}\cos(k_{11}d)]\frac{\rho}{2}e^{j(k_x)x+j(k_z+\chi)z} \\
&-[a_{11}k_{11}^2\cos(k_{11}d)+b_{11}k_{11}^2\sin(k_{11}d)]\frac{\rho^2}{8}e^{j(k_x+3q)x+j(k_z+\chi)z} \\
&-[a_{11}k_{11}^2\cos(k_{11}d)+b_{11}k_{11}^2\sin(k_{11}d)]\frac{\rho^2}{8}e^{j(k_x-q)x+j(k_z+\chi)z} \\
&-[a_{11}k_{11}^2\cos(k_{11}d)+b_{11}k_{11}^2\sin(k_{11}d)]\frac{\rho^2}{4}e^{j(k_x+q)x+j(k_z+\chi)z}
\end{aligned}
$$

For Lower Boundary

$e^{j(k_x-q)x+j(k_z-\chi)z}$	$a_{-1-1}-\frac{\xi^2}{4}a_{-1-1}k_{-1-1}^2+b_{-10}k_{-10}-\frac{\xi^2}{8}a_{-1-1}k_{-1-1}^2$
$e^{j(k_x-q)x+j(k_z)z}$	$\frac{\xi}{2}b_{-1-1}k_{-1-1}+a_{-10}-\frac{\xi^2}{4}a_{-10}k_{-10}^2+b_{-11}k_{-11}$
$e^{j(k_x-q)x+j(k_z+\chi)z}$	$-\frac{\xi^2}{8}a_{-1-1}k_{-1-1}^2+b_{-10}k_{-10}+a_{-11}k_{-11}-\frac{\xi^2}{4}a_{-11}k_{-11}^2$
$e^{j(k_x)x+j(k_z-\chi)z}$	$a_{0-1}k_{0-1}-\frac{\xi^2}{4}a_{0-1}k_{0-1}^2+\frac{\xi}{2}b_{00}k_{00}-\frac{\xi^2}{8}a_{01}k_{01}^2$
$e^{j(k_x)x+j(k_z)z}$	$\frac{\xi}{2}b_{0-1}k_{0-1}+a_{00}k_{00}-\frac{\xi^2}{4}a_{00}k_{00}^2+b_{01}k_{01}$
$e^{j(k_x)x+j(k_z+\chi)z}$	$-\frac{\xi^2}{8}a_{0-1}k_{0-1}^2+\frac{\xi}{2}b_{00}k_{00}+a_{01}-\frac{\xi^2}{4}a_{01}k_{01}^2$
$e^{j(k_x+q)x+j(k_z-\chi)z}$	$a_{1-1}-\frac{\xi^2}{4}a_{1-1}k_{1-1}^2+\frac{\xi}{2}b_{10}k_{10}-\frac{\xi^2}{8}a_{11}k_{11}^2$
$e^{j(k_x+q)x+j(k_z)z}$	$\frac{\xi}{2}b_{1-1}k_{1-1}+a_{10}-\frac{\xi^2}{4}a_{10}k_{10}^2+\frac{\xi}{2}b_{11}k_{11}$
$e^{j(k_x+q)x+j(k_z+\chi)z}$	$-\frac{\xi^2}{8}a_{1-1}k_{1-1}^2+\frac{\xi}{2}b_{10}k_{10}+a_{11}-\frac{\xi^2}{4}a_{11}k_{11}^2$

For Upper Boundary

$e^{j(k_x-q)x+j(k_z-\chi)z}$

$$a_{-1-1}\cos(k_{-1-1}d)+b_{-1-1}\sin(k_{-1-1}d)-\frac{\rho^2}{4}a_{-1-1}k_{-1-1}^2\cos(k_{-1-1}d)-\frac{\rho^2}{4}b_{-1-1}k_{-1-1}^2\sin(k_{-1-1}d)$$
$$+\frac{\rho}{2}a_{0-1}k_{0-1}\sin(k_{0-1}d)-\frac{\rho}{2}b_{0-1}k_{0-1}\cos(k_{0-1}d)-\frac{\rho^2}{8}a_{1-1}k_{1-1}^2\cos(k_{1-1}d)-\frac{\rho^2}{8}b_{1-1}k_{1-1}^2\sin(k_{1-1}d)$$

$e^{j(k_x-q)x+j(k_z)z}$

$$a_{-10}\cos(k_{-10}d)+b_{-10}\sin(k_{-10}d)-\frac{\rho^2}{4}a_{-10}k_{-10}^2\cos(k_{-10}d)-\frac{\rho^2}{4}b_{-10}k_{-10}^2\sin(k_{-10}d)$$
$$+\frac{\rho}{2}a_{00}k_{00}\sin(k_{00}d)-\frac{\rho}{2}b_{00}k_{00}\cos(k_{00}d)-\frac{\rho^2}{8}a_{10}k_{10}^2\cos(k_{10}d)-\frac{\rho^2}{8}b_{10}k_{10}^2\sin(k_{10}d)$$

$e^{j(k_x-q)x+j(k_z+\chi)z}$

$$a_{-11}\cos(k_{-11}d)+b_{-11}\sin(k_{-11}d)-\frac{\rho^2}{4}a_{-11}k_{-11}^2\cos(k_{-11}d)-\frac{\rho^2}{4}b_{-11}k_{-11}^2\sin(k_{-11}d)$$
$$+\frac{\rho}{2}a_{01}k_{01}\sin(k_{01}d)-\frac{\rho}{2}b_{01}k_{01}\cos(k_{01}d)-\frac{\rho^2}{8}a_{11}k_{11}^2\cos(k_{11}d)-\frac{\rho^2}{8}b_{11}k_{11}^2\sin(k_{11}d)$$

$e^{j(k_x)x+j(k_z-\chi)z}$

$$a_{0-1}\cos(k_{0-1}d)+b_{0-1}\sin(k_{0-1}d)+\frac{\rho}{2}a_{-1-1}k_{-1-1}\sin(k_{-1-1}d)-\frac{\rho}{2}b_{-1-1}k_{-1-1}\cos(k_{-1-1}d)$$
$$+\frac{\rho}{2}a_{1-1}k_{1-1}\sin(k_{1-1}d)-\frac{\rho}{2}b_{1-1}k_{1-1}\cos(k_{1-1}d)-\frac{\rho^2}{4}a_{0-1}k_{0-1}^2\cos(k_{0-1}d)-\frac{\rho^2}{4}b_{0-1}k_{0-1}^2\sin(k_{0-1}d)$$

$e^{j(k_x)x+j(k_z)z}$

$$a_{00}\cos(k_{00}d)+b_{00}\sin(k_{00}d)+\frac{\rho}{2}a_{-10}k_{-10}\sin(k_{-10}d)-\frac{\rho}{2}b_{-10}k_{-10}\cos(k_{-10}d)$$
$$+\frac{\rho}{2}a_{10}k_{10}\sin(k_{10}d)-\frac{\rho}{2}b_{10}k_{10}\cos(k_{10}d)-\frac{\rho^2}{4}a_{00}k_{00}^2\cos(k_{00}d)-\frac{\rho^2}{4}b_{00}k_{00}^2\sin(k_{00}d)$$

$e^{j(k_x)x+j(k_z+\chi)z}$

$$a_{01}\cos(k_{01}d)+b_{01}\sin(k_{01}d)+\frac{\rho}{2}a_{-11}k_{-11}\sin(k_{-11}d)-\frac{\rho}{2}b_{-11}k_{-11}\cos(k_{-11}d)$$
$$+\frac{\rho}{2}a_{11}k_{11}\sin(k_{11}d)-\frac{\rho}{2}b_{11}k_{11}\cos(k_{11}d)-\frac{\rho^2}{4}a_{01}k_{01}^2\cos(k_{01}d)-\frac{\rho^2}{4}b_{01}k_{01}^2\sin(k_{01}d)$$

$e^{j(k_x+q)x+j(k_z-\chi)z}$

$$a_{1-1}\cos(k_{1-1}d)+b_{1-1}\sin(k_{1-1}d)-\frac{\rho^2}{4}a_{1-1}k_{1-1}^2\cos(k_{1-1}d)-\frac{\rho^2}{4}b_{1-1}k_{1-1}^2\sin(k_{1-1}d)$$
$$+\frac{\rho}{2}a_{0-1}k_{0-1}\sin(k_{0-1}d)-\frac{\rho}{2}b_{0-1}k_{0-1}\cos(k_{0-1}d)-\frac{\rho^2}{8}a_{-1-1}k_{-1-1}^2\cos(k_{-1-1}d)-\frac{\rho^2}{8}b_{-1-1}k_{-1-1}^2\sin(k_{-1-1}d)$$

$e^{j(k_x+q)x+j(k_z)z}$

$$a_{10}\cos(k_{10}d)+b_{10}\sin(k_{10}d)-\frac{\rho^2}{4}a_{10}k_{10}^2\cos(k_{1-1}d)-\frac{\rho^2}{4}b_{10}k_{10}^2\sin(k_{10}d)$$
$$+\frac{\rho}{2}a_{00}k_{00}\sin(k_{00}d)-\frac{\rho}{2}b_{00}k_{00}\cos(k_{00}d)-\frac{\rho^2}{8}a_{-10}k_{-10}^2\cos(k_{-10}d)-\frac{\rho^2}{8}b_{-10}k_{-10}^2\sin(k_{-10}d)$$

$e^{j(k_x+q)x+j(k_z+\chi)z}$

$$a_{11}\cos(k_{11}d)+b_{11}\sin(k_{11}d)-\frac{\rho^2}{4}a_{11}k_{11}^2\cos(k_{11}d)-\frac{\rho^2}{4}b_{11}k_{11}^2\sin(k_{11}d)$$
$$+\frac{\rho}{2}a_{01}k_{01}\sin(k_{01}d)-\frac{\rho}{2}b_{01}k_{01}\cos(k_{01}d)-\frac{\rho^2}{8}a_{-11}k_{-11}^2\cos(k_{-11}d)-\frac{\rho^2}{8}b_{-11}k_{-11}^2\sin(k_{-11}d)$$

Format of the matrix should be such (First 9 rows are for the lower boundary and the last 9 rows are for the upper boundary);

$$a_{-1-1}\ a_{-10}\ a_{-11}\ a_{0-1}\ a_{00}\ a_{01}\ a_{1-1}\ a_{10}\ a_{11}\ b_{-1-1}\ b_{-10}\ b_{-11}\ b_{0-1}\ b_{00}\ b_{01}\ b_{1-1}\ b_{10}\ b_{11}$$

$e^{j(k_x-q)x+j(k_z-\chi)z}$

$e^{j(k_x-q)x+j(k_z)z}$

$e^{j(k_x-q)x+j(k_z+\chi)z}$

$e^{j(k_x)x+j(k_z-\chi)z}$

$e^{j(k_x)x+j(k_z)z}$

$e^{j(k_x)x+j(k_z+\chi)z}$

$e^{j(k_x+q)x+j(k_z-\chi)z}$

$e^{j(k_x+q)x+j(k_z)z}$

$e^{j(k_x+q)x+j(k_z+\chi)z}$

$e^{j(k_x-q)x+j(k_z-\chi)z}$

$e^{j(k_x-q)x+j(k_z)z}$

$e^{j(k_x-q)x+j(k_z+\chi)z}$

$$e^{j(k_x)x+j(k_z-\chi)z}$$

$$e^{j(k_x)x+j(k_z)z}$$

$$e^{j(k_x)x+j(k_z+\chi)z}$$

$$e^{j(k_x+q)x+j(k_z-\chi)z}$$

$$e^{j(k_x+q)x+j(k_z)z}$$

$$e^{j(k_x+q)x+j(k_z+\chi)z}$$

APPENDIX IV

Calculation of Determinant of 18 X 18 Matrix

Matrix of dispersion equation can be seen below. Each row is separated each other by sign ";".

M=

[(1-l^2*a^2/4) 0 (-n^2*a^2/8) 0 0 0 0 0 0 0 (m*a/2) 0 0 0 0 0 0 0 ;

0 (1-m^2*a^2/4) 0 0 0 0 0 0 0 (l*a/2) 0 (n*a/2) 0 0 0 0 0 0 ;

(-l^2*a^2/8) 0 (1-n^2*a^2/4) 0 0 0 0 0 0 0 (m*a/2) 0 0 0 0 0 0 0 ;

0 0 0 (1-o^2*a^2/4) 0 (-r^2*a^2/8) 0 0 0 0 0 0 0 (p*a/2) 0 0 0 0 ;

0 0 0 0 (1-p^2*a^2/4) 0 0 0 0 0 0 0 (o*a/2) 0 (r*a/2) 0 0 0 ;

0 0 0 (-o^2*a^2/8) 0 (1-r^2*a^2/4) 0 0 0 0 0 0 0 (p*a/2) 0 0 0 0 ;

0 0 0 0 0 0 (1-s^2*a^2/4) 0 (-u^2*a^2/8) 0 0 0 0 0 0 0 (t*a/2) 0 ;

0 0 0 0 0 0 0 (1-t^2*a^2/4) 0 0 0 0 0 0 0 (s*a/2) 0 (u*a/2) ;

0 0 0 0 0 0 (-s^2*a^2/8) 0 (1-u^2*a^2/4) 0 0 0 0 0 0 0 (t*a/2) 0 ;

(cos(l*d)-l^2*cos(l*d)*b^2/4) 0 0 (o*sin(o*d)*b/2) 0 0 (-s^2*cos(s*d)*b^2/8) 0 0 (sin(l*d)-l^2*sin(l*d)*b^2/4) 0 0 (-o*cos(o*d)*b/2) 0 0 (-s^2*sin(s*d)*b^2/8) 0 0 ;

0 (cos(m*d)-m^2*cos(m*d)*b^2/4) 0 0 (p*sin(p*d)*b/2) 0 0 (-t^2*cos(t*d)*b^2/8) 0
0 (sin(m*d)-m^2*sin(m*d)*b^2/4) 0 0 (-p*cos(p*d)*b/2) 0 0 (-t^2*sin(t*d)*b^2/8) 0
;
0 0 (cos(n*d)-n^2*cos(n*d)*b^2/4) 0 0 (r*sin(r*d)*b/2) 0 0 (-u^2*cos(u*d)*b^2/8) 0
0 (sin(n*d)-n^2*sin(n*d)*b^2/4) 0 0 (-r*cos(r*d)*b/2) 0 0 (-u^2*sin(u*d)*b^2/8) ;

(l*sin(l*d)*b/2) 0 0 (cos(o*d)-o^2*cos(o*d)*b^2/4) 0 0 (s*sin(s*d)*b/2) 0 0 (-
l*cos(l*d)*b/2) 0 0 (sin(o*d)-o^2*sin(o*d)*b^2/4) 0 0 (-s*cos(s*d)*b/2) 0 0 ;

0 (m*sin(m*d)*b/2) 0 0 (cos(p*d)-p^2*cos(p*d)*b^2/4) 0 0 (t*sin(t*d)*b/2) 0 0 (-
m*cos(m*d)*b/2) 0 0 (sin(p*d)-p^2*sin(p*d)*b^2/4) 0 0 (-t*cos(t*d)*b/2) 0 ;

0 0 (n*sin(n*d)*b/2) 0 0 (cos(r*d)-r^2*cos(r*d)*b^2/4) 0 0 (u*sin(u*d)*b/2) 0 0 (-
n*cos(n*d)*b/2) 0 0 (sin(r*d)-r^2*sin(r*d)*b^2/4) 0 0 (-u*cos(u*d)*b/2) ;

(-l^2*cos(l*d)*b^2/8) 0 0 (o*sin(o*d)*b/2) 0 0 (cos(s*d)-s^2*cos(s*d)*b^2/4) 0 0 (-
l^2*sin(l*d)*b^2/8) 0 0 (-o*cos(o*d)*b/2) 0 0 (sin(s*d)-s^2*sin(s*d)*b^2/4) 0 0 ;

0 (-m^2*cos(m*d)*b^2/8) 0 0 (p*sin(p*d)*b/2) 0 0 (cos(t*d)-t^2*cos(t*d)*b^2/4) 0
0 (-m^2*sin(m*d)*b^2/8) 0 0 (-p*cos(p*d)*b/2) 0 0 (sin(t*d)-t^2*sin(t*d)*b^2/4) 0 ;

0 0 (-n^2*cos(n*d)*b^2/8) 0 0 (r*sin(r*d)*b/2) 0 0 (cos(u*d)-u^2*cos(u*d)*b^2/4) 0
0 (-n^2*sin(n*d)*b^2/8) 0 0 (-r*cos(r*d)*b/2) 0 0 (sin(u*d)-u^2*sin(u*d)*b^2/4)]

Because this 18 X 18 Matrix is symbolic and determinant of this matrix requires huge memories, firstly we transferred matrix's elements in terms of "M" to take determinant.

18 X 18 Matrix in terms of M

M=

[M1_1 0 M1_3 0 0 0 0 0 0 0 M1_11 0 0 0 0 0 0 0 ;

0 M2_2 0 0 0 0 0 0 0 M2_10 0 M2_12 0 0 0 0 0 0 ;

M3_1 0 M3_3 0 0 0 0 0 0 0 M3_11 0 0 0 0 0 0 0 ;

0 0 0 M4_4 0 M4_6 0 0 0 0 0 0 0 M4_14 0 0 0 0 ;

0 0 0 0 M5_5 0 0 0 0 0 0 0 M5_13 0 M5_15 0 0 0 ;

0 0 0 M6_4 0 M6_6 0 0 0 0 0 0 0 M6_14 0 0 0 0 ;

0 0 0 0 0 0 M7_7 0 M7_9 0 0 0 0 0 0 0 M7_17 0 ;

0 0 0 0 0 0 0 M8_8 0 0 0 0 0 0 0 M8_16 0 M8_18 ;

0 0 0 0 0 0 M9_7 0 M9_9 0 0 0 0 0 0 0 M9_17 0 ;

M10_1 0 0 M10_4 0 0 M10_7 0 0 M10_10 0 0 M10_13 0 0 M10_16 0 0 ;

0 M11_2 0 0 M11_5 0 0 M11_8 0 0 M11_11 0 0 M11_14 0 0 M11_17 0 ;

0 0 M12_3 0 0 M12_6 0 0 M12_9 0 0 M12_12 0 0 M12_15 0 0 M12_18 ;

M13_1 0 0 M13_4 0 0 M13_7 0 0 M13_10 0 0 M13_13 0 0 M13_16 0 0 ;

0 M14_2 0 0 M14_5 0 0 M14_8 0 0 M14_11 0 0 M14_14 0 0 M14_17 0 ;

```
0 0 M15_3 0 0 M15_6 0 0 M15_9 0 0 M15_12 0 0 M15_15 0 0 M15_18 ;

M16_1 0 0 M16_4 0 0 M16_7 0 0 M16_10 0 0 M16_13 0 0 M16_16 0 0 ;

0 M17_2 0 0 M17_5 0 0 M17_8 0 0 M17_11 0 0 M17_14 0 0 M17_17 0 ;

0 0 M18_3 0 0 M18_6 0 0 M18_9 0 0 M18_12 0 0 M18_15 0 0 M18_18 ];
```

Then this matrix's determinant is calculated via such MATLAB algorithm;

```
R11=det(M);
S = str2mat(R11);
FID = fopen('Result.txt','wt+');
Count = fwrite(FID, S, 'char')
fclose(FID);
```

This algorithm run such a way; algorithm calculates determinant of matrix in terms of M and open a result.txt file then write the determinant into result.txt file.

Then we transferred determinant of 18 X 18 symbolic matrix that is in terms of M into the determinant of 18X18 symbolic matrix that includes real symbolic values.

The determinant of matrix can be seen in CD as Appendix V.

APPENDIX V

Full Expressions of Determinant of 18 X 18 Matrix

Determinant of 18X18 symbolic matrix is given at the end of the thesis in CD.